5-26-2020

Understanding Air Pollutants and Meteorology Interactions Using Chemical Transport Models

Pengfei Wang
Louisiana State University and Agricultural and Mechanical College

UNDERSTANDING AIR POLLUTANTS AND METEOROLOGY INTERACTIONS USING CHEMICAL TRANSPORT MODELS

A Dissertation

Submitted to the Graduate Faculty of the
Louisiana State University and
Agricultural and Mechanical College
in partial fulfillment of the
requirements for the degree of
Doctor of Philosophy

in

The Department of Civil and Environmental Engineering

by
Pengfei Wang
B.S., Shandong University of Science and Technology, China, 2012
M.S., Nagasaki University, Japan, 2015
August 2020

ACKNOWLEDGMENTS

I would like to thank my advisor, Dr. Hongliang Zhang, for supporting and guiding me in my academic career. Your efficient working style and positive attitude inspired me and made me a better myself.

Then, I want to show appreciation to my committee members (in alphabetical order), Dr. Barry D. Keim, Dr. William Moe, Dr. Frank Tsai, Dr. Zuo “George” Xue, and Dr. Xiuping Zhu. Thank you all for providing valuable suggestions for my dissertation and help on my campus life.

I also want to express my gratitude to my friends, instructors, CEE and LSU for giving me a memorable experience in Baton Rouge.

Finally, I would thank my parents for their care and love. Thanks to my wife, Chuanqiu. Without your support and encouragement, I could not have made this far.

TABLE OF CONTENTS

LIST OF TABLES

LIST OF FIGURES

LIST OF ABBREVIATIONS

AGL	Above the Ground Level
AOD	Aerosol Optical Depth
ARW	Advanced Research WRF
BEIS	Biogenic Emissions Inventory System
CCM	Climate-Chemistry Model
CCN	Cloud Condensation Nuclei
CH_4	Methane
CMAQ	Community Multi-scale Air Quality
CO_2	Carbon Dioxide
CTMs	Chemical Transport Models
EC	Elemental Carbon
EDGAR	Emission Database for Global Atmospheric Research
EPA	Environmental Protection Agency
FDDA	Four-Dimensional Data Assimilation
FINN	Fire Inventory from the National Center for Atmospheric Research
FNL	Final Analysis
GE	Gross Error

GOCART	Goddard Global Ozone Chemistry Aerosol Radiation and Transport
MADE	Modal Aerosol Dynamics Model for Europe
MB	Mean Bias
MCIP	Meteorology-Chemistry Interface Processor
MDA8	Daily Maximum 8 h average
MEGAN	Model for Emissions of Gases and Aerosols from Nature
MEIC	Multi-resolution Emission Inventory for China
MFB	Mean Fractional Bias
MFE	Mean Fractional Error
MNB	Mean Normalized Bias
MNE	Mean Normalized Error
MODIS	Moderate Resolution Imaging Spectroradiometer
NAQS	National Air Quality Station
NCAR/ACOM	National Center for Atmospheric Research/Atmospheric Chemistry Observations & Modeling
NCDC	National Climate Data Center
NCEP	National Centers for Environmental Prediction
NCP	North China Plain

NEI	National Emissions Inventory
NH_4^+	Ammonium
NMM	Nonhydrostatic Mesoscale Model
NO_3^-	Nitrate
NOAH	Air Force and Hydrologic Research Lab
NOx	Oxides of nitrogen
O_3	Ozone
OBS	Observation
OC	Organic Carbon
PBL	Planetary Boundary Layer
PM_{10}	coarse particulate matter
$PM_{2.5}$	fine particulate matter
POA	Primary Organic Aerosol
PRE	Prediction
RACM-KPP	Regional Atmospheric Chemistry Mechanism of using the Kinetic Pre-Processor
RADM2	Regional Acid Deposition Model, 2nd generation
REAS2	Regional Emission inventory in ASia version 2
RH	Relative Humidity

RMSE	Root Mean Square Error
RRTM	Rapid and accurate Radiative Transfer Model
SCB	Sichuan Basin
SMOKE	Sparse Matrix Operator Kernel Emissions
SO_4^{2-}	Sulfate
SOA	Secondary Organic Aerosol
SORGAM	Secondary ORGanic Aerosol Model
SR	Solar Radiation
SREF	Short Range Ensemble Forecast
SVOCs	Semi-Volatile Organic Compounds
T2	Temperature at 2 meters
US	United States
VOCx	Volatile Organic Compounds
WD	Wind Direction
WF	With feedback
WHO	World Health Organization
WOF	Without feedback
WRF	Weather Research and Forecasting

WRF/Chem	Weather Research and Forecasting model with Chemistry
WS	Wind Speed
YSU	Yonsei University

ABSTRACT

Air pollution is a worldwide threat to human health and ecosystems, especially in developing countries. After being emitted to the atmosphere, air pollutant concentrations are determined by chemical and physical processes including transport, transformation, and deposition, which are largely affected by meteorological variations. In turn, pollutants such as fine particulate matter ($PM_{2.5}$) affect meteorology by impacting solar radiation and cloud condensation processes. Thus, it is important and necessary to understand the interactions between air pollutants and meteorology for better designing effective air pollution control strategies and forecasting weather. In this study, two chemical transport models (CTMs) are applied to understand the interactions between air pollutants and meteorology in different areas. One model is the Community Multi-scale Air Quality (CMAQ) model and the other is the Weather Research and Forecasting model with Chemistry (WRF/Chem). Four cases are studied, the first case studies the responses of ozone (O_3) and $PM_{2.5}$ concentrations to variations in meteorology in China from 2013 to 2015. It is found that emission reductions in 2014 and 2015 effectively reduced $PM_{2.5}$ concentrations by 23.9 and 43.5 $\mu g/m^3$, respectively, but was partially counteracted by unfavorable meteorology. Reduction of primary PM and gaseous precursors led to 13.4 and 16.5 ppb increase of daily maximum 8 h average (MDA8) concentrations in the summertime in 2014 and 2015 in comparison to 2013, which was likely caused by the increase of solar actinic flux due to PM reduction. The other case understands the uncertainties caused by meteorology in simulating summertime O_3 from 2016 to 2018 over the Southeast United States. WRF/Chem showed good performance in O_3 simulation over Southeast US, especially along the coastal areas. The O_3 simulation is sensitive to the meteorology uncertainties. The ensemble was more reliable than any individual run in this simulation. The last two cases simulate the feedbacks of air pollutants on meteorological

conditions and related changes in pollutant concentrations in the Sichuan Basin (SCB), China and Africa, respectively. Aerosol radiation decreased surface temperature by 1-2 ℃, wind speed (WS) by ~ 0.3 m/s, planetary boundary layer (PBL) height by 10-20 %, solar radiation (SR) by ~ 30 %, and precipitation by 0.02-0.2 mm, while increased relative humidity (RH) by up to 2-4 % in January, which resulted in up to 10 μg/m^3 increase of $PM_{2.5}$ in January and 2 ppb decrease of O_3 in July in SCB. In the simulation of Africa, $PM_{2.5}$ concentration was higher in January and lower in August while O_3 showed no significant seasonal and distribution variance. Aerosol radiative effects reduced solar radiation at the ground by as much as 20 w/m^2 in January and 40 w/m^2 in August, lowering the temperature by 1 °C in January and 0.5 °C in August on average, decreased WS by ~0.1 m/s, and reduced PBL height by up to 120 m in both months, while slightly increased RH (2-4%).

CHAPTER 1. INTRODUCTION

$PM_{2.5}$ is the fraction of PM with aerodynamic diameters less than or equal to 2.5μm. $PM_{2.5}$ is a major air pollutant around the world due to its adverse effects on crop harvest, human health, and climate [1-4]. $PM_{2.5}$ is a mixture of primary components including trace metals, elemental carbon (EC) and organic carbon (OC) and secondary components including sulfate (SO_4^{2-}), ammonium (NH_4^+), nitrate (NO_3^-) and secondary organic aerosols (SOA) [5-7]. Primary components are those directly released into the atmosphere including dust or sea salt from natural sources and EC or trace metals from anthropogenic sources. Secondary components such as SO_4^{2-}, NO_3^-, NH_4^+, and SOA are those particles formed by chemical reactions of gaseous species in the atmosphere [8]. The increase of $PM_{2.5}$ was proved to be accompanied by an increase in mortality due to respiration and cardiovascular diseases [9-13]. $PM_{2.5}$-related illnesses could cause extra hospital visits and loss of work time, leading to economic impact in $PM_{2.5}$ polluted areas [14-16].

O_3 is an important photochemical oxidant as well as a major air pollutant in the troposphere and could lead to agricultural loss and human health problems [17-21]. Besides the stratospheric-tropospheric exchange, O_3 is predominantly created by photochemical reactions of oxides of nitrogen (NOx) and volatile organic compounds (VOCs) [22-25]. Due to the high oxidizing ability, elevated ground-level O_3 is harmful to human health by irritating skin, eyes, respiratory tract, and aggravate asthma and bronchial inflammation [26]. Chronic O_3 exposure can also lead to impaired photosynthesis and altered gene expression, which results in cell death and crop yield losses on wheat, soybean, and maize [27, 28].

Meteorology affects the concentration and distribution of primary air pollutants and influences the formation of secondary pollutants consequently [29, 30]. The chemical pathways for the formation of secondary inorganic components of $PM_{2.5}$ mainly include gas-phase photochemical oxidation

reaction, the heterogeneous reaction on the surface of particles, and liquid-phase oxidation reaction inside the particles [31, 32]. Solar radiation changes could lead to variations of atmospheric stability, which will affect transport and dispersion of pollutants as well as the rates of photochemical reactions [33-35]. Wind speed and direction will influence the accumulation and dispersion of pollutants [36, 37]. With the increase of precipitation, PM concentration will decrease since wet deposition is its main sink, while O_3 changes can be neglected because of the low solubility of O_3 and its precursors in water [38-41]. The higher temperature is expected to aggravate O_3 pollution because it is favorable for photochemical reactions [42-44].

After being emitted to the atmosphere, atmospheric aerosols are not only influenced by meteorology changes but also impact the climate by changing incoming and outcoming solar radiation into and out of the earth's system. The aerosol radiation effect contains direct, indirect and semi-direct effects [45]. The direct aerosol radiative effect includes any direct interactions between aerosol particles and solar radiation that change the amount of solar radiant energy, such as scatting and absorption [46, 47]. Acting as cloud condensation nuclei (CCN), aerosol particles could increase the number of cloud droplets and scattering areas or enlarge the cloud lifetime and therefore enhance cloud albedo. This is the "indirect aerosol radiative effect". Some aerosols such as soot, which have a strong ability in absorbing solar radiation could release energy as heat radiation. The energy could heat the air mass, increasing its static stability, and may also cause cloud droplets evaporation, and then affect the climate by reducing cloud. This is called "semidirect aerosol radiative effect" [48, 49]. After carbon dioxide (CO_2) and methane (CH_4), O_3 is the third-largest greenhouse gas and will heat the atmosphere by absorbing long-wave radiation from the earth system [50]. It also decreases net primary plant productivity by impacting photosynthesis due to its oxidative stress [51-53].

Many studies have focused on the interactions of air pollutants and meteorological conditions. By investigating the observation data of $PM_{2.5}$ concentration and meteorological data such as temperature, wind, humidity in Beijing during 2007-2008, Wang et al. [54] diagnosed and identified the impact of meteorological conditions on air pollutants and found condensation is favorable for the formation of a secondary aerosol. Huang et al. [55] studied the aerosol-PBL interaction by comparing the observation data of $PM_{2.5}$ with the reanalysis meteorological data during 2010-2016. They indicate that aerosol could impact meteorology by blocking solar radiation, which leads to a cooler surface. In addition to the surface dimming, the warming of the upper air brought by aerosols will increase the stability and stagnation of the air, which will worsen the dispersion of air pollutants. A statistical analysis of O_3, temperature, and mortality through thin plate regression splines in nine French cities in 2003 was conducted by Filleul et al. [56], the risk of deaths related to O_3 and temperature ranged from 10.6% to 174.7% in different cities.

Besides the statistical methods, CTMs are widely used to analyze the interactions between air pollutants and meteorological condition changes as well. The coupled WRF/CMAQ modeling system (Weather Research and Forecasting (WRF) and CMAQ) was used in January 2013 over the North China Plain (NCP) to simulate the aerosol–meteorology interactions. Wang et al. [57] found a high concentration of $PM_{2.5}$ produced a decrease in solar radiation and heading to a more stable PBL. The higher PBL stability prevents the dispersion process, which results in an enhanced $PM_{2.5}$ concentration. The WRF/Chem model was used to simulate the aerosol direct effects on radiation and aerosol indirect effects on meteorological factors over Europe during June and July in 2006 [58]. The GRAPES/CUACE model has been applied to simulate the feedbacks on the radiation budget, PBL and haze formation caused by aerosols over Jing-Jin-Ji, China in 2008 [59]. To simulate the aerosol indirect and direct feedback effects on meteorology and air pollutant

concentrations, the WRF/Chem model is used over Poland [60]. The meteorology effect on air pollutions has been estimated in Melbourne, Australia during 1999-2006 [61]. $PM_{2.5}$, O_3, and NO_2 are showing significant response to meteorology changes of PBL, winds, especially temperature. Langner et al. [62] indicate the importance of climate impact on O_3 in connection with summer extreme event by using one online climate-chemistry model (CCM) and four offline CTMs to simulate the future climate change on surface O_3 between 2000-2009 and 2040-2049 over Europe.

Statistical analysis studies of the pollutant-meteorology interactions highly rely on observation, which is costly and usually time and space limited. CTMs can offer much larger spatial and longer temporal distribution with high resolution. Current air pollution studies paid more attention to first-tier cities, my study of all the capital cities cover the whole China will be a great supplement, particularly it considered the changes of $PM_{2.5}$ and O_3 connected with meteorological influence. Air pollution problems in second or third-tier cities areas like SCB or developing areas like Africa are not well studied. This study will provide information for understanding the current pollution situation and help to make future emission control policies. Meteorology uncertainties are the biggest impact factor for O_3 forecasting besides emission. My study will be of great importance for air pollution investigation in those emission well-controlled areas like the United States (U.S.). Thus, it is both essential and crucial to investigate the interactions between air pollutants and meteorology.

It is assumed that unfavorable meteorology may offset the positive impacts of emission reduction on air pollution control. **The first objective** is to use the WRF/CMAQ system to simulate $PM_{2.5}$ and O_3 concentrations in 2013-2015 over China and compare it with observation data at 31 provincial capital cities to examine the response of $PM_{2.5}$ and O_3 to meteorological changes. The concentrations or distribution variations of air pollutants are presumed to bring changes in

meteorology. **The second objective** is to apply the WRF/Chem to simulate $PM_{2.5}$ and O_3 over the SCB in China with the consideration of aerosol radiative feedback effect. This objective can offer information about the influence on meteorological variables from air pollutions. It is supposed that using different initial and boundary conditions for meteorology in CTM may lead to different results of O_3 simulation. **The third objective** is to simulate O_3 over the Southeast US from 2016 to 2018 using the ensemble WRF/Chem driven by the Short Range Ensemble Forecast (SREF) outputs. This study focused on the meteorology uncertainties in the areas that anthropogenic emissions were well controlled. It is a hypothesis that including aerosol radiative feedbacks in the model simulation might improve the prediction of meteorology variables and air pollutants. **The last objective** is to simulate $PM_{2.5}$ and O_3 over the whole continent of Africa in January and August 2015 by using WRF/Chem. This study would be valuable for analyzing air pollution impact on meteorology for the places where have large meteorology variation and emission potential like Africa. **With the accomplishment of all four objectives, this study** emphasizes the significance of considering the interactions of air pollutants and meteorological conditions in air pollution control management.

CHAPTER 2. RESPONSES OF $PM_{2.5}$ AND O_3 CONCENTRATIONS TO CHANGES OF METEOROLOGY AND EMISSIONS IN CHINA

2.1 Introduction

Developing countries such as China have been suffering from air pollution countrywide with the rapid development of industrialization and urbanization. $PM_{2.5}$ is the major concern due to its adverse effects on human health, visibility, ecosystems, and climate [1-4, 63, 64]. Annual concentrations of $PM_{2.5}$ in the majority of the cities in China are more than 5 times higher than the World Health Organization (WHO) guideline of 10 $\mu g/m^3$ [65-67]. Total premature mortality of 1.3 million in China has been estimated due to $PM_{2.5}$ related diseases such as chronic obstructive pulmonary disease and lung cancer [68]. Besides, O_3 is attracting increasing attention during the increase of concentrations in many areas [17-19]. O_3 is a secondary pollutant formatted from photochemical reactions between NO_x and VOCs and leads to both human health damages and agricultural loss [22-25, 69].

To reduce the severe air pollution, the Chinese government has taken enormous efforts since 2013 and targeted to reduce $PM_{2.5}$ concentrations by 25% in major metropolitan areas by 2017 [70]. Due to strict control measures, annually-averaged $PM_{2.5}$ concentrations in major regions have decreased continuously these years [71]. It was observed that $PM_{2.5}$ concentrations did not always decrease and even increased in a few instances. For example, in December 2015, the concentrations of $PM_{2.5}$ were much higher than in previous years [72, 73]. At the same time, O_3 concentrations increased in Beijing, Shanghai, Guangzhou, and Chengdu from 2013 to 2015 [74]. The industry, business, scientific communities, and the public are all concerned as these stringent

This chapter was previously published as: Wang, P., Guo, H., Hu, J., Kota, S. H., Ying, Q., & Zhang, H. (2019). Responses of PM2.5 and O3 concentrations to changes of meteorology and emissions in China. Science of the Total Environment, 662, 297-306.

emission control measures are made at a high price of increasing cost in industrial production and inconveniently affects daily life.

Concentrations of air pollutants are significantly influenced by both emissions and meteorology conditions [41, 75]. Reducing emissions could decrease the primary PM and precursors of secondary PM directly, but also change the atmospheric processes, whose nonlinear characteristics may cause uncertain changes in PM and O_3 [76, 77]. For example, Huang et al. [78] reported that 30-77% of $PM_{2.5}$ in severe pollution events were contributed by the secondary aerosol formation in Beijing, Shanghai, Guangzhou, and Xi'an, thus reducing primary emissions may have little effects. O_3 formation is controlled by the ratios of VOCs to NOx in specific locations and improper changes of emissions would cause unchanged or increase of concentrations [29, 79]. Li et al. [80] reported that the increasing O_3 was related by the slowing down of hydroperoxyl radicals sink caused by PM reduction in addition to the changes in emissions of its precursors. Regional transport could increase the concentration of air pollutants in certain locations[81-83].

Although climate change is believed not likely to significantly offset efforts to reduce $PM_{2.5}$ [84], year to year variations of meteorology would lead to inconsistent changes in $PM_{2.5}$. Unfavorable meteorology leads to an increase in air pollutants even when emissions remain unchanged [85-89]. Meteorological conditions even play a dominant role compared with emission control in some cases [90]. O_3 formation is favored by high temperatures, low humidity, and wind speed [91]. Meteorology impacts on PM are more variable, based on the diversity of PM components. Stagnant meteorology with low wind speed leads to less dispersion of PM [92]. High temperatures can increase oxidation and production of sulfate but reduce nitrate through more volatilization from particle to gas [93, 94]. Biogenic semi-volatile organic compounds (SVOCs) could also increase due to high temperature, and the partitioning to SOA could be very uncertain.

Thus, it is important to identify the roles of meteorology variations and emission controls in concentration changes of air pollutants to assess the effectiveness of emission control measures and address potential problems. In this study, we investigated the responses of $PM_{2.5}$ and O_3 concentrations to meteorology variations and emission controls at all the provincial capital cities in China based on the national wide ambient measures and chemical transport model simulations during 2013-2015.

2.2 Methods

The hourly $PM_{2.5}$ and O_3 concentrations at monitoring sites within the 31 provincial capital cities from March 2013 to December 2015 were downloaded from the publishing website of China National Environmental Monitoring Center (http://113.108.142.147:20035/emcpublish/). The regions of China and the locations of 31 cities are shown in Figure 1 and Table 1. The MDA8 concentrations in this analysis were calculated as the highest of 17 consecutive 8-hr averages of hourly O_3 concentrations. All the measurements conducted at the multiple national air quality monitoring sites were averaged to the city level for analysis. The data were validated and sanity check was conducted as previous studies [95-97].

Table 1. List of the provincial capital cities in different regions of China.

Region	**City list**
North	1 Beijing, 2 Tianjin, 3 Shijiazhuang, 4 Taiyuan, and 5 Huhehaote.
Northeast	6 Shenyang, 7 Changchun, and 8 Haerbin.
East	9 Shanghai, 10 Nanjing, 11 Hangzhou, 12 Hefei, 13 Fuzhou, 14 Nanchang, and 15 Jinan.
South Central	16 Zhengzhou, 17 Wuhan, 18 Changsha, 19 Guangzhou, 20Nanning, and 21 Haikou.
Southwest	22 Chongqing, 23 Chengdu, 24 Guiyang, 25 Kunming, and 26 Lasa.
Northwest	27 Xian, 28 Lanzhou, 29 Xining, 30 Yinchuan, and 31 Wulumuqi.

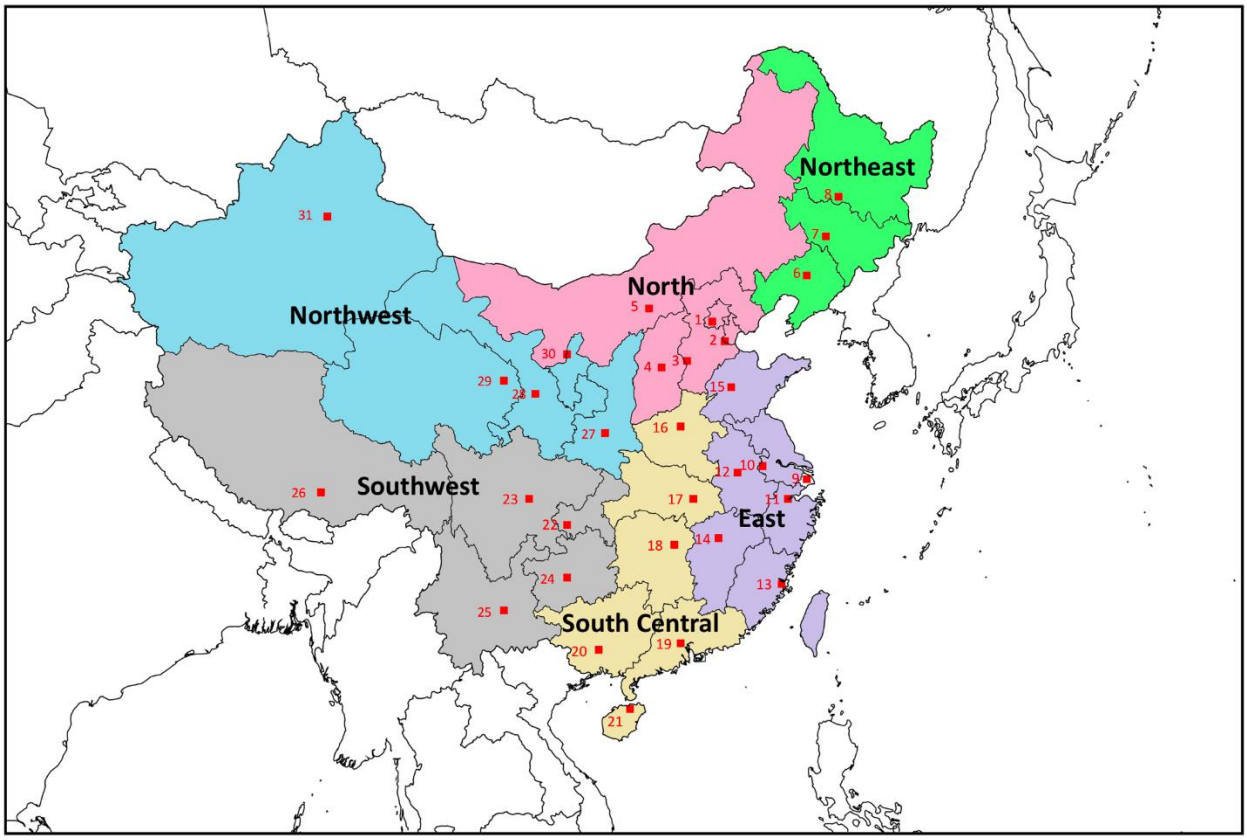

Figure 1. Simulation domain covering China and surrounding countries. The numbers of the cities are constant with Table 1.

An updated version of CMAQv5.0.1 was applied to simulate O_3 and $PM_{2.5}$ from 2013 to 2015. Details about the changes made to improve the model performance of SOA and sulfate can be found in previous studies [98, 99]. The model used a 36 km×36 km horizontal resolution domain that covers China and surrounding countries (Figure 1). Multi-resolution Emission Inventory for China (MEIC) (http://www.meicmodel.org) was used for the monthly anthropogenic emissions from China and emissions of surrounding countries were from Regional Emission inventory in ASia version 2 (REAS2) [100]. Biogenic emissions were generated using the Model for Emissions of Gases and Aerosols from Nature (MEGAN) version 2.10. The meteorological inputs were generated using WRF v3.6.1 with initial and boundary conditions from the National Center for Environmental Prediction (NCEP) Final Analysis (FNL) Operational Model Global Tropospheric

Analyses dataset [101]. The model performance has been validated against all available observations in 2013 [99, 102-104].

The changes in pollutant concentrations were calculated based on differences in observations at different time spans (eqn-1). The inter-annual changes were based on concentrations from March to December in each year, as no observations were available in January and February of 2013. December was selected to represent the heavily polluted wintertime for $PM_{2.5}$ and summer months (June, July, and August) were used for O_3. The anthropogenic emissions of the CMAQ simulations remained unchanged in all three years so that the changes in predicted pollutant concentrations are only due to change in meteorological conditions and biogenic emissions (eqn-2). The changes caused by differences in anthropogenic emissions were then calculated by subtracting changes due to meteorology from total observation changes (eqn-3).

$$\Delta C_{i,j} = Obs_{i,j} - Obs_{i,2013} \quad \text{(eqn-1)}$$

$$\Delta M_{i,j} = Pre_{i,j} - Pre_{i,2013} \quad \text{(eqn-2)}$$

$$\Delta E_{i,j} = \Delta C_{i,j} - \Delta M_{i,j} \quad \text{(eqn-3)}$$

- $\Delta C_{i,j}$ represents the change in observation of pollutant i from the year 2013 to year j,
- $Obs_{i,j}$ represents the averaged observation of pollutant i in year j,
- $\Delta M_{i,j}$ is the change of pollutant i in year j due to meteorology and biogenic emissions compared to 2013,
- $Pre_{i,j}$ is the averaged prediction of pollution i in year j,
- $\Delta E_{i,j}$ indicates the change of pollutant i in year j due to anthropogenic emission changes compared to 2013.

It should be noted that the method used in this study is a rough estimation of pollutant concentrations changes due to meteorology and emission changes. Due to the complexity of atmospheric processes, the "real" contributions of meteorology and emission changes cannot be ideal differentiated. The analysis was conducted in all the 31 provincial capital cities in China as a national overview.

2.3 Results and discussions

2.3.1 Model validation

Performance of meteorology simulation by WRF for 2013 has been validated previously and the statistics of temperature at 2 meters (T2), WS, and WD at 10 meters and RH at first layer calculated by Hu et al. [105]. The benchmarks are recommended by Emery et al. [106] for an MM5 model simulation with a resolution of 4–12 km in U.S.. The values that exceeded the benchmark are represented in bold. The same for Table 2 and 3 (OBS means observation; PRE means prediction; MB means bias; RMSE is root mean square; error GE is gross error). The benchmarks suggested by Emery et al. [106] are also listed and compared. The model performance for 2014 and 2015 is generally comparable to that of 2013, as shown in Table 2 and 3, respectively. For T2, prediction results are slightly higher in November and lower in other seasons than observations. The MB values are usually within benchmarks of ≤±0.5 in fall and winter. The GE values of T2 are larger than the benchmark (≤2.0) except September and December in 2014. GE values of WS meet the benchmark (≤2.0) in all months though WS is over predicted. MB values are within benchmark (≤±0.5) in summer and RMSE values are within benchmarks (≤2.0) from June to September in both years. For WD, there are four months within benchmark (MB ≤±10) in 2014 and 7 months in 2015. RH predictions are close to observations with MB of ±2.0% in most months.

Table 2. Meteorology performance of 12 months in 2014. OBS means observation, PRE means prediction, MB means bias, GE is gross error, and RMSE is root mean square error. The benchmarks are suggested by Emery et al. [107]. Values exceeded the benchmark are represented in bold.

		Jan	Feb	Mar	Apr	May	Jun	Jul	Aug	Sep	Oct	Nov	Dec	Bench-mark
T2(K)	OBS	269.3	269.6	277.6	284.3	289.6	294.2	296.9	296.2	291.3	284.9	277.7	269.9	
	PRE	268.6	268.1	276.4	283.7	288.8	293.4	296.1	295.5	290.7	284.8	277.8	269.6	
	MB	**-0.7**	**-1.5**	**-1.2**	**-0.6**	**-0.8**	**-0.8**	**-0.7**	**-0.6**	-0.5	-0.1	0.1	-0.2	≤±0.5
	GE	**3.1**	**3.2**	**2.9**	**2.5**	**2.6**	**2.5**	**2.5**	**2.3**	1.3	**2.4**	**2.5**	1.9	≤2.0
	RMSE	4.2	4.3	3.9	3.4	3.5	3.4	3.4	3.1	3.1	3.2	3.4	3.8	
WS(m/s)	OBS	3.5	3.5	3.7	3.6	3.7	3.3	3.4	3.2	3.2	3.4	3.3	3.5	
	PRE	4.7	4.8	4.7	4.4	4.4	3.7	3.8	3.8	3.8	4.4	4.4	4.9	
	MB	**1.2**	**1.3**	**1.0**	**0.8**	**0.7**	-0.4	0.4	**0.6**	**0.6**	**1.0**	**1.0**	**1.3**	≤±0.5
	GE	1.9	2.0	1.8	1.7	1.7	1.4	1.4	1.5	1.5	1.7	1.7	2.0	≤2.0
	RMSE	**2.5**	**2.5**	**2.4**	**2.1**	**2.2**	1.9	1.9	2.0	2.0	**2.2**	**2.3**	**2.6**	≤2.0
WD(°)	OBS	214.4	191.0	207.7	192.2	193.4	168.4	184.1	176.2	176.4	184.1	203.2	225.2	
	PRE	234.1	195.1	225.4	204.1	207.4	172.6	196.8	180.4	175.8	187.3	211.3	248.1	
	MB	**17.8**	4.1	**15.7**	**11.4**	**12.7**	6.2	**12.3**	6.9	3.5	6.6	**10.4**	**20.1**	≤±10
	GE	**47.9**	**47.9**	**45.9**	**47.3**	**45.8**	**48.7**	**47.1**	**47.8**	**47.8**	**45.9**	**47.8**	**45.6**	≤±30
	RMSE	65.3	65.6	63.4	64.7	63.0	65.8	64.0	65.0	65.2	63.6	65.4	62.7	
RH(%)	OBS	74.5	75.2	69.9	64.3	61.2	66.6	67.5	70.2	67.9	69.2	71.9	75.7	
	PRE	72.0	74.4	72.0	63.9	63.1	68.6	69.2	71.8	69.0	69.6	71.3	71.4	
	MB	-2.5	-0.8	2.1	-0.4	1.9	2.0	1.7	1.6	1.1	0.5	-0.6	-4.3	
	GE	13.3	11.9	12.9	13.2	13.5	12.3	12.3	11.2	11.8	13.1	12.9	14.9	
	RMSE	17.4	15.5	16.4	16.8	17.2	15.6	15.7	14.3	15.0	16.7	16.8	20.1	

Table 3. Meteorology performance of 12 months in 2015. OBS means observation, PRE means prediction, MB means bias, GE is gross error, and RMSE is root mean square error. The benchmarks are suggested by Emery et al. [107]. Values exceeded the benchmark are represented in bold.

		Jan	Feb	Mar	Apr	May	Jun	Jul	Aug	Sep	Oct	Nov	Dec	Bench-mark
T2(K)	OBS	270.4	272.4	277.4	284.3	290.0	293.5	297.0	296.4	291.0	284.9	277.7	272.6	
	PRE	270.0	271.5	276.3	283.6	289.3	293.0	296.3	295.7	290.4	284.5	278.0	272.6	
	MB	-0.5	**-0.9**	**-1.0**	**-0.7**	**-0.7**	-0.4	**-0.6**	**-0.7**	**-0.6**	-0.4	0.3	0	≤±0.5
	GE	**2.9**	**2.9**	**2.8**	**2.6**	**2.5**	**2.4**	**2.4**	**2.3**	**2.3**	**2.5**	**2.5**	**2.8**	≤2.0
	RMSE	3.9	3.8	3.7	3.5	3.4	3.2	3.3	3.1	3.0	3.3	3.3	3.8	
WS(m/s)	OBS	3.5	3.6	3.6	3.7	3.7	3.4	3.4	3.2	3.28	3.5	3.3	3.5	
	PRE	4.8	4.8	4.6	4.6	4.3	3.9	3.8	3.6	4.0	4.5	4.4	4.7	
	MB	**1.3**	**1.2**	**1.0**	**0.8**	**0.6**	0.5	0.4	0.4	**0.7**	**1.0**	**1.1**	**1.2**	≤±0.5
	GE	1.9	1.9	1.8	1.7	1.6	1.5	1.5	1.4	1.5	1.7	1.8	1.9	≤2.0
	RMSE	**2.5**	**2.5**	**2.3**	**2.3**	**2.1**	2.0	1.9	1.9	2.0	**2.2**	**2.3**	**2.4**	≤2.0
WD(°)	OBS	215.2	206.2	201.1	184.9	193.1	171.3	177.9	170.9	176.8	200.7	180.7	208.7	
	PRE	231.6	220.4	214.3	190.6	206.6	177.1	185.5	172.4	176.4	209.0	180.3	222.3	
	MB	**15.9**	**13.9**	**12.7**	7.5	**12.3**	7.0	8.6	4.4	4.1	9.9	4.9	**14.0**	≤±10
	GE	**47.3**	**46.2**	**46.1**	**45.1**	**47.3**	**48.2**	**47.2**	**48.9**	**46.7**	**45.0**	**48.0**	**47.3**	≤±30
	RMSE	64.8	63.6	63.4	62.4	64.7	65.4	64.3	66.3	63.9	62.6	65.8	64.7	
RH(%)	OBS	77.8	75.8	71.7	67.3	61.4	66.5	67.7	68.9	70.0	66.1	76.3	73.8	
	PRE	75.0	73.1	71.1	68.1	62.4	68.1	70.5	71.5	71.2	66.9	75.8	73.9	
	MB	-2.8	-2.8	-0.6	0.8	1.0	1.5	2.8	2.6	1.2	0.8	-0.5	0.1	
	GE	13.3	12.3	12.9	12.8	13.2	11.8	11.8	11.3	11.4	13.6	11.9	12.5	
	RMSE	18.1	16.1	16.4	16.5	17.0	15.2	15.1	14.5	14.6	17.4	15.7	16.8	

Table 4. Model performance on O_3-1h, MDA8, $PM_{2.5}$, PM_{10}, from March to December 2013. OBS is mean observation, PRE is mean prediction, MFB is mean fractional bias, MFE is mean fractional error, MNB is mean normalized bias, and MNE is mean normalized error. The performance criteria for $PM_{2.5}$ are suggested by EPA [108], and the performance criteria for O_3 are suggested by EPA [109]. Values exceeded the criteria are represented in bold.

		Mar	Apr	May	Jun	Jul	Aug	Sep	Oct	Nov	Dec	Criteria
O_3-1h (ppb)	OBS	53.96	57.73	65.37	67.72	65.7	68.3	60.73	57.97	49.18	46.53	
	PRE	58.09	61.76	66.91	67.82	63.23	66.47	59.5	54.92	45.66	42.09	
	MFB	0.08	0.09	0.05	0.01	-0.01	-0.01	0.01	-0.03	-0.05	-0.09	
	MFE	0.29	0.27	0.25	0.3	0.29	0.28	0.27	0.26	0.27	0.32	
	MNB	**0.16**	**0.17**	0.11	0.1	0.06	0.06	0.07	0.03	0.01	-0.01	$\leq \pm 0.15$
	MNE	**0.34**	**0.32**	0.28	**0.33**	**0.31**	0.3	0.29	0.26	0.26	0.28	≤ 0.3
MDA8 (ppb)	OBS	50.4	47.44	52.59	54.36	51.79	54.03	48.63	48.03	40.31	38.92	
	PRE	48.81	51.49	57.86	59.58	54.05	58.07	50.64	48.48	40.6	40.7	
	MFB	-0.05	0.07	0.1	0.08	0.03	0.06	0.04	0.01	-0.01	0.01	
	MFE	0.29	0.24	0.24	0.28	0.26	0.26	0.25	0.24	0.25	0.27	
	MNB	0.03	0.13	**0.16**	**0.16**	0.09	0.12	0.1	0.06	0.03	0.07	$\leq \pm 0.15$
	MNE	0.29	0.28	0.28	**0.32**	0.28	0.29	0.27	0.25	0.24	0.27	≤ 0.3
$PM_{2.5}$ ($\mu g/m^3$)	OBS	81.68	62.07	60.12	60.83	45.52	47.1	56.08	85.69	88.93	123.73	
	PRE	66.12	43.24	39.28	41.6	31.31	39.07	52.24	56.09	80.21	126.83	
	MFB	-0.24	-0.4	-0.47	-0.41	-0.48	-0.31	-0.21	-0.42	-0.17	-0.07	$\leq \pm 0.6$
	MFE	0.59	0.63	0.68	0.69	0.72	0.65	0.62	0.64	0.6	0.59	≤ 0.75
	MNB	0.04	-0.16	**-0.19**	-0.09	-0.17	-0.01	0.11	-0.16	0.17	0.3	
	MNE	0.61	0.54	0.58	**0.63**	0.63	0.64	0.68	0.56	0.7	0.75	
PM_{10} ($\mu g/m^3$)	OBS	151.39	121.56	111.90	96.95	79.90	85.04	98.27	136.02	150.27	178.78	
	PRE	74.72	52.48	45.37	46.58	35.59	44.63	57.53	65.12	90.22	136.26	
	MFB	-0.59	-0.73	-0.79	-0.68	-0.78	-0.65	-0.54	-0.65	-0.48	-0.34	
	MFE	0.74	0.83	0.89	0.82	0.88	0.79	0.73	0.77	0.72	0.63	
	MNB	-0.31	-0.43	-0.45	-0.35	-0.44	-0.35	-0.24	-0.36	-0.16	-0.04	
	MNE	0.56	0.58	0.62	0.62	0.63	0.59	0.60	0.59	0.64	0.62	

Table 4 shows the statistics of model performance of different pollutants including 1-hour peak O_3 (O_3-1h), MDA8 O_3, $PM_{2.5}$, and coarse particulate matter (PM_{10}). Mean observations, mean predictions, mean fractional bias (MFB), mean fractional error (MFE), mean normalized bias (MNB), and mean normalized error (MNE) were calculated for each month from March to December 2013. The performance criteria suggested by EPA [108] were used for $PM_{2.5}$ and the performance criteria of EPA [109] were used for O_3. Values that exceeded the criteria are denoted in bold. The overall model performance on O_3-1h and MDA8 O_3 meet the criteria suggested by US

EPA [109] in most months. O_3-1h MNB values of March and April were slightly higher than the criteria of 0.15, and O_3-1h MNE values of March, April, June and July were higher than the benchmark of 0.3. MDA8 had higher MNB in May and June and MNE in June than criteria. Negative MFB values show that $PM_{2.5}$ was under-predicted but all within the suggested benchmark of 0.6 [110]. More details can be found in Hu et al. [105].

2.3.2 Annual $PM_{2.5}$

Figure 2 shows the annual observed $PM_{2.5}$ concentrations in the base year (2013) at the cities, the changes in observed concentrations, as well as the changes due to emissions and meteorology in 2014 and 2015 compared to 2013. The exact values are shown in Table 5. The annual values in most cities in 2013 were above 50 μg/m^3 with the highest average of 95.4 μg/m^3 in north China. All cities experienced a decrease of $PM_{2.5}$ in 2014 with more than ~20 μg/m^3 decrease in Shijiazhuang, Nanjing, Chongqing, Xi'an and Wulumuqi. Concentration changes due to meteorology were all larger than zero except at Haikou, Kunming, indicating that meteorology in 2014 was more favorable to high $PM_{2.5}$. The increases of $PM_{2.5}$ due to meteorology were up to 20 μg/m^3 in Beijing, Tianjin, Haerbin, Wuhan, Changsha, Chongqing, Chengdu, and Xi'an. These cities are scattered in different regions, showing that the meteorological effects are different even within the same region.

Meteorology changes in 2014 and 2015 affected the concentrations of $PM_{2.5}$ in comparison to 2013. Both primary and secondary components of $PM_{2.5}$ increased in 2014 and 2015and inland areas are found more vulnerable to meteorology especially in 2015 (Figure 3). OTHER is the sum of inexplicit components. In 2015, there is a 30% increase (24.6 μg/m^3 in concentration) on average in all cities. The increase has the same pattern in both years referring to the component species and regions, while the amounts can be doubled in 2015 comparing to 2014 in all regions except

Northwest. Sulfate, nitrates, and ammonium are the top three contributors, accounting for 80-90% of the total increase. The changes in meteorological parameters in Figure 4 could explain the differences. In most regions, temperature, WS and planetary boundary layer (PBL) height were lower, and RH was higher in 2014 than the base year. These conditions are favorable for higher pollution than the base year. Emission control was effective as concentration changes were less than zero in all cities. The emission induced changes were estimated to be larger than 20 μg/m^3 in most cities and up to 50 μg/m^3 in Shijiazhuang, Nanjing, Wuhan, Chengdu, and Xi'an.

Table 5. Responses of $PM_{2.5}$ and O_3 concentrations to changes of meteorology and emissions in China.

	2013 Observation	**2014-2013**			**2015-2013**		
		Obs.	**Met and biogenic emissions**	**Anthropogenic emissions**	**Obs.**	**Met and biogenic emissions**	**Anthropogenic emissions**
Annual $PM_{2.5}$(μg/m^3)							
All cities	74.6	-12.5	11.5	-23.9	-18.9	24.6	-43.5
North	95.4	-15.0	16.3	-31.3	-27.2	28.4	-55.7
Northeast	77.3	-7.9	10.6	-18.6	-8.9	22.6	-31.4
East	73.3	-14.3	10.5	-24.8	-19.7	27.9	-47.6
South Central	70.3	-10.1	14.3	-24.3	-16.0	37.9	-53.9
Southwest	57.4	-10.0	9.3	-19.3	-15.5	16.7	-32.2
Northwest	76.2	-15.5	7.3	-22.8	-22.5	9.4	-31.9
December $PM_{2.5}$(μg/m^3)							
All cities	109.8	-32.4	-8.6	-27.1	-18.6	54.5	-73.1
North	105.0	-17.6	-7.9	-9.7	24.4	91.5	-67.1
Northeast	127.3	-40.7	-9.2	-31.4	-8.7	97.7	-106.4
East	130.3	-52.4	-5.4	-61.5	-41.1	41.1	-82.2
South Central	118.5	-48.8	-12.1	-36.8	-44.8	72.7	-117.6
Southwest	81.8	-17.6	1.6	-19.2	-27.8	29.5	-57.3
Northwest	93.0	-9.6	-19.4	9.8	4.4	13.5	-9.1
Summertime MDA8 O_3 (ppb)							
All cities	38.2	13.4	-3.2	16.7	16.5	-1.8	18.3
North	47.3	19.0	-8.7	27.7	15.0	-2.4	17.5
Northeast	36.1	20.0	-4.5	24.5	21.3	-0.5	21.8
East	37.4	12.4	-1.1	13.5	12.8	-2.1	14.9
South Central	35.7	14.7	-1.5	16.2	19.2	-4.2	23.3
Southwest	38.1	6.2	-3.7	9.9	13.3	0.2	13.1
Northwest	34.7	11.0	-1.6	12.7	20.1	-0.9	21.1

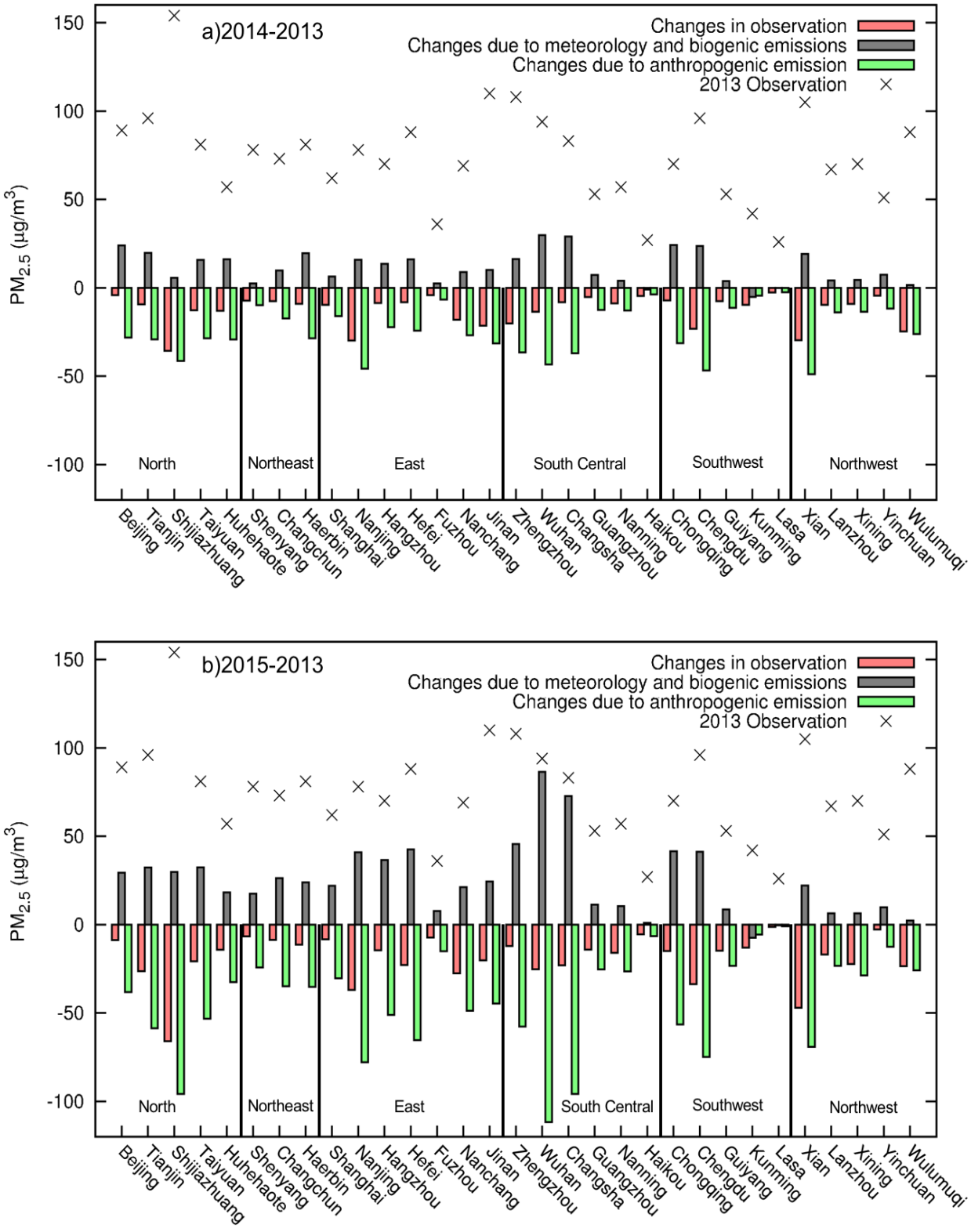

Figure 2. Changes in annual averaged $PM_{2.5}$ concentrations in the provincial capital cities in 2014 and 2015 compared to 2013 due to changes in meteorology + biogenic emissions and anthropogenic emissions.

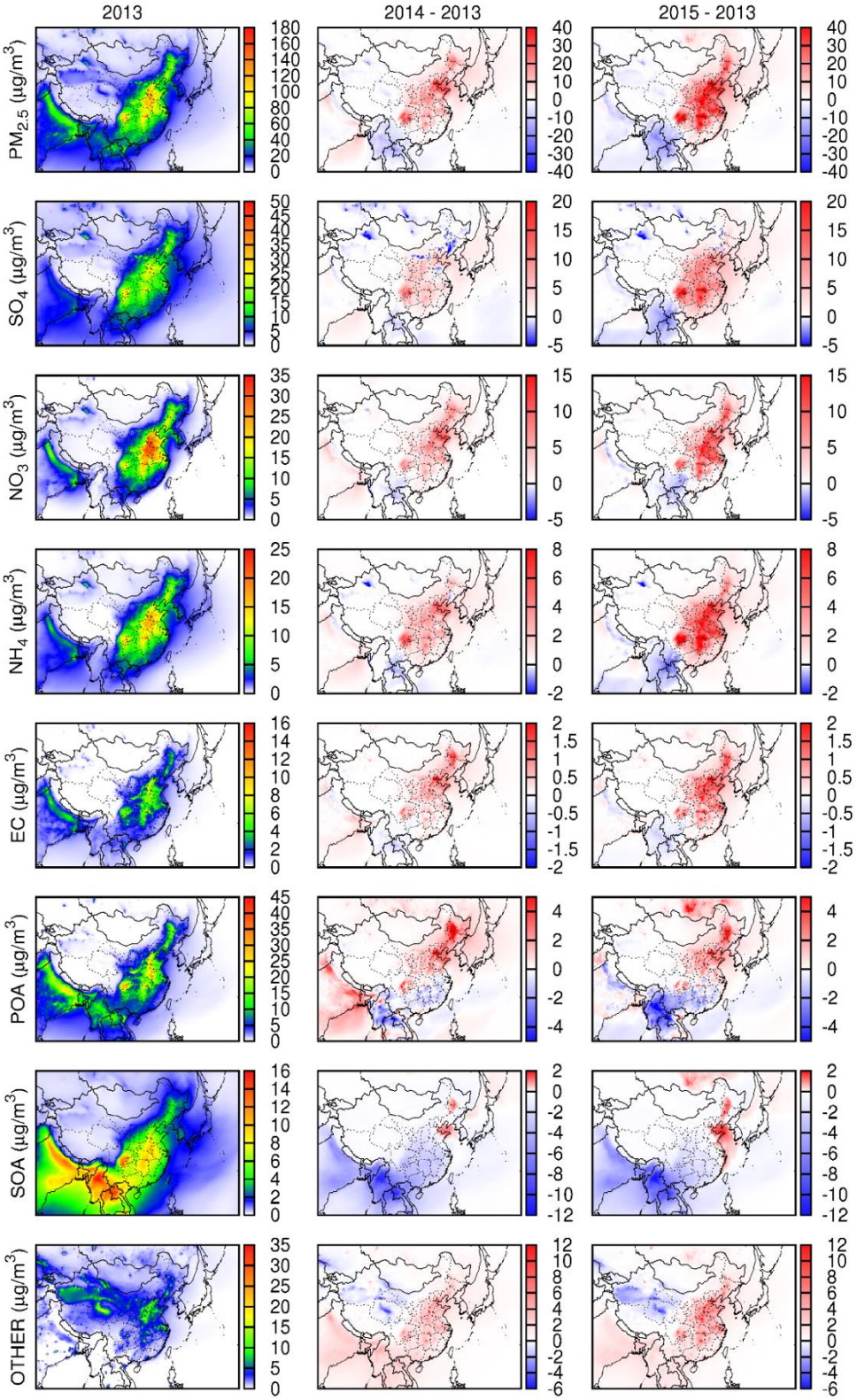

Figure 3. Predicted annual $PM_{2.5}$ and its major components in 2013 and the changes due to meteorology in 2014 and 2015. OTHER is the sum of inexplicit components.

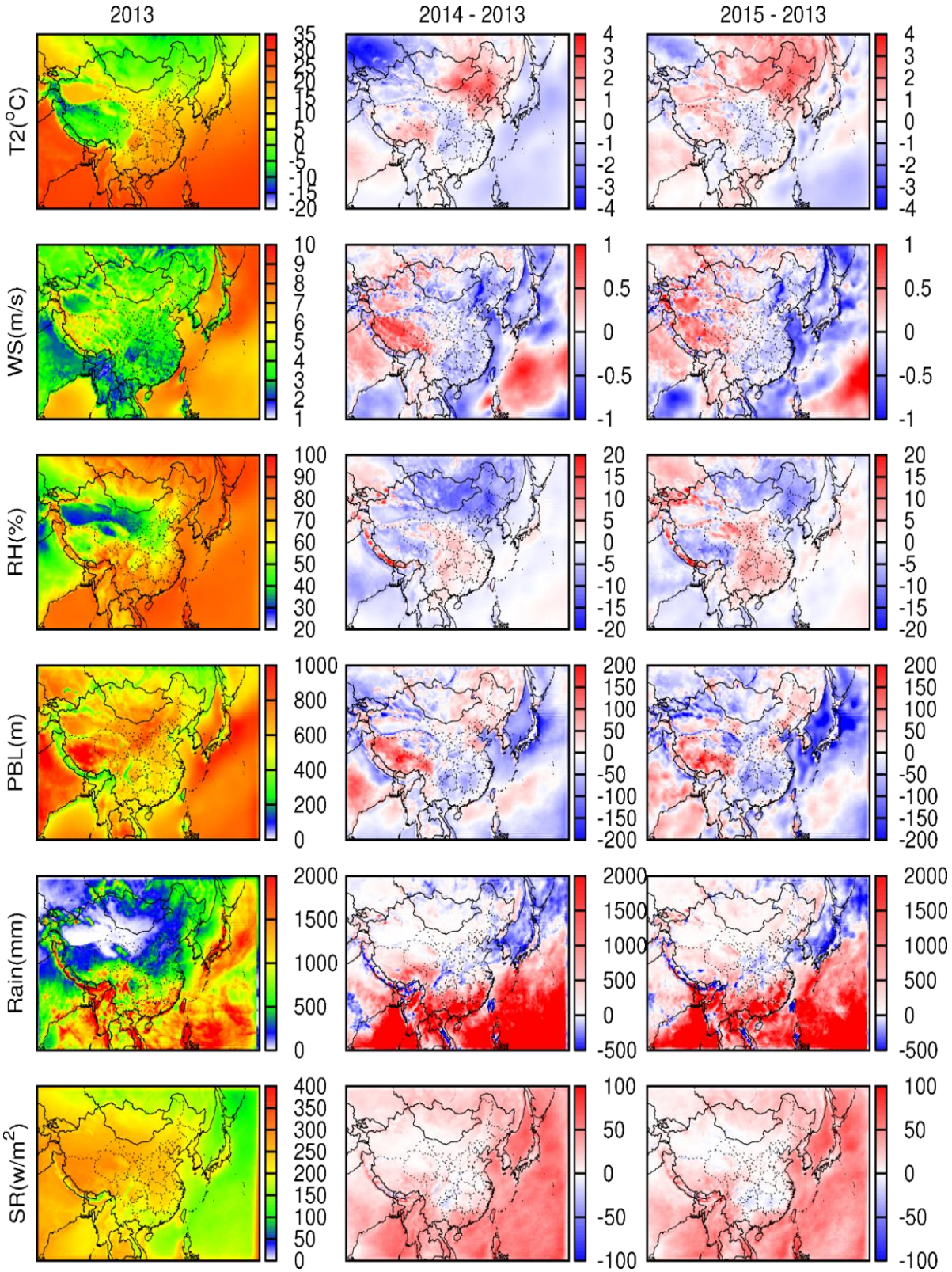

Figure 4. Annual averaged meteorological parameters in 2013 and the differences from 2014 and 2015 to 2013. T2 is temperature at 2 meters above ground, WS is wind speed, RH is relative humidity, PBL is planetary boundary layer height, and SR is the shortwave radiation at surface.

In 2015, $PM_{2.5}$ concentrations decreased overall in all cities with the largest change of over 60 $\mu g/m^3$ in Shijiazhuang and an average of 27.2 $\mu g/m^3$ in north China. Compared with 2014, similar meteorology changes such as low temperature, WS and PBL height and even higher RH were observed. Meteorology was also not favorable for pollution dispersion, with changes being greater than 25 $\mu g/m^3$ in most cities in north, northeast, east and south-central regions (Figure 3). Wuhan and Changsha had the highest increase of >70 $\mu g/m^3$. Specifically, primary components (EC, POA, and part of OTHER) only accounted for less than 10% of the total while the rest are all secondary species. The role of emission control was more significant with more than 30 $\mu g/m^3$ decreases in all regions and over 100 $\mu g/m^3$ reductions in Shijiazhuang, Wuhan, and Changsha.

2.3.3 Winter $PM_{2.5}$

$PM_{2.5}$ pollution in China is more severe in winter time, thus it is key to evaluate the changes in those months. Figure 5 shows the changes of $PM_{2.5}$ in December when severe pollution events happen frequently. The observed $PM_{2.5}$ in all cities were greater than 50 $\mu g/m^3$ except Lasa, with the highest concentrations of 200 $\mu g/m^3$ in Hefei and Wuhan. In December 2014, $PM_{2.5}$ concentrations decreased in all cities except Wulumuqi. Meteorology was favorable for decreasing pollution in most cities in North, Northeast, East, South Central, and Northwest with the average decreases of -7.9, -9.2, -5.4, -12.1 and -19.4, respectively (Table 5). The largest decrease due to meteorology was greater than 50 $\mu g/m^3$ in Zhengzhou and Xi'an. Compared to 2013, December 2014 had similar rain and SR, lower temperature, and RH, and higher WS and PBL (Figure 6). The lower RH reduced the possibility of secondary PM formation and the higher WS was beneficial for the decrease of both primary and secondary PM by diffusion and transportation [41]. Nitrate ranked first in the total decrease with 30%, which equals to the combination of sulfate and ammonium. POA, SOA, and EC took the rest share as ~15%, 8%, and less than 5%, respectively.

Thus, all major components of $PM_{2.5}$ decreased in all areas except East and Northeast China (Figure 7).

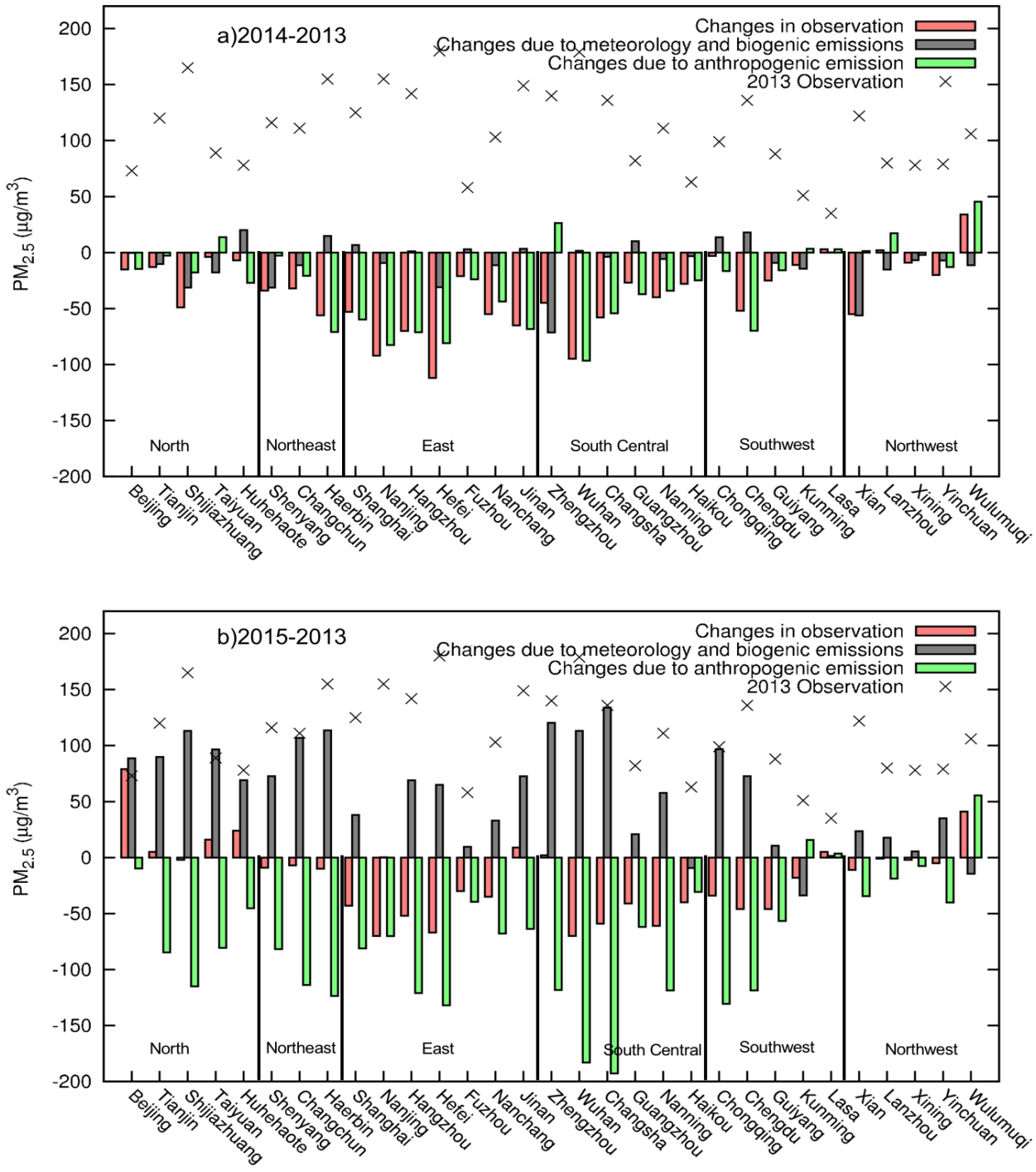

Figure 5. Changes in $PM_{2.5}$ concentrations in the provincial capital cities in December 2014 and 2015 compared to 2013 due to changes in meteorology+ biogenic emissions and anthropogenic emissions.

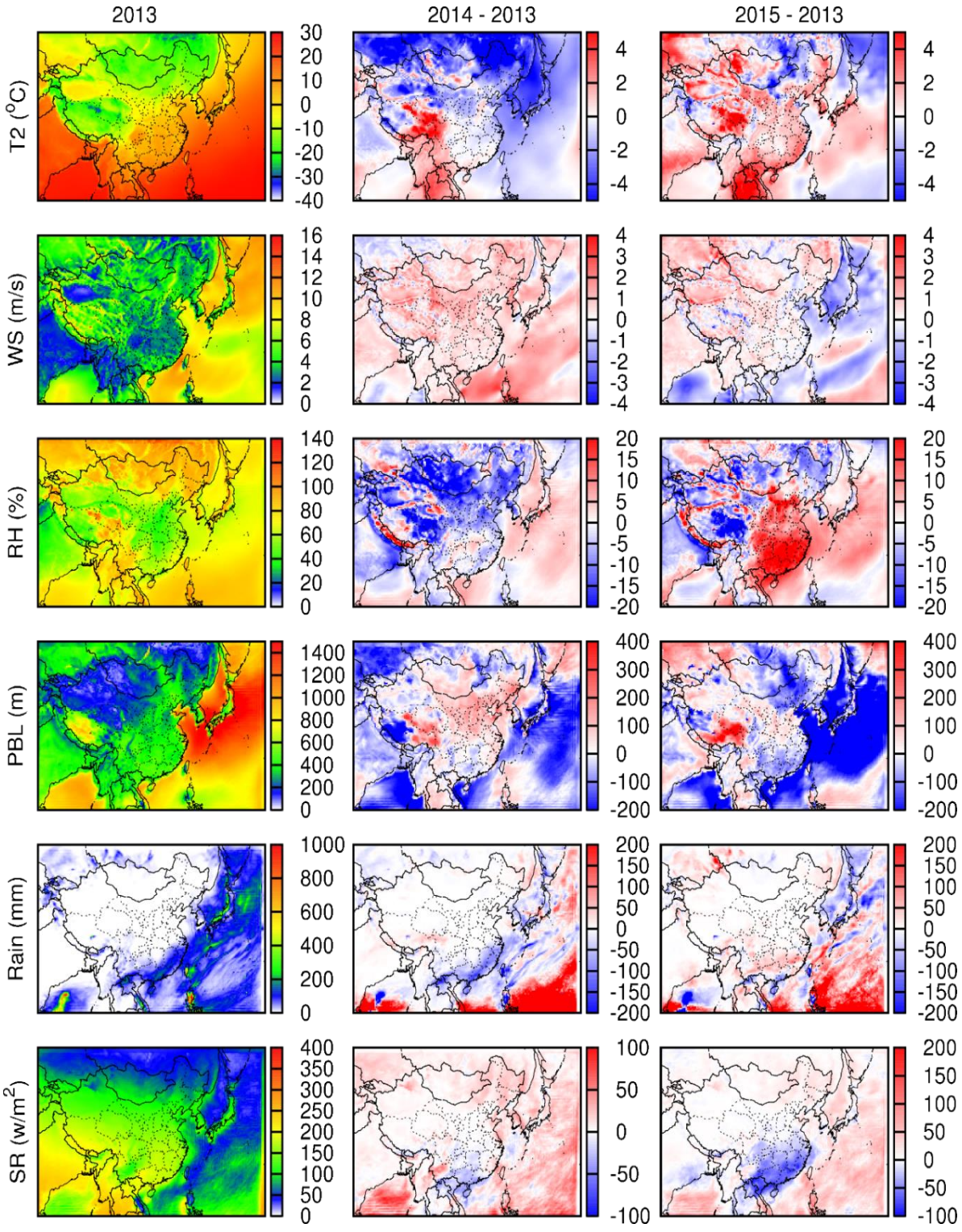

Figure 6. Averaged meteorological parameters in December 2013 and the differences from 2014 and 2015 to 2013. T2 is temperature at 2 meters above ground, WS is wind speed, RH is relative humidity, PBL is planetary boundary layer height, and SR is the shortwave radiation at surface.

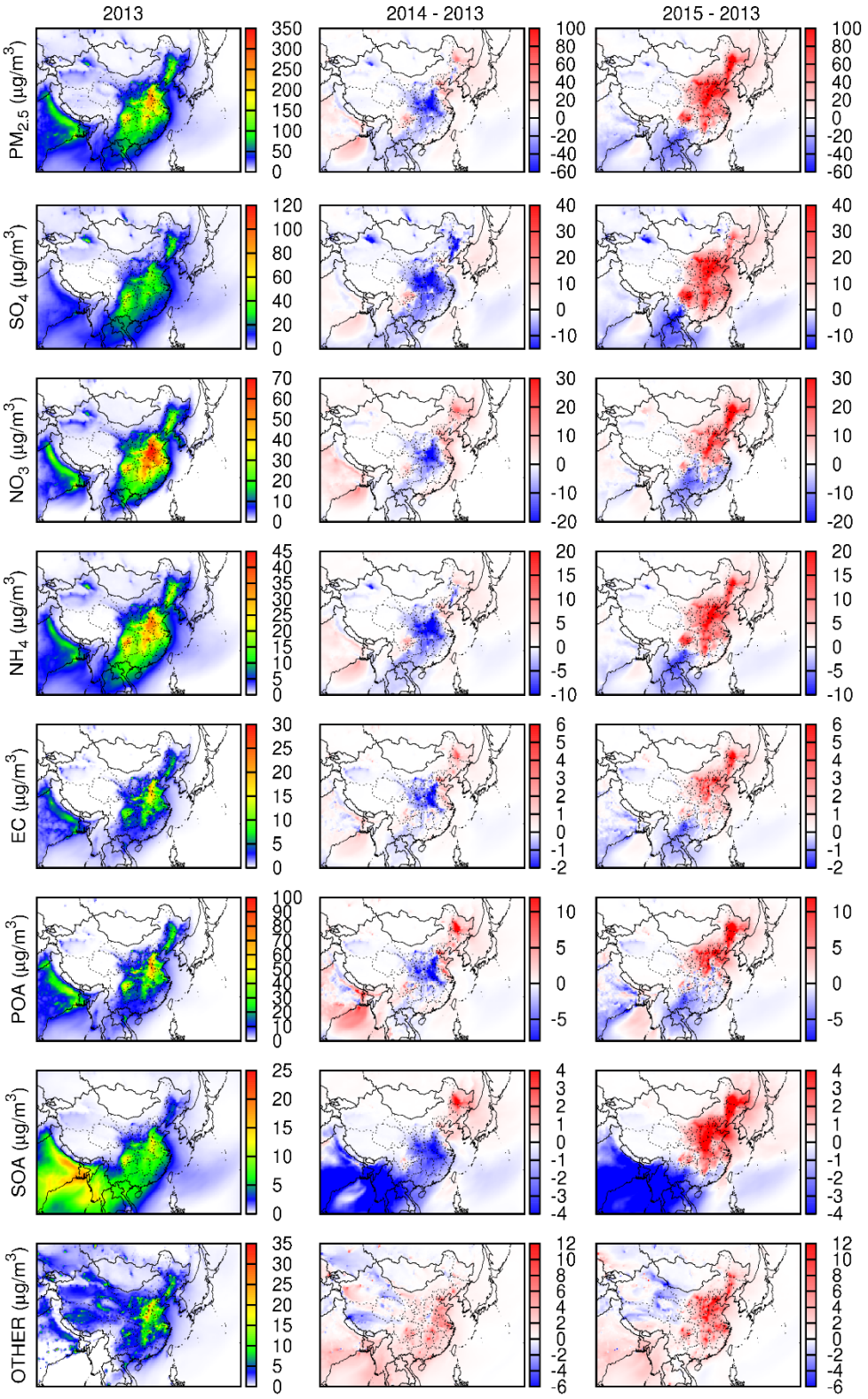

Figure 7. Predicted December $PM_{2.5}$ and its major components in 2013 and the changes due to meteorology in 2014 and 2015. OTHER is the sum of inexplicit components.

In December 2015, the $PM_{2.5}$ concentrations increased greatly in Beijing and Wulumuqi, remained similar in most cities in North, Northeast, and Northwest, and decreased significantly in other regions (Figure 5b). Meteorology played a significant role in the changes of concentrations in almost all cities, leading to the increases of 54.5 $\mu g/m^3$ and 91.5 $\mu g/m^3$, 97.7 $\mu g/m^3$, 41.1 $\mu g/m^3$, 72.7 $\mu g/m^3$ in North, Northeast, East and South Central, respectively (Table 5). The changes attributed to meteorology were up to 90 $\mu g/m^3$ in Beijing, and 130 $\mu g/m^3$ in Changsha. All $PM_{2.5}$ components increased due to meteorology, especially in the regions of North, Northeast and part of East and South-Central China as shown in Figure 7. Secondary inorganic aerosols (SIA, including sulfate, nitrate, and ammonia) contributed the most with contributions of 35%, 15%, and 15% to the total increase by sulfate, nitrate, and ammonia, respectively. POA accounted as much as 10 -15% in the Northeast. Spatially, nitrate, EC, and POA are more likely to increase in the Northeast while sulfate increased in North, East and South-Central areas. Ammonia and SOA increased in all four regions. The major reason is that secondary PM formations were more favorable with slightly higher temperatures, similar WS, much higher RH, and lower PBL (Figure 6). RH plays a major role as high RH leads to more SIA formation [41, 111, 112]. RH increase leads to more aerosol water and higher sulfur oxidation ratio (SOR) and nitrogen oxidation ratio (NOR) for more sulfate and nitrate formation [113]. Ammonium is semi-volatile and considered to be in equilibrium with its gas-phase precursor in general. Thus, more ammonium in aerosol phase is favored by high RH [114]. Anthropogenic emission changes led to a limited reduction of $PM_{2.5}$ concentrations in Beijing, but worked significantly for most cities, with more than 160 $\mu g/m^3$ directions in Changsha and Wuhan, helping reduce $PM_{2.5}$ concentrations under unfavorable meteorological conditions.

2.3.4 Summer O_3

O_3 has higher concentrations in summer due to more intensive photochemical reactions. Figure 8 shows the changes of MDA8 O_3 in summer months (June, July and August) in all capital cities. Averaged MDA8 O_3 in summer 2013 were 30-60 ppb, except in Haerbin, Fuzhou, and Haikou, where concentrations were lower. MDA8 O_3 increased greatly in 2014 and 2015 at most cities with the largest increase of 20-40 ppb in Beijing, Huhehaote, Haerbin, Fuzhou, Jinan, and Zhengzhou. Generally, changes in meteorology conditions and biogenic emissions in summer of both 2014 and 2015 were not the reason for the overall increases. The MDA8 O_3 concentrations would have decreased by 5-10 ppb in most cities due to changes in meteorology and biogenic emissions alone, except in some cities in East, South Central, and Southwest China, where concentrations would have increased slightly by less than 10 ppb. Figure 9 shows that even though northern China experienced decrease and southern China would have experienced an increase in both 2014 and 2015, the changes were not significant as meteorology conditions (Figure 10) did not vary dramatically in summer. In 2014 and 2015 summer, the temperature, PBL and WS was lower, RH was comparable, rain and SR was slightly higher, compared to the base year summer in southern China. Some meteorology factors may have a counter effect on the change of O_3 concentrations. For example, lower temperature usually leads to less O_3 formation due to lower photochemical reaction rates [115].

Therefore, the observed large changes of O_3 concentrations are mostly due to anthropogenic emission changes. As shown in Figure 8, changes of MDA8 O_3 due to emission changes of precursors are greater than 0, except at Hefei in 2014 and Shijiazhuang in 2015. Beijing experienced greater than 30 and 20 ppb increases in 2014 and 2015, respectively. The highest increase occurred in Jinan (~40ppb) in both 2014 and 2015.

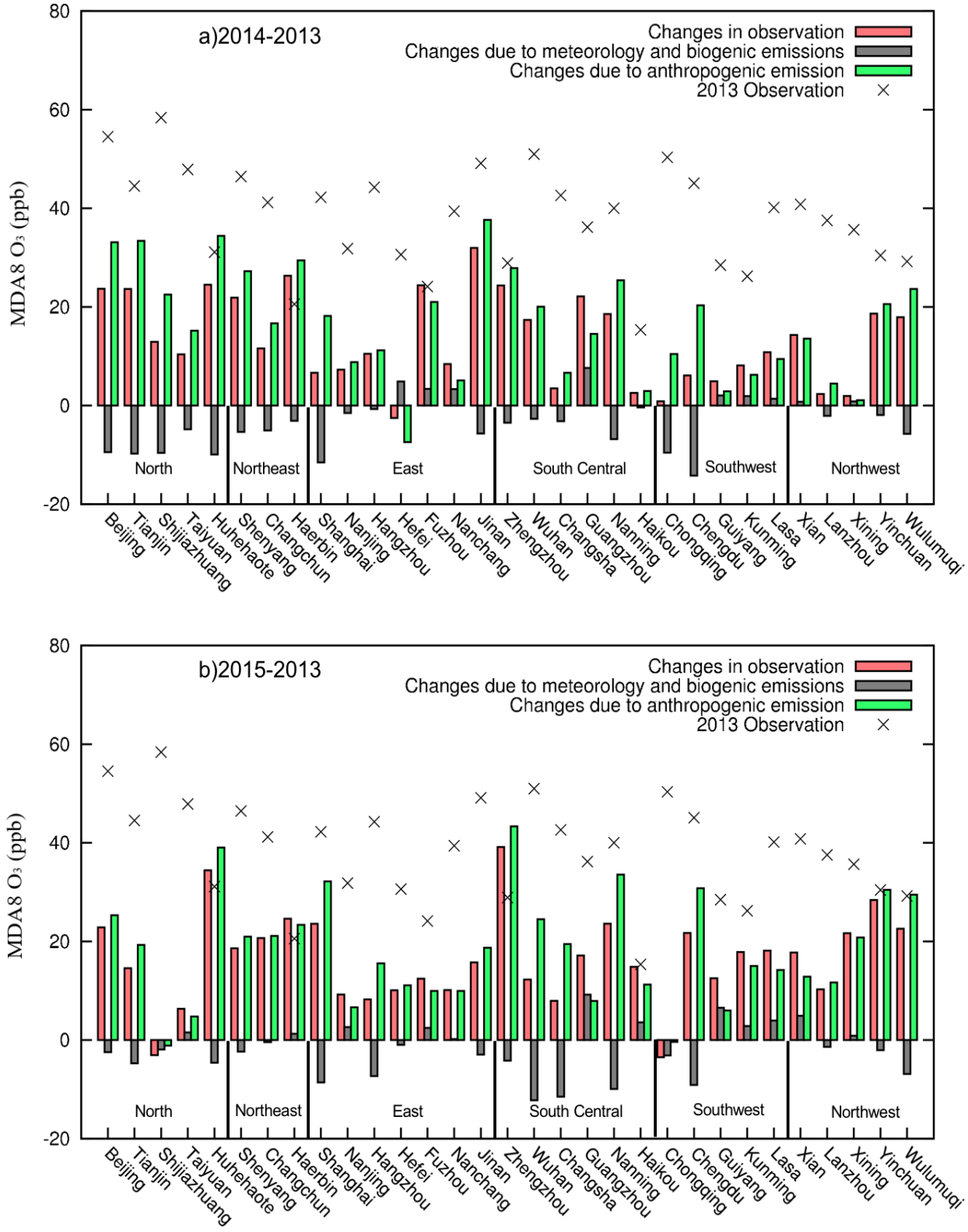

Figure 8. Changes in MDA8 O_3 concentrations in the provincial capital cities in summer months (June, July, and August) in 2014 and 2015 compared to 2013 due to changes in meteorology + biogenic emissions and anthropogenic emissions.

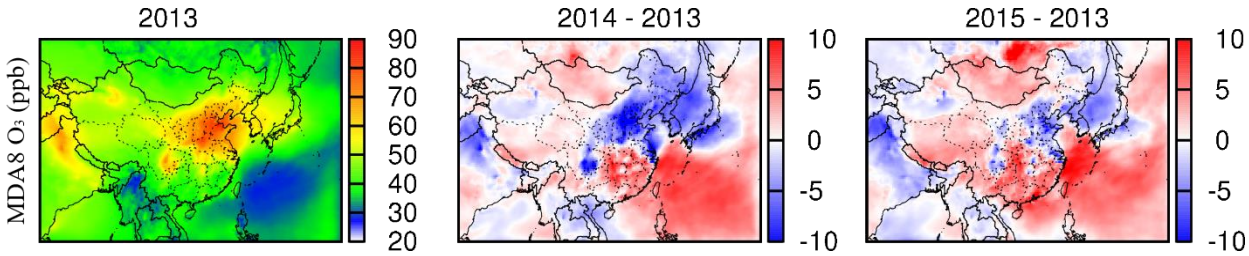

Figure 9. Predicted summer MDA8 O_3 in 2013 and the changes due to meteorology in 2014 and 2015.

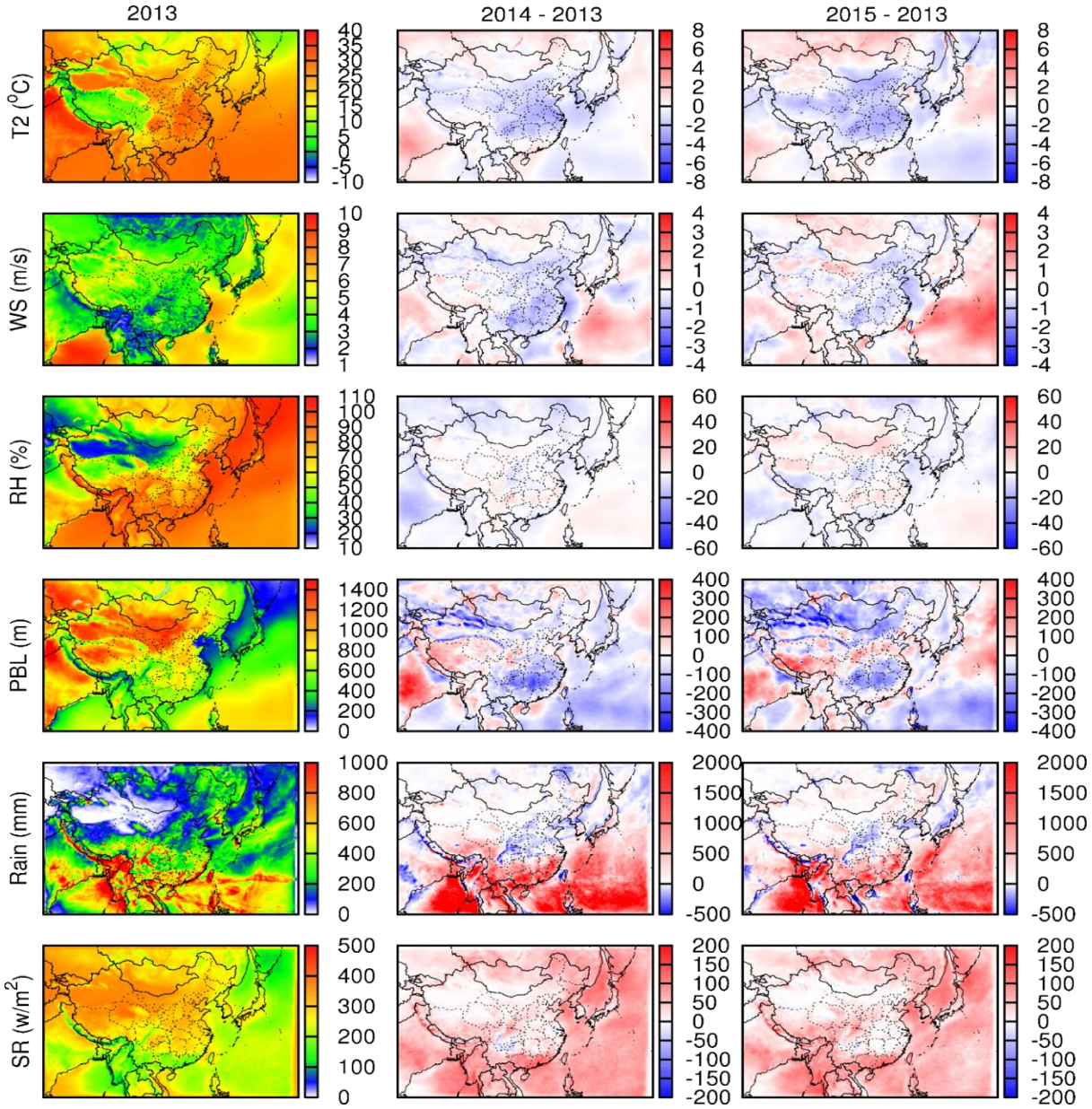

Figure 10. Averaged meteorological parameters in summer 2013 and the differences from 2014 and 2015 to 2013. T2 is temperature at 2 meters above ground, WS is wind speed, RH is relative humidity, PBL is planetary boundary layer height, and SR is the shortwave radiation at surface.

The increase of O_3 with reduced anthropogenic emissions can be explained by two reasons. First, $PM_{2.5}$ is the focus of pollution control in China and current emission control measures are all PM-related, i.e. reducing primary PM, SO_2, and NO_x, while control of VOCs is not targeted seriously. The decrease of $PM_{2.5}$ concentrations reduced the scattering and absorption of sunlight, increased UV radiation, and led to higher MDA8 O_3 [116]. The other reason is reducing NO_x reduces the O_3 titration in urban areas, where O_3 formation is VOC-limited, thus leads to higher O_3 concentrations. There is a O_3 isopleth figure at five of the 31 cities in summer episodes in 2013 from a previous study [117]. The x-axis shows the ratio of input VOC emissions, y-axis shows ratio of input NOx emissions, and unit of O_3 on contour line is ppb. It shows that under the conditions in summer 2013, O_3 concentrations in different areas in China were controlled by different factors. In northern city Beijing, O_3 in more likely controlled by NO_x, however, reducing NO_x only by 40% only leads to less than 10, 4, and 4 ppb in June, July and August, respectively. In eastern and southern cities Shanghai and Guangzhou, reducing NO_x leads to an increase of O_3. In Northwest and Southwest cities Xi'an and Chongqing, reducing NO_x by 40% leads to a small amount of O_3 decrease. Since it is not clear about the changes in the emissions of NO_x and VOCs, as well as the changes of VOCs speciation from 2013 to 2014 and 2015, fully explaining the increase of O_3 is impossible. However, this phenomenon indicates the importance of studying O_3 when controlling $PM_{2.5}$.

2.4 Conclusion

In summary, the changes of $PM_{2.5}$ and O_3 concentrations due to meteorology and emission control from the base year (2013) to 2014 and 2015 were analyzed based on ambient measurements and simulations with CMAQ. It is found that emission controls in 2014 and 2015 were effective, but they were counteracted by unfavorable meteorology in some events. Compared with the base year, the decrease of annual averaged $PM_{2.5}$ in all cities due to emission control were 23.9 $\mu g/m^3$ and

43.5 μg/m^3 in the year 2014 and 2015, respectively. The contributions of meteorology and biogenic emission to the increase of annual averaged $PM_{2.5}$ were 11.5 μg/m^3 and 24.6 μg/m^3 the two years. Especially, meteorology conditions caused severe air pollution events in December 2015 with increasing $PM_{2.5}$ concentrations due to meteorology of up to 88.7 μg/m^3 in Beijing. In contrast, reducing primary PM and gaseous PM precursors led to increasing of O_3 concentrations, especially in the summer. Averagely, 16.7 and 18.3 ppb increases were caused by emission reduction in all the 31 capital cities in 2014 and 2015 compared with the base year (2013). This could be caused by the increase of photolysis rate after PM emission was reduced and change of the relative abundance of NOx and VOCs when NO_x and VOCs emissions were changed. This study emphasizes the importance of considering meteorology and O_3 formation in controlling $PM_{2.5}$.

CHAPTER 3. MODELING $PM_{2.5}$ AND O_3 WITH AEROSOL FEEDBACKS USING WRF/CHEM OVER THE SICHUAN BASIN, SOUTHWESTERN CHINA

3.1 Introduction

$PM_{2.5}$ and O_3 are two major pollutants for air pollution, having adverse effects to crop harvest, human health, and climate [1-4, 17-21]. $PM_{2.5}$ is a mixture of primary components including heavy metals, OC, EC and secondary components including SO_4^{2-}, NO_3^-, NH_4^+, and SOA [5-7]. $PM_{2.5}$ pollution has been proved to be accompanied with an increase in mortality due to respiration and cardiovascular diseases [9-13]. $PM_{2.5}$-related illnesses could cause extra hospital visits and loss of work time, leading to economic impact [14-16]. As the fourth and seventh leading risk factors for premature mortality globally, indoor and outdoor PM pollution was expected to have caused over 3.5 and 3.2 million global premature deaths in 2010, respectively [118]. Asian areas shared 80% of those global premature deaths [119]. Besides stratospheric-tropospheric exchange, O_3 in the troposphere is predominantly generated by photochemical reactions of NOx and VOCs [22-25]. Due to high oxidization, elevated O_3 is harmful to human health by irritating skin, eyes, respiratory tract, and aggravate asthma and bronchial inflammation [120]. Chronic O_3 exposure can also lead to impaired photosynthesis and altered gene expression, which results in cell death and crop yield losses [27, 28]. One hundred ten million tons of crop losses on wheat, soybean, and maize in 2010 were due to O_3 globally and Asia had a share of 35% [119].

Concentrations of air pollutants rely on two key factors of emissions and meteorology. After being emitted to the atmosphere, pollutants go through chemical and physical processes including

This chapter was previously published as: Wang, Pengfei, Xue Qiao, and Hongliang Zhang. "Modeling $PM_{2.5}$ and O_3 with aerosol feedbacks using WRF/Chem over the Sichuan Basin, southwestern China." Chemosphere (2020): 126735.

transport, chemical transformation, and deposition, which are highly affected by meteorology [7, 121, 122]. Besides, aerosols also impact meteorology by directly changing incoming and outcoming solar radiation and indirectly acting as CCN [48, 49, 123, 124]. Aerosols could increase the number of cloud droplets and scattering areas or enlarge the cloud lifetime and therefore enhance cloud albedo. The changes in meteorology will then affect air pollution formation, resulting in complex interactions between meteorology and pollutants, which are not fully understood.

Being heavily polluted over the past decades, many air quality studies have been done in China, but most focused on more developed cities such as Beijing, Shanghai and Guangzhou [67, 125, 126]. With an area of 0.22 million km^2 and a population of 108.1 million in 2015, the SCB in Southwestern China is severely affected by air pollution owing to its high anthropogenic emissions and the basin landform [127-130]. It is also one of the most cloudy areas, indicating a possible strong interaction between meteorology and air pollutants [130-134]. Considering aerosol radiation feedback would improve the simulation accuracy for the understanding formation and sources of air pollutants. Many studies have investigated aerosol radiation effect over global domains [135-140]. However, to the best of our knowledge, no such studies have been done for the SCB.

Therefore, WRF/Chem, V3.7.1 was applied in this study to simulate $PM_{2.5}$ and O_3 and understand the effects of aerosol radiation feedbacks for the SCB in January and July 2015. It is hypothesized that considering aerosol radiation feedbacks is important in understanding air pollution formation in the SCB.

3.2 Methods

3.2.1 Model description and application

WRF/Chem is a version of WRF being coupled online with a chemistry module so that meteorological and chemical components are predicted simultaneously. It is capable of simulating aerosol radiative feedbacks on atmospheric processes [141, 142]. In this study, the WRF/Chem V3.7.1 is implemented over the SCB with nested domains. The 36km domain covers entire China and surrounding countries in East Asia area, while the nested 12-km domain covers the 18 cities in the SCB and adjacent areas. The initial and boundary conditions for WRF were provided using the NCEP FNL datasets with 6 hours temporal resolution and 1° × 1° spatial resolution. The mozbc developed by National Center for Atmospheric Research/Atmospheric Chemistry Observations & Modeling (NCAR/ACOM) was used to modify wrfbdy_d0x to get chemical boundary condition files [143]. The simulation periods were January and July in 2015 to represent wintertime and summertime and each run covered 31 days with 3 days spin-up. In Sichuan Basin, $PM_{2.5}$ peak values usually appear in January while O_3 peak values show in July [144-147]. The RADM2 (Regional Acid Deposition Model, 2nd generation) gas-phase chemical mechanism and the Modal Aerosol Dynamics Model for Europe (MADE) with the secondary organic aerosol model (SORGAM) were used[141]. Physical options included NOAH land surface model [148], YSU boundary layer physics [149], RRTM longwave and Goddard shortwave radiation schemes [150, 151], and Grell 3D ensemble cumulus parameterization with shallow convection and radiative feedback [152]. The configuration of WRF/Chem is described in Table 6.

Table 6. The configuration of WRF/Chem.

Process	WRF/Chem
Long-wave radiation	RRTM
Short-wave radiation	Goddard
Land-surface model	Noah
Boundary layer scheme	YSU
Photolysis scheme	Fast-J
Gas-phase mechanism	RADM2
Aerosol model	MADE/SORGAM

To investigate the effect of aerosol radiation feedbacks on meteorology and air quality, two simulation scenarios were performed and compared. The first one is the baseline scenario without feedbacks (WOF). The other scenario (WF) contains aerosol direct radiation effects. Other than the difference in aerosol radiation feedback effects, the two scenarios were identical in emission inputs and model setup, and the difference between them (WF-WOF) represents the influence of aerosol radiation direct effects.

3.2.2 Emission Inventory

The anthropogenic emissions were generated based on the Emission Database for Global Atmospheric Research (EDGAR) v4.3 (http://edgar.jrc.ec.europa.eu/overview.php?v=432_AP), including precursors of $PM_{2.5}$ and O_3 (NOx, carbon monoxide, ammonia, and sulfur dioxide and VOCs), as well as primary PM components. The sectorial EDGAR inventories were categorized into six source categories: agriculture, industries, energy, residential activities, off-road and on-road transport. The monthly emissions were processed to hourly level depended on weekly and diurnal emission profiles specific to sources allocation profiles as mentioned in [7, 153]. The weekly profiles are obtained from European Monitoring and Evaluation Programme (EMEP) emission inventory (https://www.emep.int/) and the final report WRAP (Western Regional Air Partnership) mobile source emission inventory update [154-156]. According to EMEP, the weekdays emissions are

higher than weekends by 25% for power plants and 35% for residential and industry. By analyzing the data of vehicle class, state, and roadway type from EPA with the vehicle activity database from Federal Highway Administration, the weekly and diurnal profiles for transport were developed [156]. The diurnal profiles of NH_3 are modified base on the profiles of fertilizer in Chinkin et al. [157]. The profiles of other four categories are calculated rely on the profiles developed by Olivier et al. [158]. The specific values were modified slightly to reflect the differences in different inventories based on communications with inventory experts. Tables 7 and 8 show the final weekly and diurnal profiles used in this study. The emissions from biomass burning were based on the Fire Inventory from the National Center for Atmospheric Research (NCAR) (FINN) [159].

3.2.3 Model validation

The model performance was validated by comparing meteorological observations and air pollutant concentrations with simulation results. Meteorological observations were obtained from the National Climate Data Center (NCDC), including WS and WD at 10 meters above the ground level (AGL) and T2 and RH at 2 meters AGL. Hourly $PM_{2.5}$ and O_3 concentrations at monitoring sites were downloaded from the China National Environmental Monitoring Center (https://www.aqistudy.cn). There are 1434 and 101 meteorological stations in the 36km and 12km domains, respectively and there are 94 National Air Quality Station (NAQS) in total within the SCB (Figure 11).

Table 7. Weekly profiles for five emission categories.

	Monday	Tuesday	Wednesday	Thursday	Friday	Saturday	Sunday
Power	0.125	0.125	0.125	0.125	0.125	0.188	0.187
Industry	0.135	0.135	0.135	0.135	0.135	0.163	0.162
Residential	0.135	0.135	0.135	0.135	0.135	0.163	0.162
Transport	0.155	0.155	0.155	0.155	0.155	0.117	0.108
Agriculture	0.143	0.143	0.143	0.143	0.143	0.143	0.142

Table 8. Diurnal profiles for five emission categories.

Power	0.0333	0.0313	0.0313	0.03	0.0313	0.0346	0:00 - 6:00
	0.0388	0.0446	0.0488	0.0509	0.0488	0.0488	6:00 - 12:00
	0.0484	0.0479	0.0479	0.0471	0.0459	0.0448	12:00 - 18:00
	0.0438	0.0427	0.0425	0.0417	0.0396	0.0354	18:00 - 24:00
Industry	0.0311	0.0311	0.0318	0.0348	0.0373	0.0394	0:00 - 6:00
	0.0423	0.0456	0.0476	0.0505	0.0539	0.0547	6:00 - 12:00
	0.0518	0.0522	0.0526	0.0489	0.0447	0.0423	12:00 - 18:00
	0.0394	0.0365	0.0352	0.0331	0.0323	0.0311	18:00 - 24:00
Residential	0.0148	0.0148	0.0148	0.0148	0.0148	0.0203	0:00 - 6:00
	0.0507	0.0634	0.0659	0.0655	0.0558	0.0486	6:00 - 12:00
	0.0452	0.0444	0.0423	0.0402	0.0423	0.0465	12:00 - 18:00
	0.0592	0.0634	0.0575	0.0571	0.0423	0.0156	18:00 - 24:00
Transportation	0.0083	0.0042	0.0021	0.0021	0.0038	0.01	0:00 - 6:00
	0.0363	0.0767	0.0771	0.0584	0.0517	0.05	6:00 - 12:00
	0.0542	0.0596	0.0604	0.0663	0.0855	0.0863	12:00 - 18:00
	0.0625	0.0438	0.0313	0.0258	0.025	0.0188	18:00 - 24:00
NH_3	0.0201	0.0201	0.0201	0.0201	0.0201	0.0201	0:00 - 6:00
	0.0281	0.0411	0.0702	0.0822	0.0732	0.0822	6:00 - 12:00
	0.0863	0.0802	0.0602	0.0411	0.0411	0.0281	12:00 - 18:00
	0.0291	0.0291	0.0291	0.0291	0.0291	0.0201	18:00 - 24:00

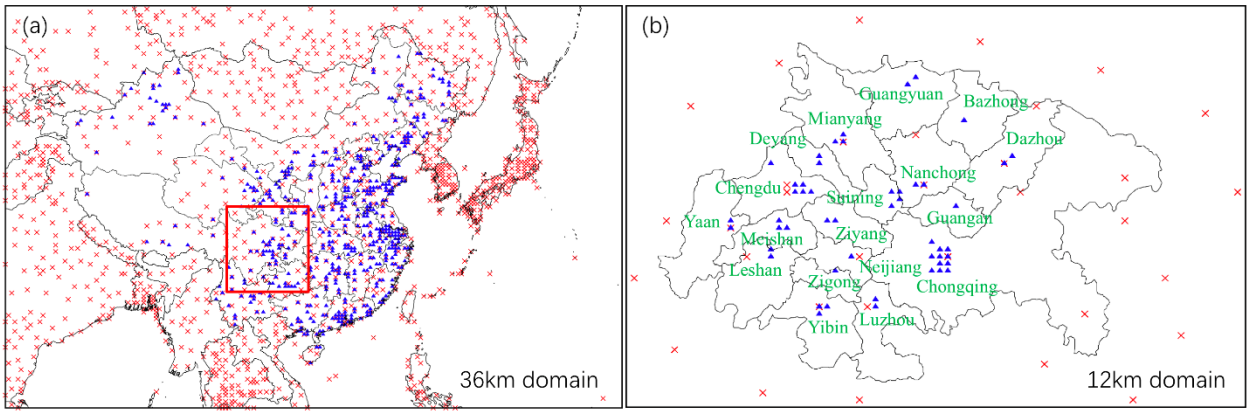

Figure 11. (a) Locations of domains and meteorological stations (red cross X) (b) Locations of national air quality stations (blue triangle △) in the SCB.

3.3 Results and discussions

3.3.1 Model validation

3.3.1.1 Meteorology

The WRF model performance was validated for January and July of 2015 over the SCB. The MB, RMSE, and GE were used to compare observations and simulations. Details and comparison with benchmarks suggested by Emery et al. [107] are shown in Table 9. T2 was under-predicted in both January and July since MBs values are negative (-1.0 K and -0.8 K, respectively). While WS was over-predicted in the two months, as MBs are 1.1 m/s in January and 0.6 m/s in July. Although prediction was not in the same pattern for WD (over-predicted in January and under-predicted in July), MBs of WD was within the benchmark in both months. The statistics were further compared with relevant benchmarks. For T2, both MB and GE were exceeding benchmarks by 20% to 50%. MB of WD was within the benchmark while GE was exceeding benchmarks by 100% in both months. GE of WS achieved the benchmark values while MB was larger than benchmarks by at least 20%. RMSE of WS is exceeding the benchmark in January by 15%. It should be mentioned that exceeding the benchmark value does not mean failure of the simulation because the benchmark value was based on MM5 simulations for the eastern United States with horizontal grid resolutions of 12km and 4 km. The WRF model predictions were generally reliable since the model performance statistics are similar to other studies applying WRF over China [105, 134, 160].

Table 9. Meteorology performance of January and July in 2015. OBS means observation, PRE means prediction, MB means bias, GE is gross error, and RMSE is root mean square error. The benchmarks are suggested by Emery et al. [107]. Values exceeded the benchmark are represented in bold.

		Jan	Jul	Benchmark
T2(K)	OBS	277.6	294.8	
	PRE	276.6	294.0	
	MB	**-1.0**	**-0.8**	≤±0.5
	GE	**3.0**	**2.4**	≤2.0
	RMSE	4.0	3.2	
WS(m/s)	OBS	3.0	2.8	
	PRE	4.2	3.4	
	MB	**1.1**	**0.6**	≤±0.5
	GE	1.8	1.4	≤2.0
	RMSE	**2.3**	1.8	≤2.0
WD(°)	OBS	172.4	161.5	
	PRE	170.8	151.6	
	MB	6.4	-0.5	≤±10
	GE	**56.6**	**63.2**	≤±30
	RMSE	73.5	80.1	
RH(%)	OBS	75.9	69.4	
	PRE	71.2	73.6	
	MB	-4.7	4.2	
	GE	14.2	11.9	
	RMSE	18.2	15.1	

3.3.1.2 $PM_{2.5}$ and O_3

The model performance on $PM_{2.5}$ and MDA8 O_3 were assessed by using mean observations, mean predictions, MFB, MFE, MNB and MNE, as shown in Table 10 and 11. $PM_{2.5}$ were within criteria (≤ ±0.6 for MFB and ≤ 0.75 for MNB) for all the cities both in January and July. The model simulations also well captured the day-to-day variations and peaks of $PM_{2.5}$ in most SCB cities in January (Figure 12). In July, the $PM_{2.5}$ simulation missed several peaks at the beginning of the month but captures most of the other peaks (Figure 13). In terms of O_3, MNB and MNE in all the cities were much larger than their criteria (≤ ±0.15 and ≤ 0.3, respectively) in January (Table 10). Although the partial reason is too many data points were lower than the cutoff concentration due to low O_3 concentrations in winter, uncertainties in emission and photochemical should be noted.

However, the relatively low MNB/MNE and MFB/MFE in almost every month indicated that MDA8 O_3 was well captured. Figure 14 indicates that MDA8 O_3 was well predicted by the trend, but some absolute values were missed in January. As shown in Table 11, more than 50% of the cities' MNB in July were within criteria and the amount for MNE was more than 67% when feedback exists. When there was no feedback, the model simulation in July was quite well in other cities. except for some slight large underprediction in Chengdu, Guangyuan, Guangan, Meishan, Neijiang and Ziyang and some overprediction in Nanchong and Ya'an. The averaged MDA8 O_3 was 50–70 ppb basin wide with no big daily oscillations in all cities in July (Figure 15). The model performance is acceptable for $PM_{2.5}$ in January and MDA8 O_3 in July.

3.3.2 Seasonal and spatial variations

$PM_{2.5}$ concentrations in the basin have significant seasonal variations (Figure 16 and 17). Simulated $PM_{2.5}$ concentrations were significantly higher in January (basin-wide average: 100 $\mu g/m^3$) than in July (basin-wide average: 40 $\mu g/m^3$) and exceeded the WHO guidelines. The $PM_{2.5}$ components showed different fractional contribution in summer and winter, while SO_4^{2-} was the top contributor in both months (Figure 16 and 17). SO_4^{2-}, primary organic aerosol (POA) and NO_3^- were the top contributors in January, which account for ~30%, ~13% and ~15% of the total $PM_{2.5.}$ In July, SO_4^{2-}, $NH^{4+,}$ and NO_3^- shared over half of the total $PM_{2.5}$ almost equally. Higher emission and unfavorable meteorology were two main results that lead to seasonal variation. More air pollutant was usually emitted during winter than summer within the basin [127]. What's worse, meteorology conditions such as lower WS and lower precipitation were usually unfavorable for the process of transformation and transport of $PM_{2.5}$ in the SCB area in both seasons [129, 161]. From Figure 18, the WS was less than 1-3 m/s basin-wide both in January and July, and the monthly precipitation was less than 1mm on average.

Table 10. Model performance on MDA8 O_3 and $PM_{2.5}$ in January 2015 with or without feedback. OBS is mean observation, PRE is mean prediction, MFB is mean fractional bias, MFE is mean fractional error, MNB is mean normalized bias, and MNE is mean normalized error. The performance criteria for $PM_{2.5}$ are suggested by EPA [108], and the performance criteria for O_3 are suggested by EPA [109]. Values exceeded the criteria are represented in bold.

MDA8 O_3 (ppb)	**WF (January)**						**WOF (January)**					
	OBS	PRE	MFB	MFE	MNB	MNE	OBS	PRE	MFB	MFE	MNB	MNE
Chengdu	17.09	40.21	0.85	0.86	**2.14**	**2.15**	17.09	40.98	0.87	0.88	**2.22**	**2.24**
Chongqing	11.79	36.48	1.08	1.08	**3.37**	**3.37**	11.79	37.06	1.09	1.09	**3.47**	**3.47**
Guangyuan	29.55	41.31	0.35	0.40	**0.61**	**0.66**	29.55	41.74	0.36	0.41	**0.64**	**0.69**
Mianyang	18.90	39.64	0.76	0.76	**2.04**	**2.04**	18.90	39.95	0.76	0.76	**2.10**	**2.10**
Nanchong	11.99	39.42	1.05	1.05	**2.34**	**2.34**	11.99	39.88	1.06	1.06	**2.38**	**2.38**
Bazhong	17.87	40.95	0.81	0.81	**1.75**	**1.75**	17.87	41.37	0.82	0.82	**1.79**	**1.79**
Deyang	25.15	39.35	0.54	0.65	**1.08**	**1.17**	25.15	40.08	0.55	0.66	**1.13**	**1.22**
Guangan	27.15	39.61	0.40	0.44	**0.63**	**0.66**	27.15	39.77	0.41	0.43	**0.64**	**0.66**
Leshan	16.80	43.98	0.94	0.94	**2.46**	**2.46**	16.80	44.22	0.94	0.94	**2.48**	**2.48**
Luzhou	18.85	39.02	0.81	0.81	**2.91**	**2.91**	18.85	39.40	0.82	0.82	**2.89**	**2.89**
Meishan	20.32	39.90	0.71	0.72	**1.64**	**1.65**	20.32	41.19	0.73	0.74	**1.74**	**1.75**
Neijiang	25.01	40.32	0.55	0.58	**1.09**	**1.12**	25.01	41.06	0.56	0.59	**1.12**	**1.14**
Suining	22.17	40.69	0.61	0.61	**1.01**	**1.01**	22.17	41.13	0.62	0.62	**1.04**	**1.04**
Yibin	21.31	41.79	0.70	0.70	**1.38**	**1.38**	21.31	42.63	0.72	0.72	**1.41**	**1.41**
Zigong	27.15	40.21	0.39	0.42	**0.54**	**0.56**	27.15	41.07	0.41	0.43	**0.57**	**0.59**
Ziyang	32.32	41.34	0.28	0.34	**0.42**	**0.47**	32.32	42.36	0.30	0.36	**0.45**	**0.50**
Ya'an	15.43	50.00	1.06	1.06	**2.47**	**2.47**	15.43	49.72	1.05	1.05	**2.45**	**2.45**
Dazhou	16.81	40.51	0.82	0.82	**1.49**	**1.49**	16.81	40.36	0.82	0.82	**1.48**	**1.48**
Criteria					$\leq \pm 0.15$	≤ 0.3					$\leq \pm 0.15$	≤ 0.3
$PM_{2.5}$ ($\mu g/m^3$)	**WF (January)**						**WOF (January)**					
	OBS	PRE	MFB	MFE	MNB	MNE	OBS	PRE	MFB	MFE	MNB	MNE
Chengdu	125.28	109.85	-0.06	0.46	0.11	0.51	125.28	106.21	-0.09	0.45	0.08	0.49
Chongqing	117.51	125.87	0.11	0.40	0.34	0.59	117.51	115.39	0.04	0.42	0.25	0.57
Guangyuan	36.83	61.23	0.50	0.59	1.12	1.20	36.83	61.77	0.51	0.59	1.14	1.21
Mianyang	78.89	92.90	0.17	0.53	0.51	0.77	78.89	89.46	0.15	0.52	0.46	0.74
Nanchong	106.95	105.75	0.01	0.45	0.20	0.55	106.95	99.38	-0.05	0.47	0.14	0.55
Bazhong	76.67	67.05	-0.09	0.42	0.05	0.44	76.67	65.99	-0.10	0.41	0.03	0.43
Deyang	102.80	105.35	0.07	0.52	0.34	0.66	102.80	101.24	0.04	0.50	0.30	0.63
Guangan	107.45	106.03	0.04	0.59	0.45	0.88	107.45	100.55	-0.01	0.60	0.38	0.85
Leshan	107.50	102.39	0.01	0.41	0.17	0.48	107.50	101.80	0.01	0.42	0.17	0.50
Luzhou	124.72	125.81	0.08	0.44	0.31	0.61	124.72	113.79	0.00	0.47	0.20	0.59
Meishan	114.28	116.18	0.06	0.42	0.25	0.53	114.28	113.90	0.05	0.43	0.23	0.53
Neijiang	126.31	115.93	-0.04	0.49	0.18	0.60	126.31	106.62	-0.11	0.52	0.10	0.60
Suining	90.56	100.13	0.13	0.51	0.57	0.87	90.56	93.98	0.08	0.51	0.49	0.83
Yibin	114.99	105.45	0.01	0.45	0.24	0.59	114.99	102.95	-0.02	0.45	0.21	0.58
Zigong	143.05	125.60	-0.06	0.50	0.16	0.59	143.05	115.89	-0.13	0.53	0.08	0.59
Ziyang	84.62	105.66	0.26	0.53	0.85	1.06	84.62	101.55	0.23	0.51	0.78	1.00
Ya'an	70.37	85.88	0.20	0.35	0.34	0.46	70.37	84.71	0.19	0.33	0.32	0.44
Dazhou	129.72	71.74	-0.50	0.68	0.27	0.56	129.72	69.60	-0.52	0.70	-0.29	0.57
Criteria			$\leq \pm 0.6$	≤ 0.75					$\leq \pm 0.6$	≤ 0.75		

Table 11. Model performance on MDA8 O_3 and $PM_{2.5}$ in July 2015 with or without feedback. OBS is mean observation, PRE is mean prediction, MFB is mean fractional bias, MFE is mean fractional error, MNB is mean normalized bias, and MNE is mean normalized error. The performance criteria for $PM_{2.5}$ are suggested by EPA [108], and the performance criteria for O_3 are suggested by EPA [109]. Values exceeded the criteria are represented in bold.

MDA8 O_3 (ppb)	**WF (July)**						**WOF (July)**					
	OBS	PRE	MFB	MFE	MNB	MNE	OBS	PRE	MFB	MFE	MNB	MNE
Chengdu	85.89	62.54	-0.27	0.38	**-0.19**	**0.35**	85.89	62.77	-0.27	0.38	**-0.18**	**0.36**
Chongqing	57.48	55.82	0.01	0.22	0.07	0.26	57.48	55.97	0.01	0.22	0.08	0.27
Guangyuan	69.46	53.62	-0.25	0.26	**-0.21**	0.22	69.46	53.57	-0.25	0.26	**-0.21**	0.23
Mianyang	68.07	54.81	-0.16	0.31	-0.02	**0.38**	68.07	54.70	-0.17	0.31	-0.01	**0.39**
Nanchong	56.27	58.42	0.09	0.31	**0.17**	**0.36**	56.27	57.54	0.08	0.32	**0.16**	**0.37**
Bazhong	62.70	51.97	-0.16	0.24	-0.13	0.22	62.70	51.80	-0.17	0.24	-0.13	0.23
Deyang	70.16	58.01	-0.15	0.26	-0.08	0.27	70.16	57.74	-0.16	0.27	-0.09	0.28
Guangan	86.23	55.41	-0.42	0.42	**-0.34**	**0.34**	86.23	54.97	-0.43	0.43	**-0.34**	**0.34**
Leshan	64.96	65.26	0.02	0.13	0.04	0.15	64.96	64.83	0.01	0.13	0.04	0.14
Luzhou	59.73	61.41	0.04	0.19	0.07	0.20	59.73	58.61	0.00	0.18	0.02	0.18
Meishan	78.57	62.14	-0.20	0.29	**-0.16**	0.27	78.57	61.84	-0.21	0.29	**-0.16**	0.27
Neijiang	77.28	60.94	-0.21	0.25	**-0.18**	0.21	77.28	59.95	-0.23	0.26	**-0.19**	0.23
Suining	53.73	58.11	0.10	0.23	**0.16**	0.28	53.73	57.75	0.10	0.22	0.15	0.27
Yibin	61.91	65.77	0.08	0.16	0.10	0.18	61.91	64.18	0.05	0.14	0.07	0.15
Zigong	62.92	61.71	-0.01	0.12	0.00	0.13	62.92	62.13	0.00	0.14	0.02	0.15
Ziyang	76.62	58.23	-0.26	0.28	**-0.21**	0.24	76.62	58.30	-0.26	0.28	**-0.21**	0.24
Ya'an	30.74	63.60	0.71	0.71	**1.17**	**1.17**	30.74	63.79	0.71	0.71	**1.18**	**1.18**
Dazhou	66.19	51.96	-0.20	0.31	-0.11	**0.32**	66.19	51.59	-0.20	0.32	-0.11	**0.33**
Criteria					$\leq \pm 0.15$	≤ 0.3					$\leq \pm 0.15$	≤ 0.3
$PM_{2.5}$ ($\mu g/m^3$)	**WF (July)**						**WOF (July)**					
	OBS	PRE	MFB	MFE	MNB	MNE	OBS	PRE	MFB	MFE	MNB	MNE
Chengdu	47.16	54.26	0.05	0.50	0.24	0.58	47.16	51.68	-0.01	0.48	0.18	0.54
Chongqing	49.94	49.57	-0.05	0.35	0.06	0.36	49.94	47.99	-0.08	0.33	0.03	0.36
Guangyuan	18.09	27.36	0.44	0.66	0.99	1.18	18.09	27.87	0.44	0.67	1.02	1.21
Mianyang	39.05	39.61	-0.01	0.50	0.14	0.52	39.05	39.01	-0.03	0.48	0.12	0.5
Nanchong	48.62	43.08	-0.17	0.48	-0.02	0.45	48.62	41.00	-0.21	0.48	-0.07	0.42
Bazhong	26.58	29.82	0.07	0.48	0.29	0.59	26.58	29.60	0.07	0.47	0.28	0.59
Deyang	39.73	50.10	0.14	0.58	0.41	0.73	39.73	47.69	0.10	0.55	0.33	0.66
Guangan	31.12	41.71	0.21	0.56	0.49	0.75	31.12	39.45	0.16	0.50	0.41	0.67
Leshan	35.61	45.53	0.11	0.53	0.36	0.68	35.61	44.50	0.09	0.50	0.33	0.64
Luzhou	39.16	53.10	0.23	0.52	0.53	0.76	39.16	49.72	0.18	0.47	0.43	0.66
Meishan	52.15	58.06	-0.04	0.52	0.18	0.57	52.15	54.33	-0.08	0.51	0.10	0.52
Neijiang	38.77	51.80	0.23	0.53	0.58	0.82	38.77	49.27	0.21	0.47	0.47	0.68
Suining	46.28	42.87	-0.11	0.54	0.10	0.57	46.28	40.44	-0.14	0.52	0.03	0.5
Yibin	38.04	47.97	0.15	0.48	0.35	0.61	38.04	45.41	0.11	0.45	0.28	0.54
Zigong	53.95	55.99	-0.02	0.42	0.13	0.47	53.95	55.50	-0.04	0.39	0.12	0.46
Ziyang	26.45	46.98	0.46	0.63	0.99	1.11	26.45	46.72	0.46	0.61	0.98	1.09
Ya'an	20.67	39.44	0.41	0.61	0.87	1.01	20.67	38.84	0.41	0.62	0.85	0.99
Dazhou	43.40	32.53	-0.32	0.51	-0.17	0.42	43.40	31.20	-0.36	0.51	-0.21	0.41
Criteria			$\leq \pm 0.6$	≤ 0.75					$\leq \pm 0.6$	≤ 0.75		

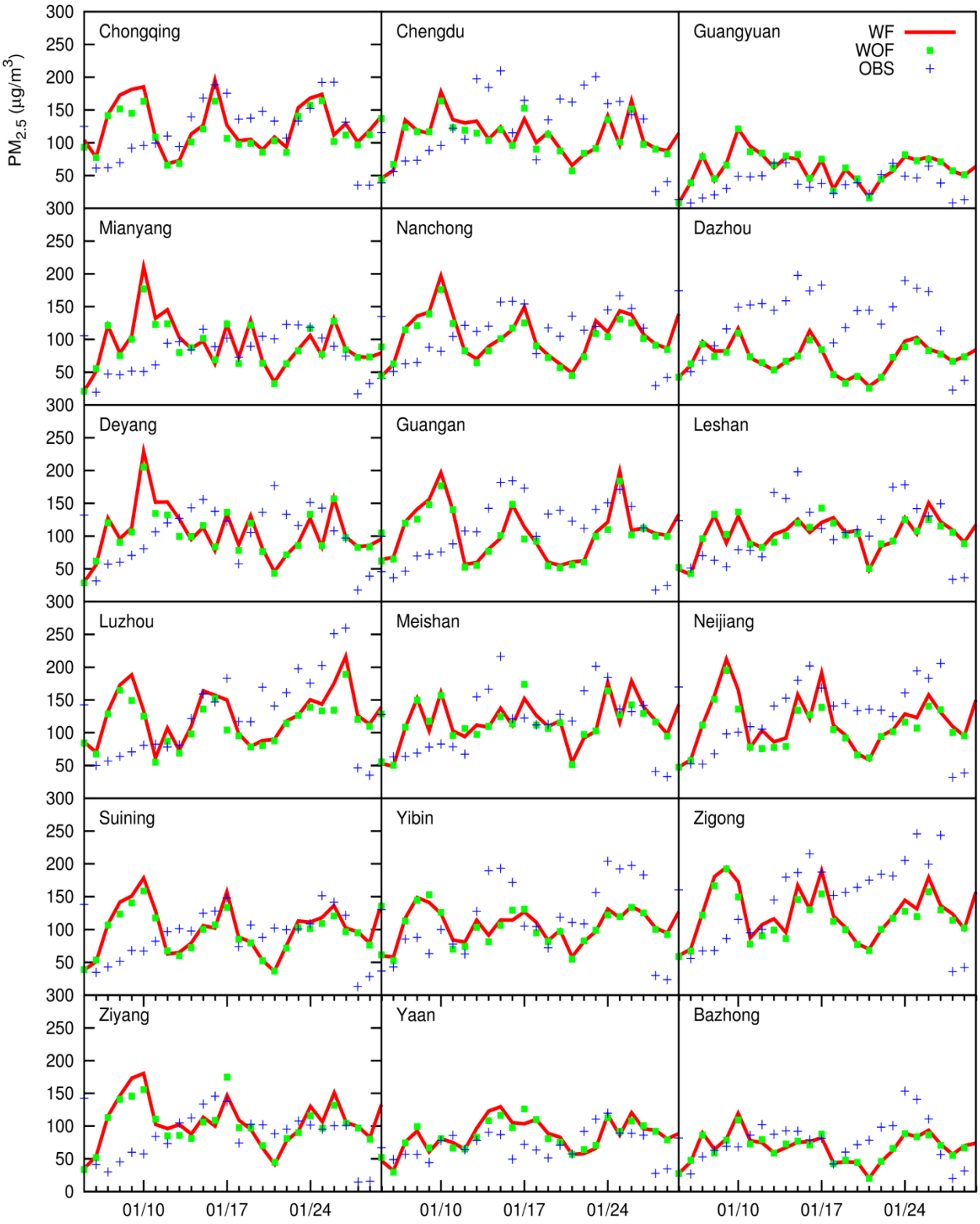

Figure 12. Predicted and observed daily $PM_{2.5}$ concentrations ($\mu g/m^3$) in the 18 cities of SCB in January. WF, WOF, and OBS indicated the $PM_{2.5}$ concentration of with feedback, without feedback and observations.

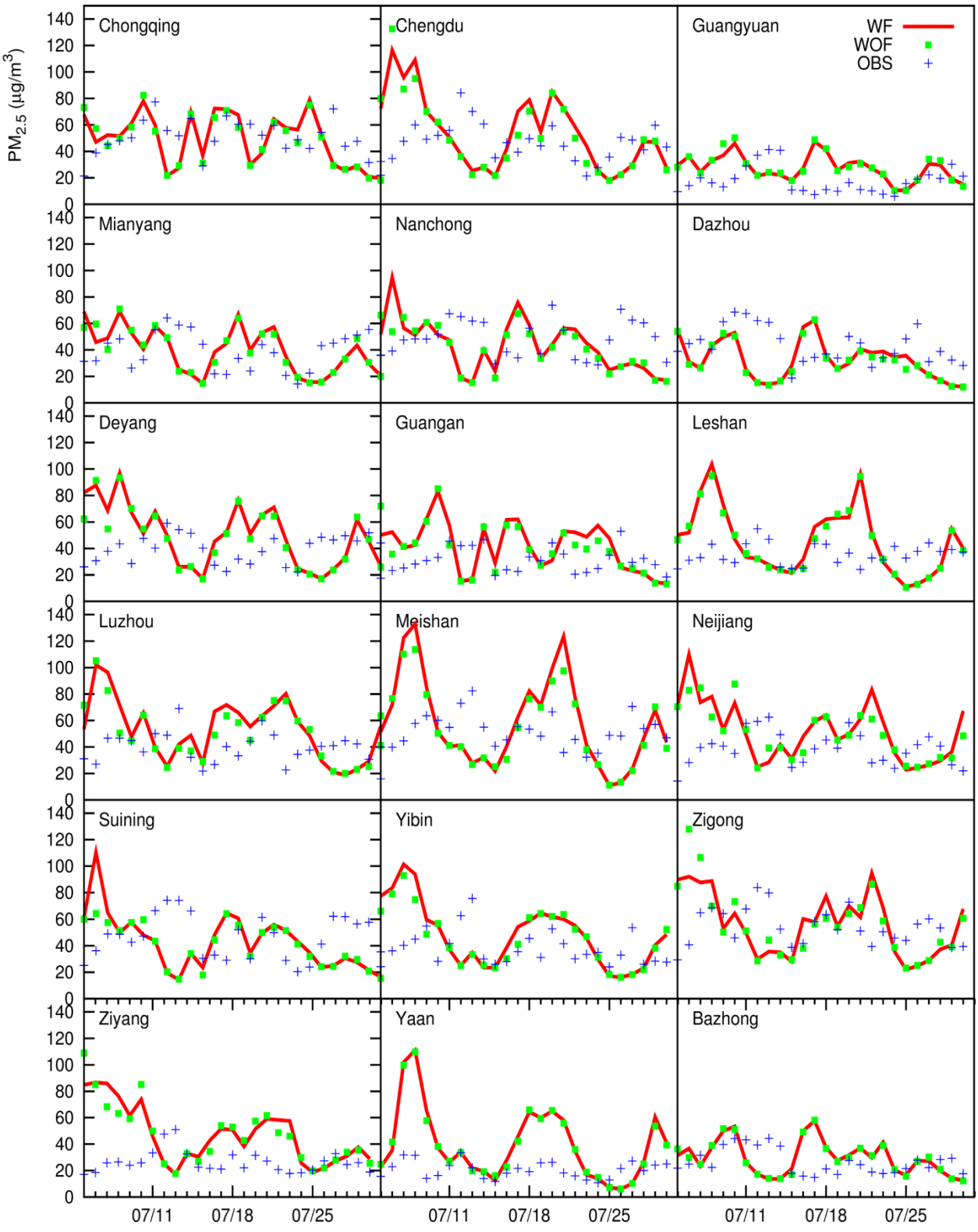

Figure 13. Predicted and observed daily $PM_{2.5}$ concentrations ($\mu g/m^3$) in the 18 cities of SCB in July. WF, WOF, and OBS indicated the $PM_{2.5}$ concentration of with feedback, without feedback and observations.

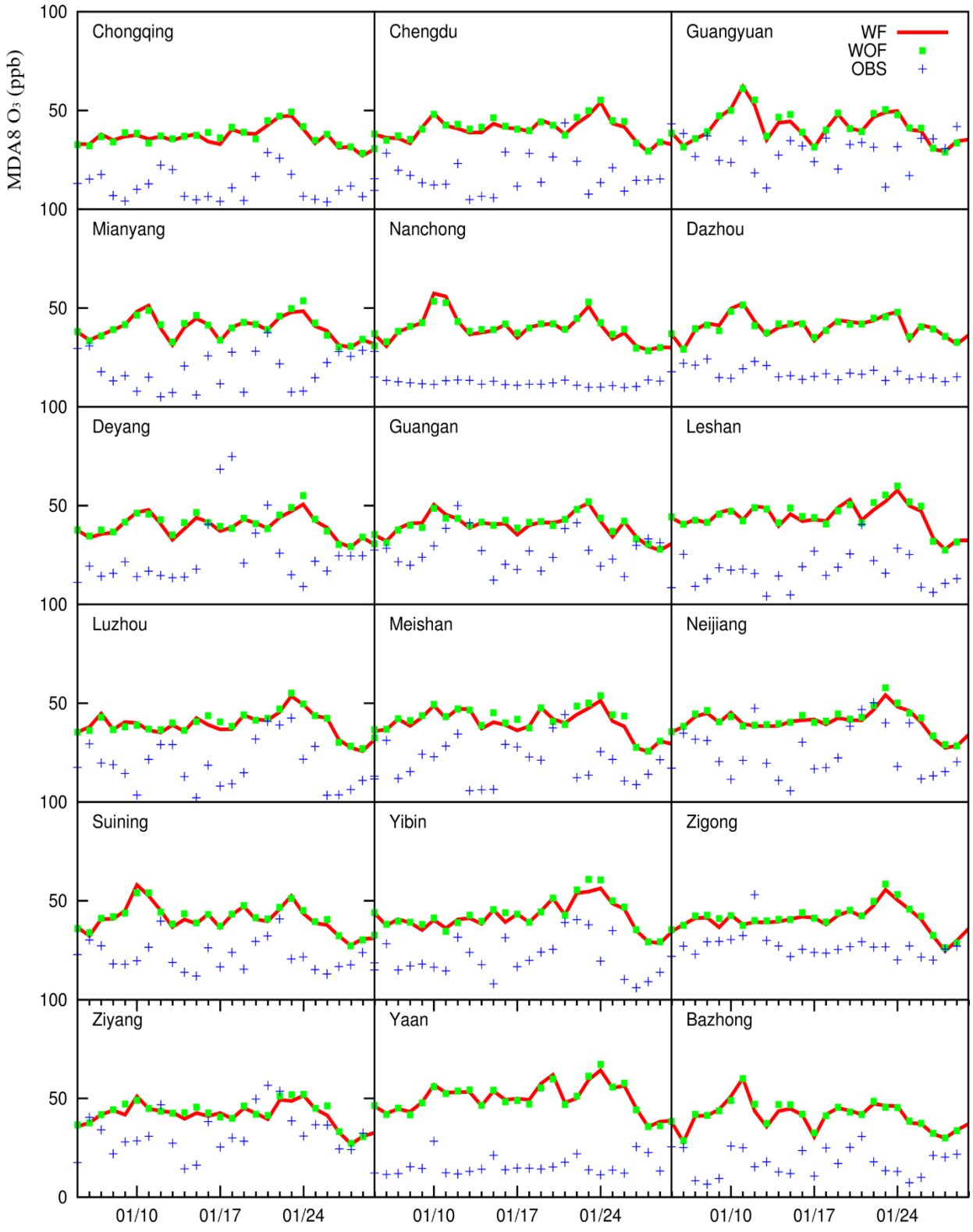

Figure 14. Predicted and observed MDA8 O_3 concentrations (ppb) in the 18 cities of SCB in January. WF, WOF, and OBS indicated the O_3 concentration of with feedback, without feedback and observations.

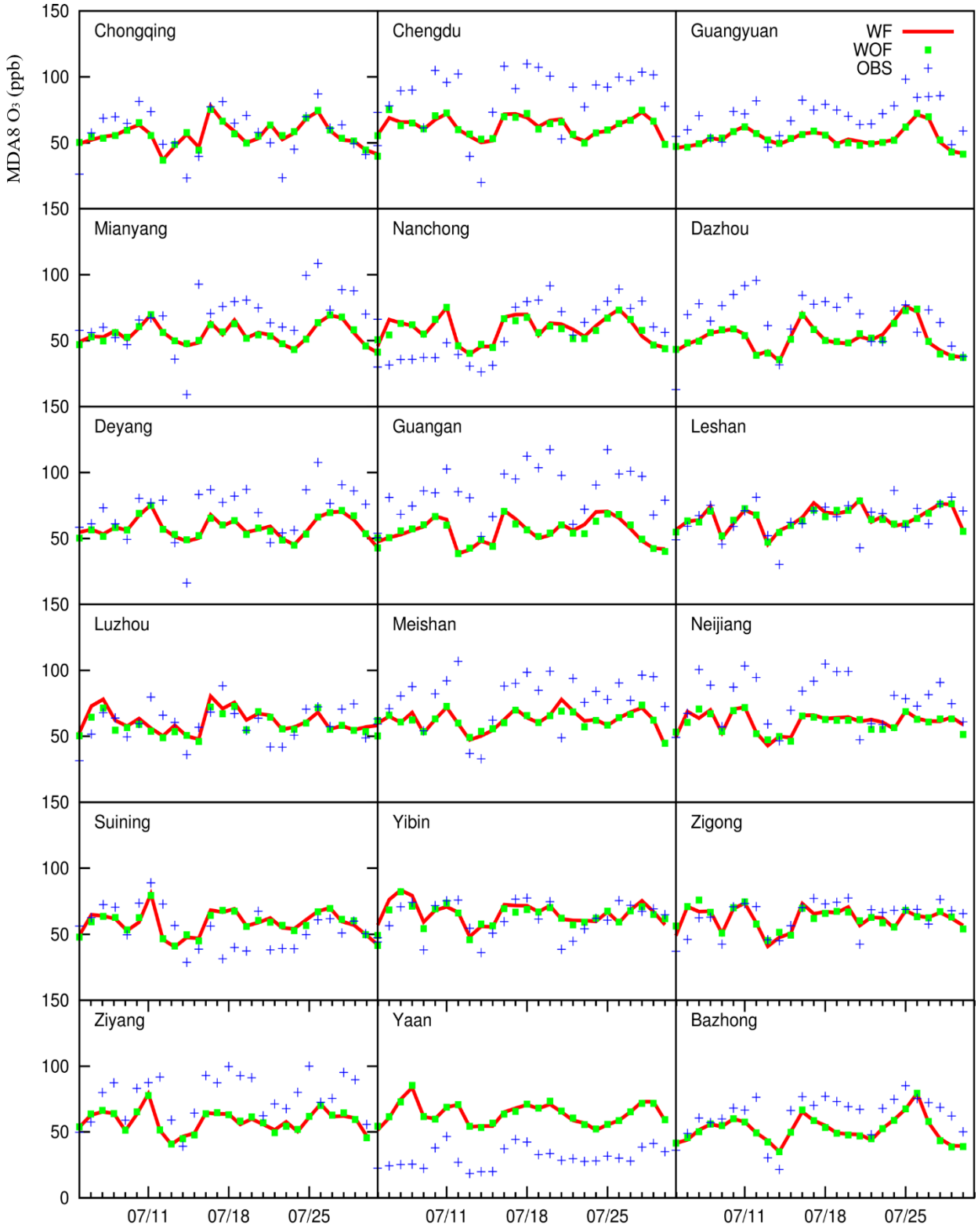

Figure 15. Predicted and observed MDA8 O_3 concentrations (ppb) in the 18 cities of SCB in July. WF, WOF, and OBS indicated the O_3 concentration of with feedback, without feedback and observations.

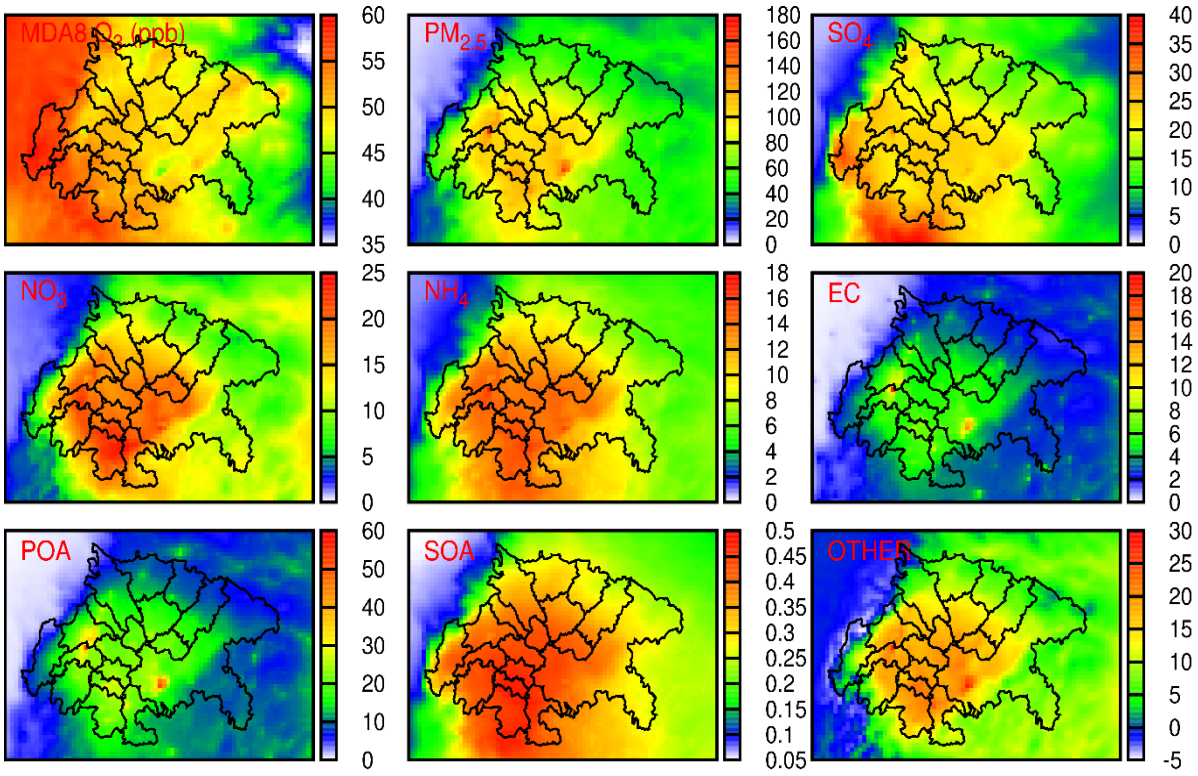

Figure 16. Predicted $PM_{2.5}$ ($\mu g/m^3$) with components and MDA8 O_3 concentrations (ppb) spatial distribution of SCB in January 2015 without feedback.

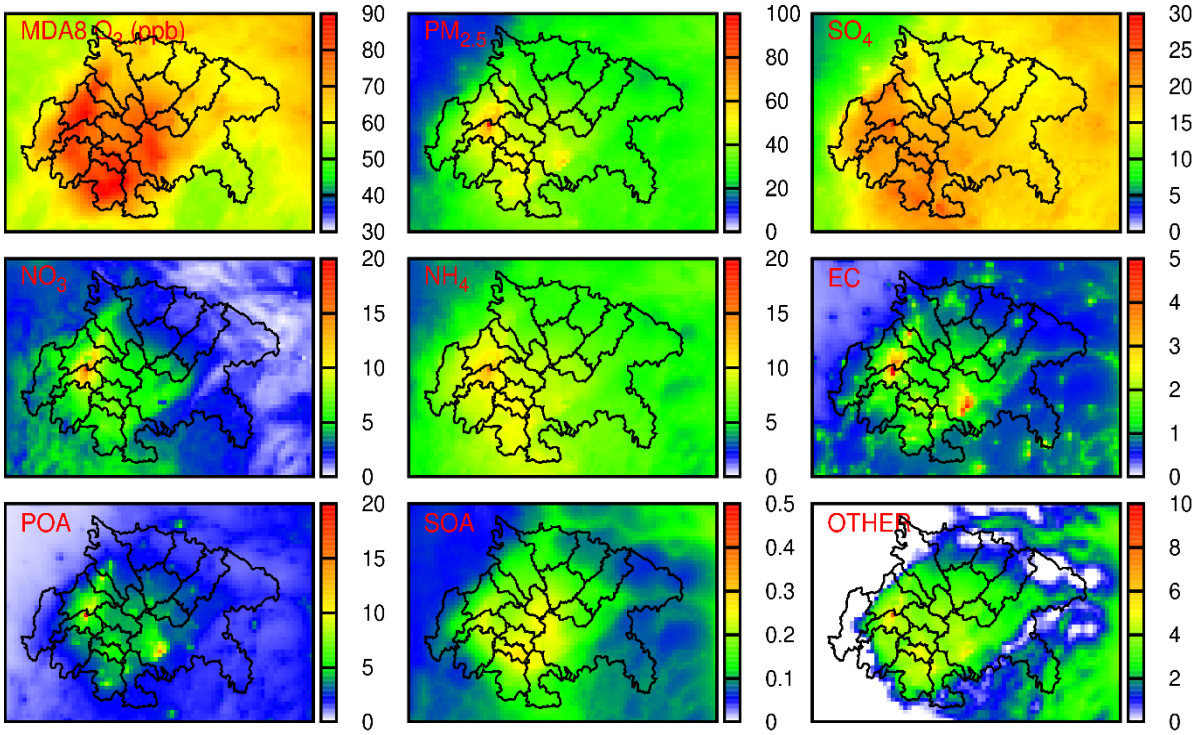

Figure 17. Predicted $PM_{2.5}$ ($\mu g/m^3$) with components and MDA8 O_3 concentrations (ppb) spatial distribution of SCB in July 2015 without feedback.

$PM_{2.5}$ concentrations gradually increased from the rim of the basin (~40 μg/m^3) to the central (~ 140 μg/m^3), with two hotspots near Chengdu and Chongqing in January (~ 120 μg/m^3) and July (~ 40 μg/m^3). This spatial pattern was associated with emissions and wind directions within the basin. The WD in SCB is usually blowing from the northeast to southeast and then travel within the basin in an counterclockwise pattern [127]. This led to an inter-city transport process of air pollutant, which can be noticed more easily during the highly polluted season of winter (Figure 16).

The MDA8 O_3 concentration was higher in summer (90 to 60 ppb from center to rim) and lower in winter (60 to 40 ppb from east to west). This seasonal pattern was associated with higher temperatures and much more solar radiation in summer, which leads to stronger photochemical production of O_3. As shown in Figure 18, the simulated temperature in summer (>30℃ on average) is more than two times in winter. Monthly average solar radiation intensity was almost three times in summer (more than 300 w/m^2) than in winter (130-160 w/m^2). Besides, according to Wang et al. [162], high $PM_{2.5}$ concentration can also decrease O_3 concentration by blocking solar radiation or consuming precursors. MDA8 O_3 concentration was in a similar pattern among 18 cities in both summer and winter, which are 50 ppb and 80 ppb on average, respectively. Megacities like Chengdu and Chongqing did not show any extreme different values compared with other cities among the basin, indicating that O_3 was largely affected by meteorological conditions than the emission of precursors.

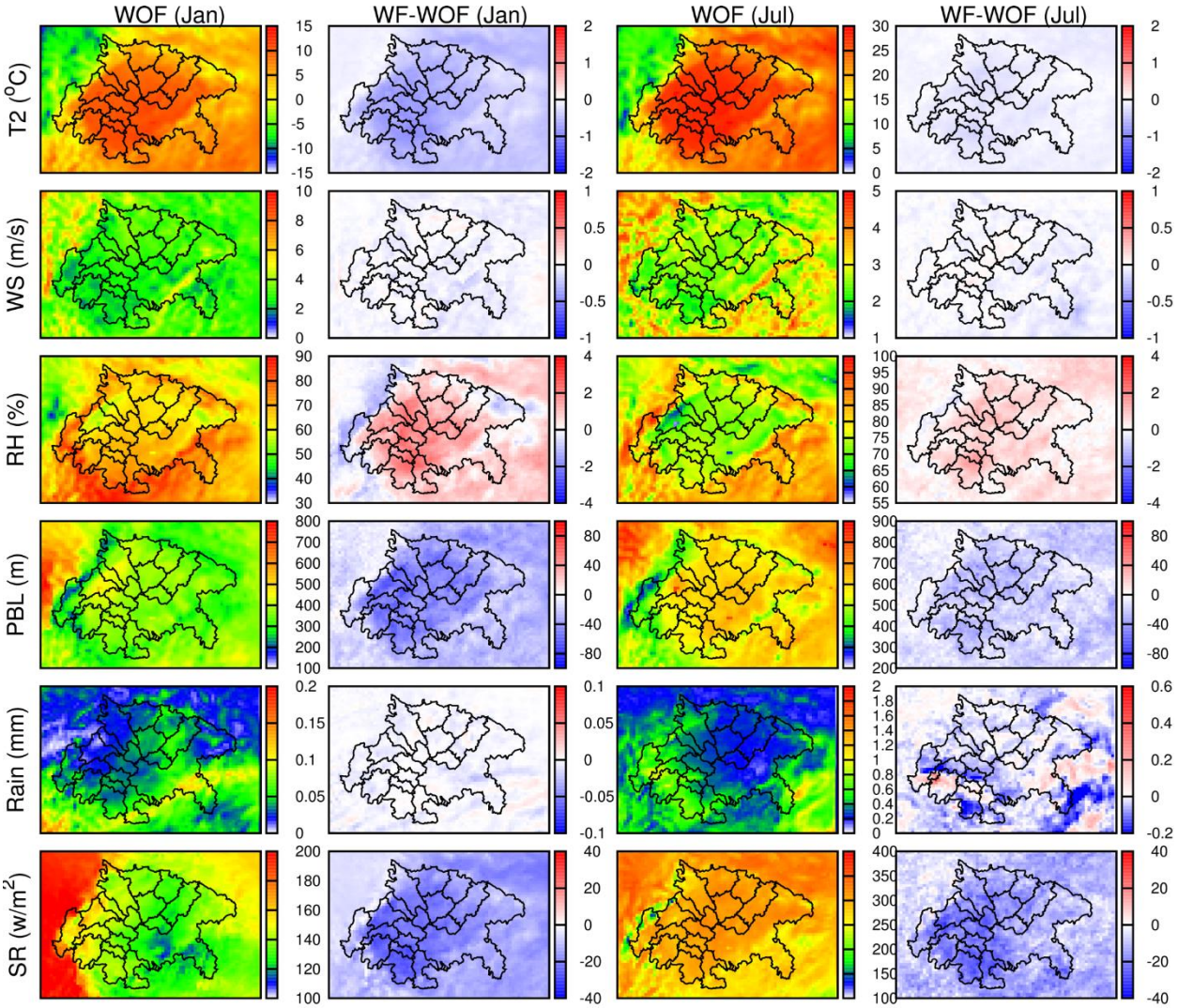

Figure 18. Averaged meteorological parameters in January and July 2015 and the differences from with feedback and without feedback. T2 is the temperature at 2 meters above ground, WS is wind speed, RH is relative humidity, PBL is planetary boundary layer height, and SR is the shortwave radiation at the surface.

3.3.3 Effects of aerosol radiation feedbacks

3.3.3.1 $PM_{2.5}$ and O_3 simulations with and without aerosol radiation feedbacks

Differences of $PM_{2.5}$ and its components and MDA8 O_3 between WF and WOF in January and July 2015 are shown in Figures 19 and 20. Aerosol radiation feedback decreased MDA8 O_3 concentration in most of the Sichuan basin by as much as 2 ppb during January. This resulted from the decreasing temperature and solar radiation directly reduced photolysis rates, which will cut the

formation of O_3 (Figure 18). In July, most areas in the south and east of the basin experienced a 1-2 ppb increase of O_3 concentration while west and northwest part of the basin had an up to 2 ppb decrease (Figure 20). The precipitation of WF in July decreased by more than 30% in comparison with WOF, which may leave more O_3 precursors in the air (Figure 18). The cloud in raining days also prevents the photochemical reactions of O_3 formation.

In January, feedback brought central basin an up to 12 μg/m^3 increase and west basin an up to 4 μg/m^3 decrease of $PM_{2.5}$. Among $PM_{2.5}$ components, NH_4^+, SOA, and POA showed a similar pattern with total $PM_{2.5}$, which increased in the central and decreased in the west. NO_3^-, EC and OTHER increased basin-wide while $NO_3^-$was the first contributor (50%) to total $PM_{2.5}$. SO_4^{2-} was in a different pattern that decreasing in most parts of the basin especially in the west and increasing in Luzhou. The changes in total $PM_{2.5}$ in July was less than 4 μg/m^3 on average. The changing pattern was like January that a slight decrease was observed in the west while the rest were increasing.

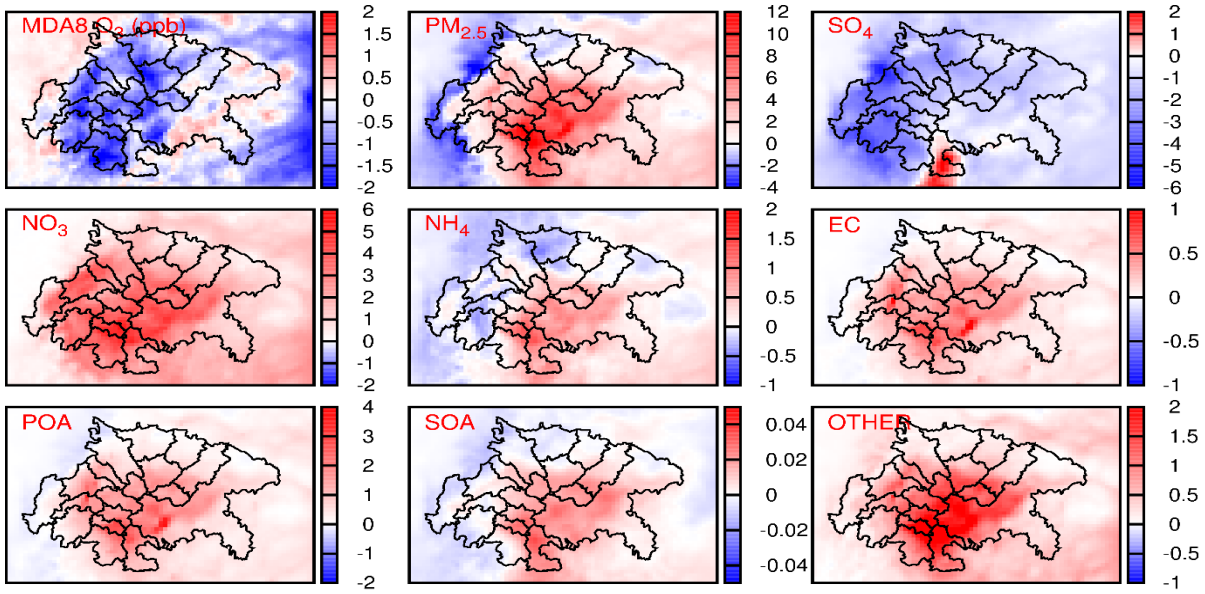

Figure 19. Differences of $PM_{2.5}$ (μg/m^3) and components and MDA8 O_3 concentrations (ppb) between WF and WOF in January 2015.

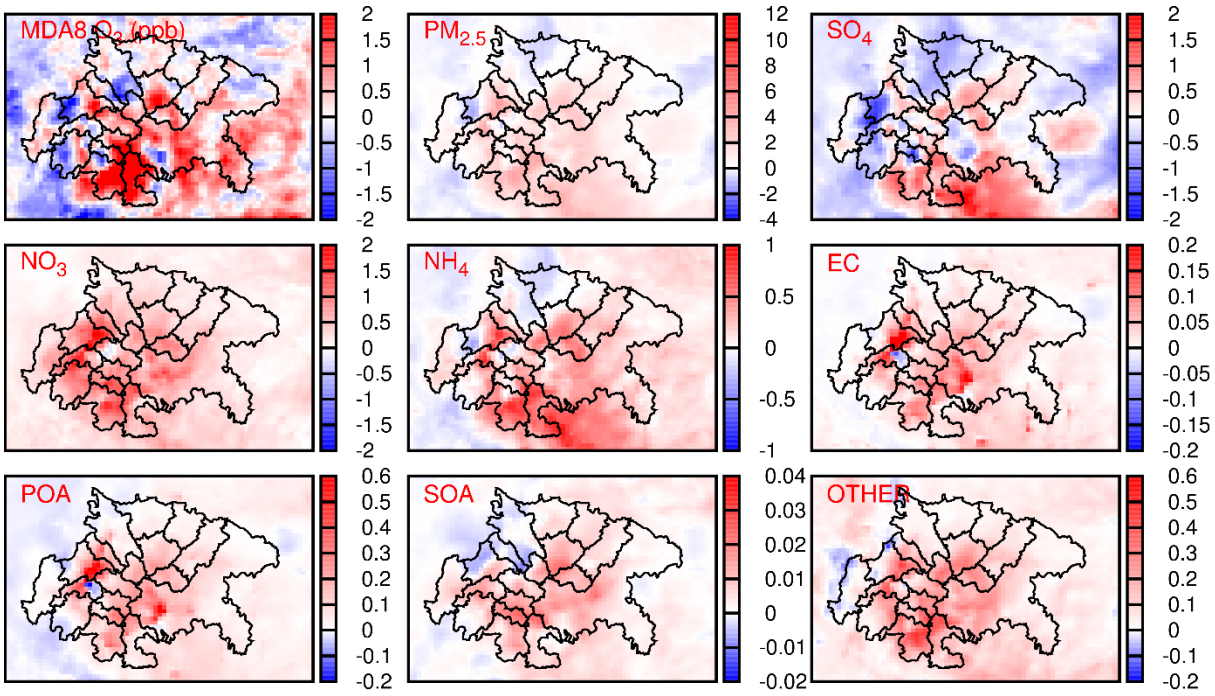

Figure 20. Differences of $PM_{2.5}$ ($\mu g/m^3$) and components and MDA8 O_3 concentrations (ppb) between WF and WOF in July 2015.

All 7 components showed quite similar spatial distribution patterns with total $PM_{2.5}$ and NO_3^- was still the first contributor. The increase of $PM_{2.5}$ was a consequence of decreases in WS, PBL, and temperature (Figure 18). Reduced PBL height indicated a more stable PBL, which further weakened the dispersion of air pollutants.

3.3.3.2 Air pollution impacts on meteorology

Figure 21 shows the temporal variations of $PM_{2.5}$ concentrations and meteorology parameters in January and July 2015 around the basin. The feedback decreased the solar radiation at the surface both in January and July. The temperature was decreasing accordingly with a larger amount in January compared with July due to the lower base value in the winter. Because of the decrease of T2 and the PBL and the increase of RH were found in both months, and changes are more visible in January than in July. WS is in a quite similar pattern and value while a slight decrease can be

found when there was feedback. The rain was reduced by feedback and bigger differences were observed in July than in January resulted from less precipitation in the winter.

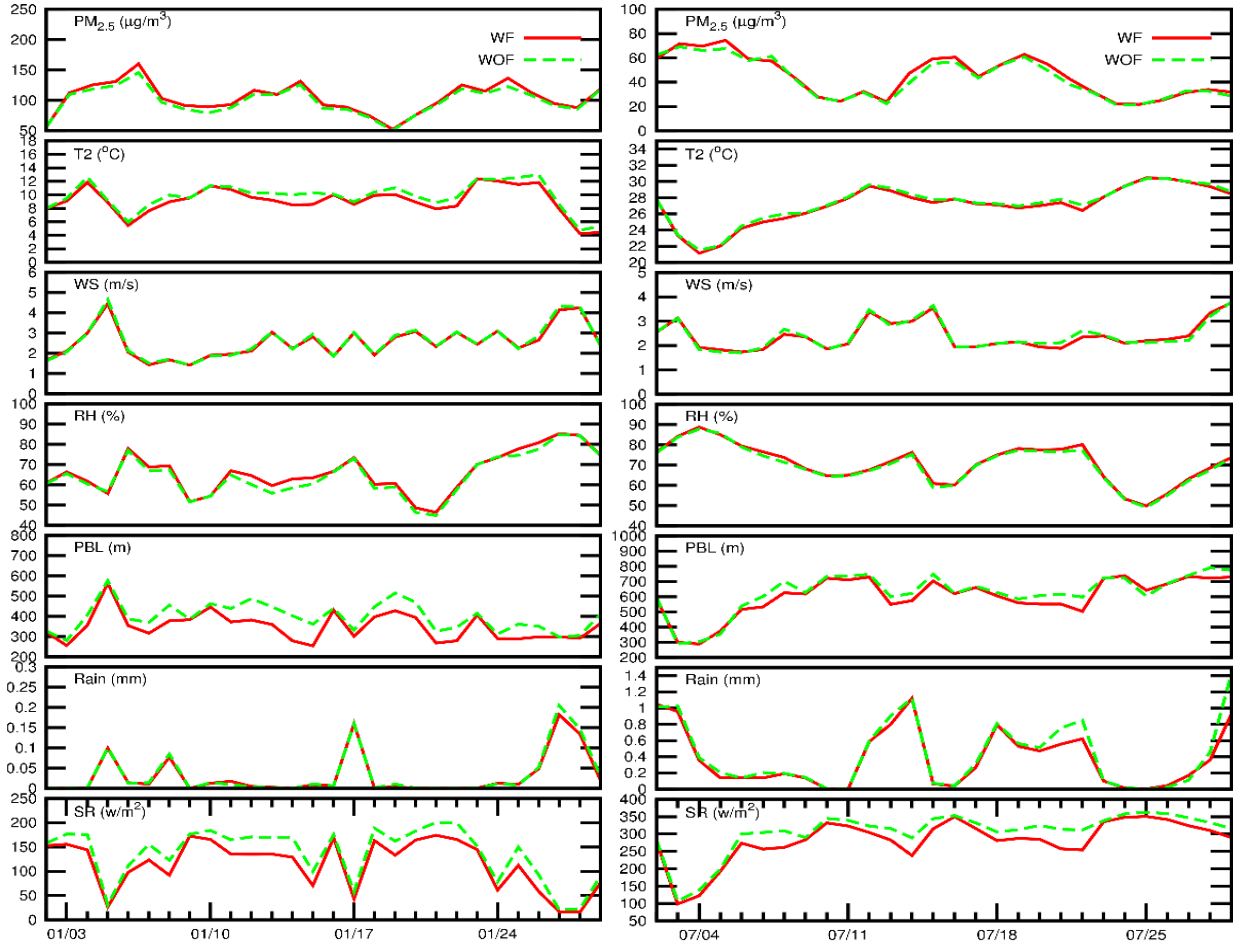

Figure 21. Temporal variations of predicted daily $PM_{2.5}$ concentrations ($\mu g/m^3$) and meteorology parameters in January and July around the basin. T2 is the temperature at 2 meters above ground, WS is wind speed, RH is relative humidity, PBL is planetary boundary layer height, and SR is the shortwave radiation at the surface.

The spatial distribution of averaged meteorological parameters in January and July 2015 of WF, WOF and their differences is shown in Figure 18. Compared to WOF, the temperature of WF decreased for 1-2℃ in January around the basin. RH increased up to 8% in most cities located in the central basin. The PBL decreased by more than 10% in the rim and 20% in the central area. Changes in precipitation in January were barely observed. Solar radiation (SR) showed a similar changing pattern with PBL, decreased ~30% when feedback was turned on.

For differences in July, changes between WF and WOF were in the same trend when compared with January but with smaller values in most meteorological parameters except precipitation. Unlike the inconspicuous changes in January, there was an apparent decrease in precipitation especially in the southwest corner of the basin for more than 30%. The temperature was slightly decreased up to 1℃ in July when there was aerosol radiation feedback. Aerosol impact radiation and temperature through different radiative effects of different aerosol components [163]. Aerosols can reduce incoming solar radiation via backscattering, which will decrease the surface temperature. WS pattern was similar as in January, changes cannot be obviously observed but the decreasing trend was certainly found. RH increased for ~5%, PBL and SR decreased for ~15% around the basin.

To quantitatively evaluate the aerosol radiation effects on $PM_{2.5}$ concentration changes and meteorology parameters, an ensemble method was used (Figure 22). The daytime (8 a.m.-4 p.m.) surface $PM_{2.5}$ concentrations at all stations were sorted from the lowest to the highest and grouped with an interval of 10 μg/m³, which produced 23 bins in January and 18 bins in July. The x-axis is the averaged concentration of $PM_{2.5}$ in each bin. The y-axis is the averaged changes caused by the feedback at all stations in each bin of each parameter. Figure 22a shows the differences in $PM_{2.5}$ concentration between WF and WOF, Figure 22b shows the percentage change of $PM_{2.5}$ by dividing the result of Figure 22a with the $PM_{2.5}$ concentration of WF. An increase in the $PM_{2.5}$ concentration brought by aerosol radiation feedback can be clearly identified from Figure 22a and b. The increasing effect was getting bigger as the $PM_{2.5}$ concentration goes high and reaching 15% in January when $PM_{2.5}$ concentration is larger than 225 μg/m³. When $PM_{2.5}$ concentration is under 35 μg/m³, the feedback effect decreased the $PM_{2.5}$ concentration for 1%. But after $PM_{2.5}$ concentration is exceeding 35 μg/m³, the percentage of changing increased almost linearly as the

$PM_{2.5}$ concentration goes high (Figure 22b) with a rate of ~7–10% per 100 μg/m³ $PM_{2.5}$. In July, absolute change and percentage changing are also in a similar changing pattern. The changing rate is as small as 7% per 100 μg/m³ $PM_{2.5}$ before the $PM_{2.5}$ concentration reached 75 μg/m³. After that, the changing grows rapidly and linearly, which reached 25% when $PM_{2.5}$ concentration was more than 175 μg/m³ (Figure 22b').

Figure 22h shows the percentage change of solar radiation that can be decreased as much as 40% as the $PM_{2.5}$ concentration goes to 150 μg/m³ and keep still afterward. This was because aerosols can absorb and scatter incoming solar radiation and resulting in reducing surface solar radiation. Lower surface solar radiation leads to a lower temperature consequently (Figure 22c). Temperature showed a similar changing pattern with solar radiation, kept decreasing to 0.6℃ from the beginning until 150 μg/m³ and became relatively stable then. From Figure 22d, the feedback decreased WS by about 0.05 m/s before 165 μg/m³ and the changes show little fluctuation afterward while with a speed of 0.05 m/s on average. The PBL was highly influenced by thermal situation and atmospheric dynamics, so PBL decreased with the reduction of temperature and WS (Figure 22f). PBL was notably decreasing within the low concentration range, which less than 150 μg/m³ and keeps the 30% changing rate after. Precipitation decreased when there was feedback but in a small range of 0.005mm during almost the whole concentration range. Since RH was determined by the temperature and water vapor, the decreasing temperature and precipitation would lead to an increase of RH, which accounted for as much as 2% in January (Figure 22e). In July, all the parameters presented the same changing pattern but slightly different amounts compare with January, such as T2, WS, PBL, SR. Feedback brought a fast decrease of RH in July when $PM_{2.5}$ concentration was less than 25 μg/m³ (Figure 22e'). Precipitation reduction is as large

as ~0.15 mm in July, which was 3-4 times of the changes in January. Lower precipitation, lower WS, and higher RH all led to an increase in PM concentration.

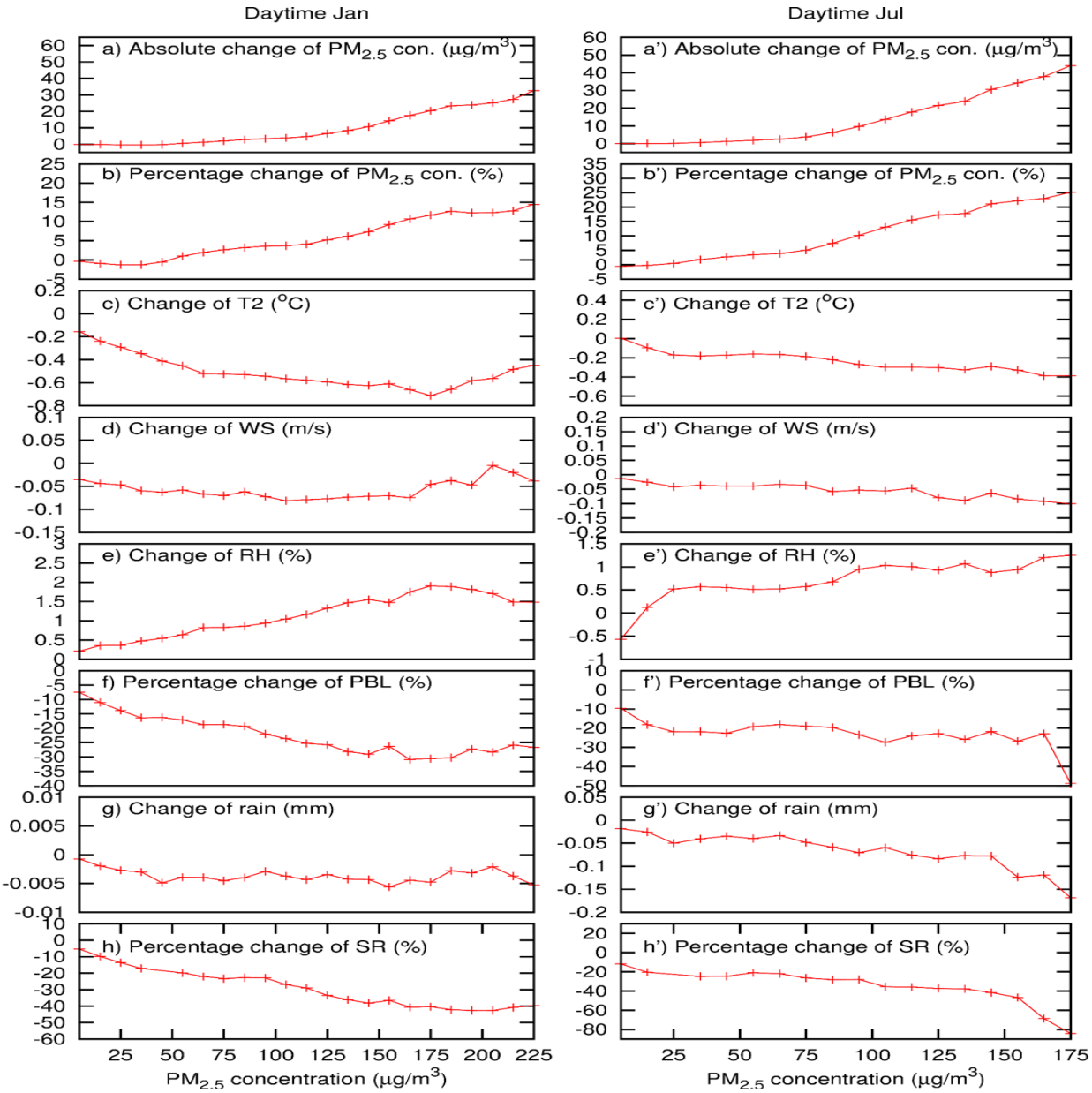

Figure 22. Changes of $PM_{2.5}$ concentrations ($\mu g/m^3$) and meteorology parameters caused by feedback around the basin, as a function of the $PM_{2.5}$ concentrations ($\mu g/m^3$) during the daytime January. The daytime (8 AM-4 PM.) surface $PM_{2.5}$ concentrations at all stations were sorted from the lowest to the highest and grouped with an interval of 10 $\mu g/m^3$, which produced 23 bins in January and 18 bins in July. The x-axis is the averaged concentration of $PM_{2.5}$ in each bin. The y-axis is the averaged changes caused by the feedback at all stations in each bin of each parameter. T2 is the temperature at 2 m above ground, WS is wind speed, RH is relative humidity, PBL is planetary boundary layer height, and SR is the shortwave radiation at the surface.

3.4 Conclusion

WRF/Chem V3.7.1 was applied to simulate air pollution and aerosol direct radiation feedbacks over the SCB and showed good capability of predicting meteorological variables and air pollutants. $PM_{2.5}$ concentration was higher in winter (~90 μg/m³) than in summer (~40 μg/m^3). Higher emission and unfavorable meteorology were two main reasons that led to seasonal variations. SO_4^{2-}, POA, and NO_3^- were the top three contributors to total $PM_{2.5}$ in winter while SO_4^{2-}, $NH_4^{+,}$ and NO_3^- shared the most in summer. O_3 concentrations of 18 cities were in similar patterns both in summer and winter, and summer concentrations were up to 80 ppb. Aerosol radiative effects reduced shortwave flux at the ground by as much as 40% in January and 80% in July, lowered the temperature by 0.6℃ in January and 0.4℃ in July in average, decreased WS by ~0.1 m/s in both seasons, reduced PBL height by 30%, while slightly increased RH (1-2 %). All those changes resulted in increases of O_3 and $PM_{2.5}$ concentrations. The feedback effects were getting bigger as the increase of $PM_{2.5}$ concentration. This study indicates that the feedbacks from air pollutants cannot be neglected in air quality simulation and should be considered in designing air pollution control strategies.

CHAPTER 4. GROUND-LEVEL OZONE SIMULATION USING ENSEMBLE WRF/CHEM PREDICTIONS OVER THE SOUTHEAST UNITED STATES

4.1 Introduction

Ground-level O_3 has adverse influences on ecosystems and human health [164-167]. Including childhood asthma, short-term exposures to O_3 are proven to have effects on respiratory and cardiovascular system [168, 169]. From a study through 95 large US urban communities, Bell et al. [170] concluded that a 10-ppb increase of O_3 in the previous week would result in a 0.64% increase in cardiovascular and respiratory-related mortality. According to Nuvolone st al. [171], 16,000 premature deaths, which equal to 192,000 years of life lost, in European countries were contributed by O_3 exposure. In a 2016 study in China, O_3 led 74200 annual premature mortality responsible for a $7.6 billion economic loss [172]. Ghude et al. [173] estimated mortality of 12,000 people by chronic obstructive pulmonary disease on a national scale in India in 2011 due to O_3 exposure. Besides health effects, elevated O_3 could influence vegetation and damage crops. From 1980 to 2011 in the U.S. , the productions of maize and soybean were reduced due to O_3 pollution by 5% and 10%, respectively [174]. Feng et al. [175] estimated the costs of O_3 induced losses in rice, wheat, and forest production in China were $7.5, $11.1, and $52.2 billion, separately.

Emission and meteorology are two key factors influencing the accuracy of predicting air pollution using CTMs [154, 176, 177]. In an O_3 simulation study in Melbourne from 1999 to 2006, Pearce et al. [61] found 26.3% of O_3 variations were due to the meteorological variables. The changes in temperature, especially when above 35°C, could lead to as much as 150% positive response for O_3. Zhang et al. [178] concluded the extreme O_3 event in October 2010 over the Southeast U.S. to the dry and warm weather conditions, which enhanced photochemical production. Jing et al. [179] also found a 53% variance of O_3 concentration resulted from meteorology from 2005 to 2013 in Chicago.

Meteorological condition plays a decisive role in the places where anthropogenic emission has been well controlled in Europe and North America [180-182]. The Toronto area experienced the highest recorded summertime O_3 in 2012 although the precursors of NOx and VOCs kept decreasing in the previous years. The high O_3 concentration was believed due to high solar radiation and transport from upwind regions [183]. Jaffe et al. [184] concluded the high O_3 in June of 2015 in the western U.S. to the unfavorable meteorological condition under the circumstance of anthropogenic emission reduction.

To address the uncertainties from emission and meteorology, ensemble methods have been applied in previous studies [185-187]. Since there was no unified theory in the field of air quality modeling, researchers constructed the ensemble in different approaches. Ensemble methods can be derived by applying several models [188-191]. Delle Monache et al. [186] conducted four photochemical models for improving simulation accuracy during an O_3 event over western Europe. The ensemble can be derived by perturbing model input parameters as well [192-197]. To determine the O_3 response to meteorological parameters, an ensemble modeling case was conducted by Dawson et al. [198] in the eastern U.S in 2001. The ensemble in nearly all the cases was initialized with slight perturbated initial conditions that reflect the inherent uncertainties in model simulations. SERF developed by the National Centers for Environmental Prediction (NCEP) of the U.S. Du et al. [199] is such an ensemble forecasting system. SREF contains 26 members from two dynamics cores: the Advanced Research WRF (ARW) and the Nonhydrostatic Mesoscale Model (NMM) of WRF. There are a control run and 12 runs with different perturbed initial conditions including initial condition, physics, and land surface in each dynamics core [200].

In this study, MDA8 O_3 over the Southeast U.S. was conducted for one week in each summer of the year from 2016 to 2018 using ensemble WRF/Chem. Model performance was validated by

comparing with air quality data collected at outdoor monitors from the U.S. Environmental Protection Agency (US EPA) [201]. This study would provide information for using ensemble meteorological inputs to improve CTMs performance.

4.2 Methods

The Weather Research and Forecasting model with Chemistry (WRF/Chem) V3.7.1 was applied to simulate MDA8 O_3 in the Southeast U.S. with a horizontal resolution of 12 km × 12 km (Figure. 23). WRF v3.7.1 was used to generate meteorological inputs with the Four-Dimensional Data Assimilation (FDDA) input from SREF. The NCEP SREF system has been developed and run since April 2001 [199, 202]. The version of SREF used in this study is a 26-member ensemble evenly split between the Advanced Research WRF (ARW) dynamical core and the Nonhydrostatic Mesoscale Model (NMM) that were both executed on a 32 km grid. Each dynamics core has 12 runs with 6 positive and 6 negative perturbed initial conditions and 1 control run [200].

Figure 23. Domain of Southeast U.S. with state names.

The National Emissions Inventory (NEI) 2011 and State Annual Emissions Trend data were applied to generate anthropogenic emissions for 2016 to 2018 [203]. Biogenic emissions were produced using the Biogenic Emissions Inventory System (BEIS) v3.14 integrated with the Sparse Matrix Operator Kernel Emissions (SMOKE) emission processing model (version 3.5.1) developed by US EPA. The emissions from biomass burning were generated based on the FINN [204].

The observation data from EPA was used to validate the simulation results and helped to decide the simulation periods. Continuous 7 days with high observed O_3 concentrations during summer were picked in each year. In specific, those were June 25 to July 02 in 2016, July 18 to 24 in 2017 and June 04 to 10 in 2018. The simulations started three days before each period with three days spin up.

4.3 Results and discussions

4.3.1 Model validation

The model performance statistics of O_3 are shown in Table 12. Mean observations, mean predictions, MFB, MFE, MNB, and MNE was calculated during each week in the three years. O_3 was well predicted as the MNB and MNE in all the three years were all within the criteria suggested by EPA [108], although the model showed slightly overprediction in 2018 (positive MNB) and underprediction in 2016 and 2017 (negative MNB). Figure 24 shows the observation (obs) and prediction (ensemble) values of weekly averaged MDA8 O_3 concentration in each monitor station in the Southeast U.S. during the three years. For 2016, the low values in Florida and East Coast areas were well captured by the ensemble. The simulations showed good results in Arkansas, Louisiana, and Mississippi while several peak values were missed in the middle and north parts of

Southeast U.S. In 2017, the model performed well especially in the East Coast and Gulf of Mexico Coastal areas, while some high values were neglected in North Carolina and South Carolina, Virginia, and Kentucky. In 2018, almost all stations were slightly underpredicted except several stations in the middle and Florida.

Table 12. Model performance of O_3 in three years. OBS is mean observation, PRE is mean prediction, MFB is mean fractional bias, MFE is mean fractional error, MNB is mean normalized bias, and MNE is mean normalized error. The performance criteria for O_3 are suggested by EPA[109].

		2016	2017	2018	Criteria
MDA8 O_3 (ppb)	OBS	44.56	43.54	43.13	
	PRE	41.31	38.74	43.32	
	MFB	-0.07	-0.12	0.02	
	MFE	0.17	0.20	0.19	
	MNB	-0.04	-0.09	0.08	$\leq \pm 0.15$
	MNE	0.18	0.18	0.23	≤ 0.3

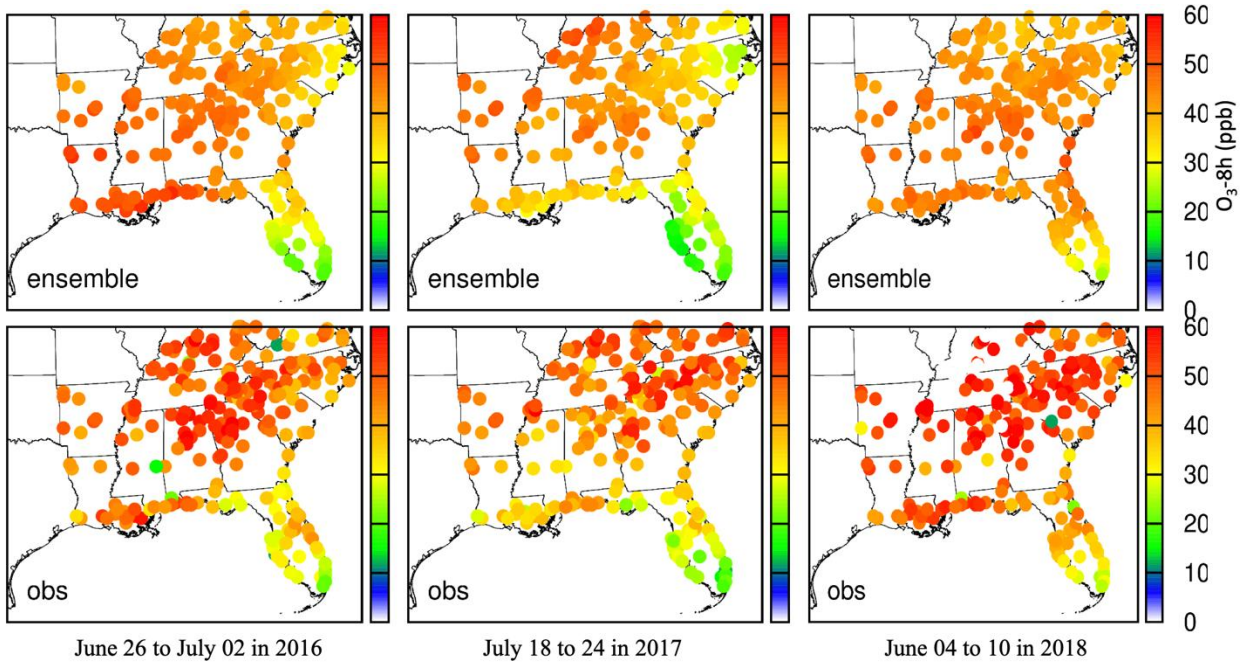

Figure 24. Averaged MDA8 O_3 concentration of ensemble prediction and observation from EPA. Units are ppb.

4.3.2 Variances of O_3 and meteorological conditions

The ensemble model had 26 members generated based on two dynamic cores. To better illustrate the differences between the ensemble, the standard division of MDA8 O_3 prediction and meteorological parameters in three years is shown in Figure 25.

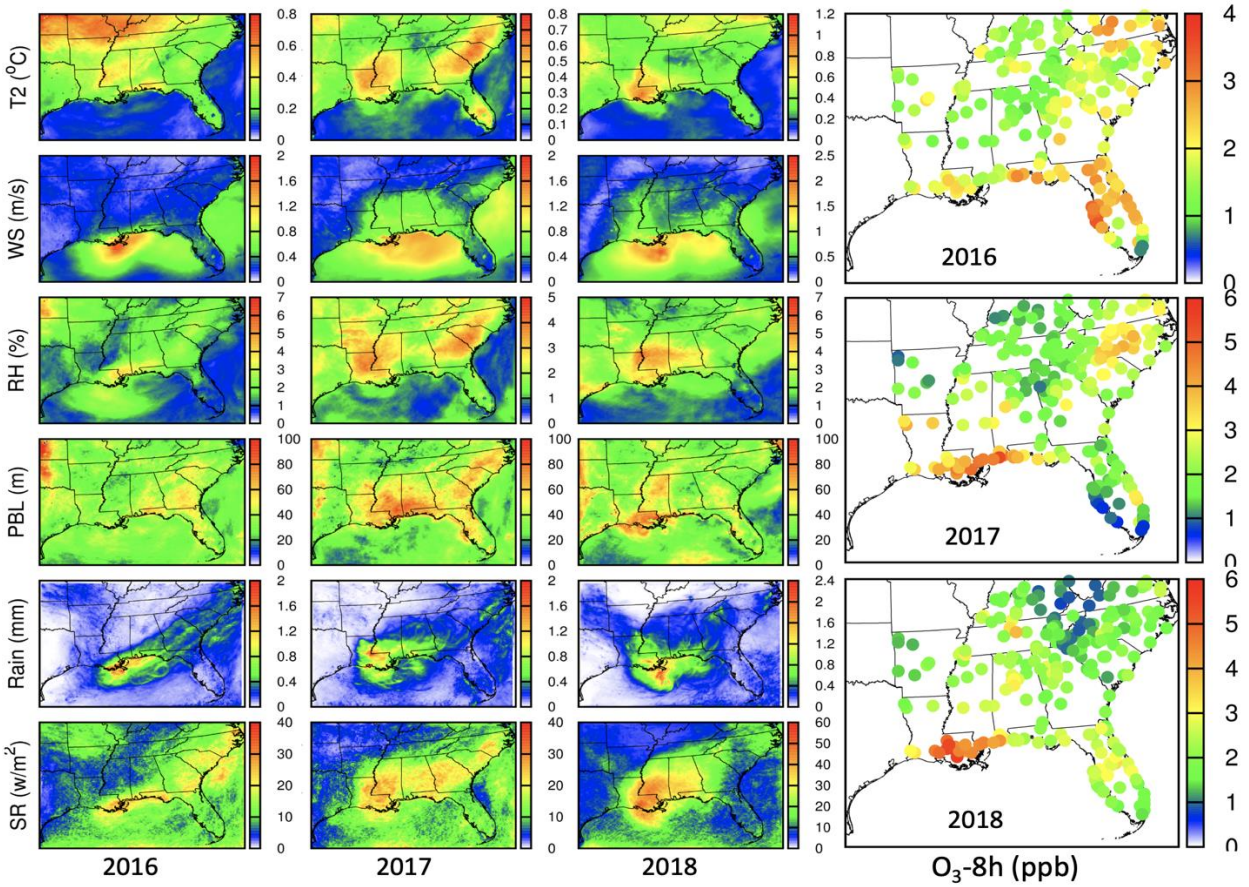

Figure 25. Standard deviation of weekly averaged MDA8 O_3 and meteorological parameters in three years. T2 is temperature at 2 meters above ground, WS is wind speed, RH is relative humidity, PBL is planetary boundary layer height, and SR is the shortwave radiation at surface.

The standard deviation in 2016 ranged from 1 to 4 ppb and the largest fluctuation happened in the coastal areas along with Louisiana, Florida, and Virginia. The standard deviation in 2017 was up to 6 ppb in the Gulf of Mexico coastal area near Louisiana and Mississippi. The highest standard deviation in 2018 was 6 ppb and was found near the Baton Rouge and New Orleans area. The O_3 oscillation caused by the ensemble meteorology accounted for at least 10% of the averaged O_3

concentration in the domain. O_3 is a product of photochemical reactions and solar radiation could dominate O_3 variability and concentration. The distribution of SR was consistent with the distribution of the O_3 standard deviation. Other parameters including T2 and precipitation (Rain) showed a similar pattern with SR, which enhanced the variation of O_3. Besides local production, transport is another important reason for the accumulation of O_3 [205]. Besides the coastline in the Gulf of Mexico, relative high wind speed variances were found in Northeast coastlines, which may enlarge the variances of O_3 concentration.

4.3.3 Root Mean Square Error

In this section, we examined the model accuracy by calculating RMSE of all the ensemble members. Figure 26 provides RMSE of all ensemble members with the observation result in three cities in three weeks of each year. Atlanta usually had the highest O_3 concentrations while Miami had the lowest and Baton Rouge experienced the largest fluctuation. These were the reasons for choosing those three cities.

The ensemble did have a noticeable range of errors in all the members, which indicated the impact of uncertainty from meteorological conditions. In Miami, the ensemble showed great performance in 2017 with less than 5.50 ppb errors in the whole week in all members. The errors in 2017 were relatively larger than that in 2016, especially on June 27, 2016. In Miami, the ensemble showed a similar pattern among members in 2016 and 2017. Both peak and valley values appeared among different members on the same day from June 05 to 07 in 2018. For example, on June 05, ARW-n2 showed an error as large as 11.50 ppb, while ARW-p2 showed the lowest error of 0.06. Except for low errors in certain days (July 01 in 2016, July 20, 22 and 23 in 2017, and June 07 in 2018), Atlanta experienced higher errors compared with Miami in almost all the days in 2018.

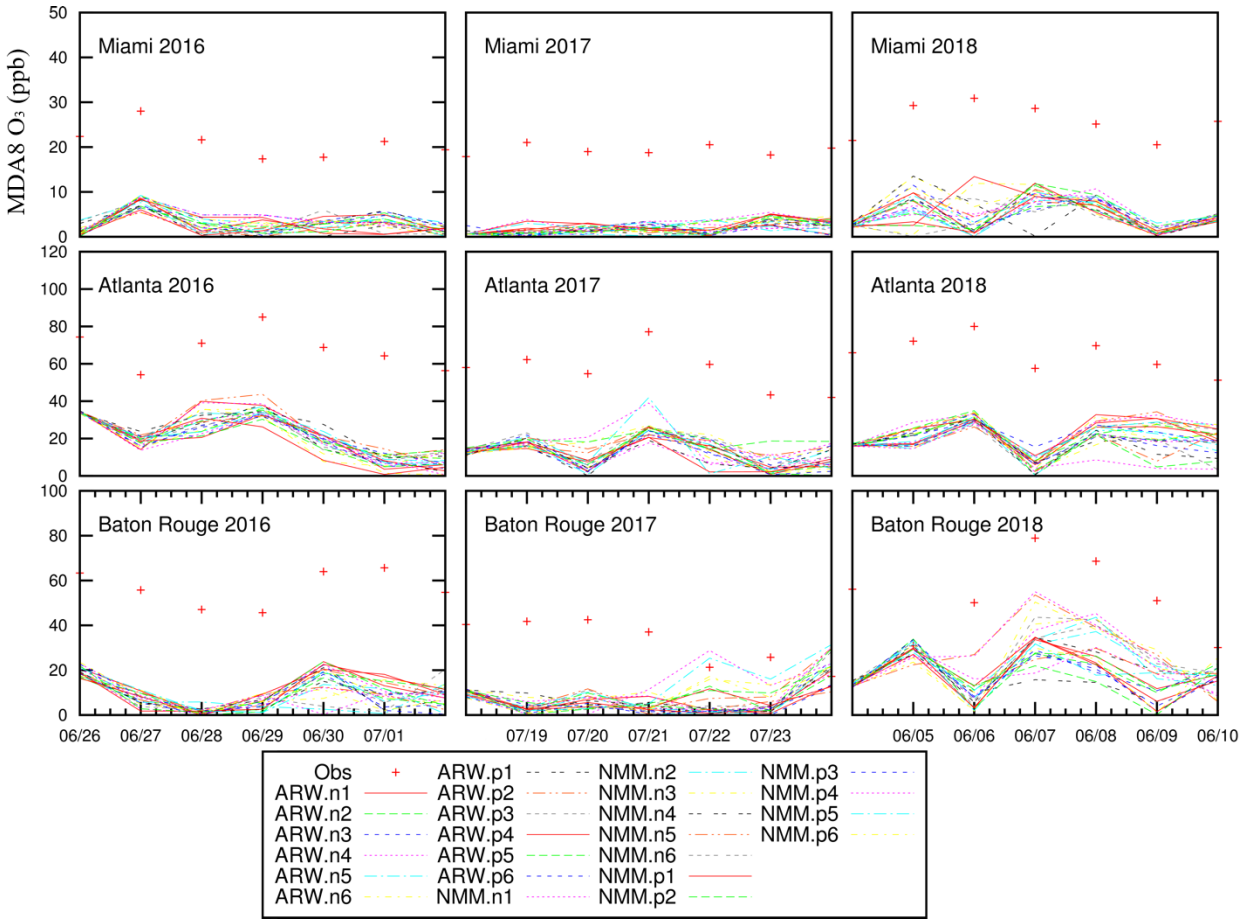

Figure 26. Root mean square errors of ensemble members and observed MDA8 O_3 in each week of three years in three cities.

For Baton Rouge, large variance of errors was found in certain days especially in 2018. On June 30, 2016, and July 22, 2017, 20–30 ppb differences were found between ensemble members. Ensemble members presented visible different performances since June 6 in 2018 although some members showed error as low as 0.15 ppb on a certain day (NMM-p2 on June 09). On July 22 and 24 of 2017 and June 05 of 2018, more than 100% of errors were observed compared with observation values. The ensemble performances were highly dependent on city and time. There was not one individual case that works well in all cities and in all three years, which in turn proved the advantage of using ensemble than using an individual member in the model simulation.

4.3.4 Evaluation and ranked histogram

Figure 27, 28 and 29 show the ensemble prediction and observed MDA8 O_3 concentrations along with RMSE in three cities in three years. The ensemble method showed benefit of capturing the peak values that individual run. For Miami in 2016, the NMM-n2, NMM-n4 and NMM-n6 cases showed better potential in catching the peak values than other cases. In 2017, although the peak value was overpredicted and the valley value was underpredicted in most cases, all the prediction results showed a similar pattern of a compact range with observation. Within the range of 1.69 to 3.41 ppb, Miami in 2017 showed the lowest RMSE in the three cities during the three years. In 2018, the top two observation values were overpredicted for a large scale in all the cases except ARW-n1 and ARW-p3. The low values were also underpredicted, which resulted in a relatively large RMSE. For Atlanta, underprediction from all ensemble members was observed in three years. Almost all the RMSE were larger than 20 ppb in 2016 and 2018. All the members missed the peak and valley values in 2016. In 2018, only member NMM-n1 caught the valley values of Atlanta. In 2017, the NMM-n4 member was better in capturing the top value than other members. In Baton Rouge, many members did well by reproducing the peak values and valley values in 2016. In 2017, all the peak values were overpredicted, but some members have closely predicted the valley values (ARW-n1, ARW-n6, ARW-p3, NMB-n1, NMB-n2, NMB-n6). In 2018, the members showed a disarray pattern of prediction and even the lowest RMSE was as large as 16.09 ppb (NMB-n4).

Figure 30 shows the distribution of observed O_3 values from the lowest to highest for all three cities in three years. The rank histogram plots were made by placing the prediction values of all the 26 ensemble members in 8 bins with the head and tail bin outside the observation spread. Rank histogram plots are usually used to evaluate the effectiveness of how the ensemble results covered the observation. A perfect ensemble will have equivalent probability through the bins resulting in a flat histogram plot.

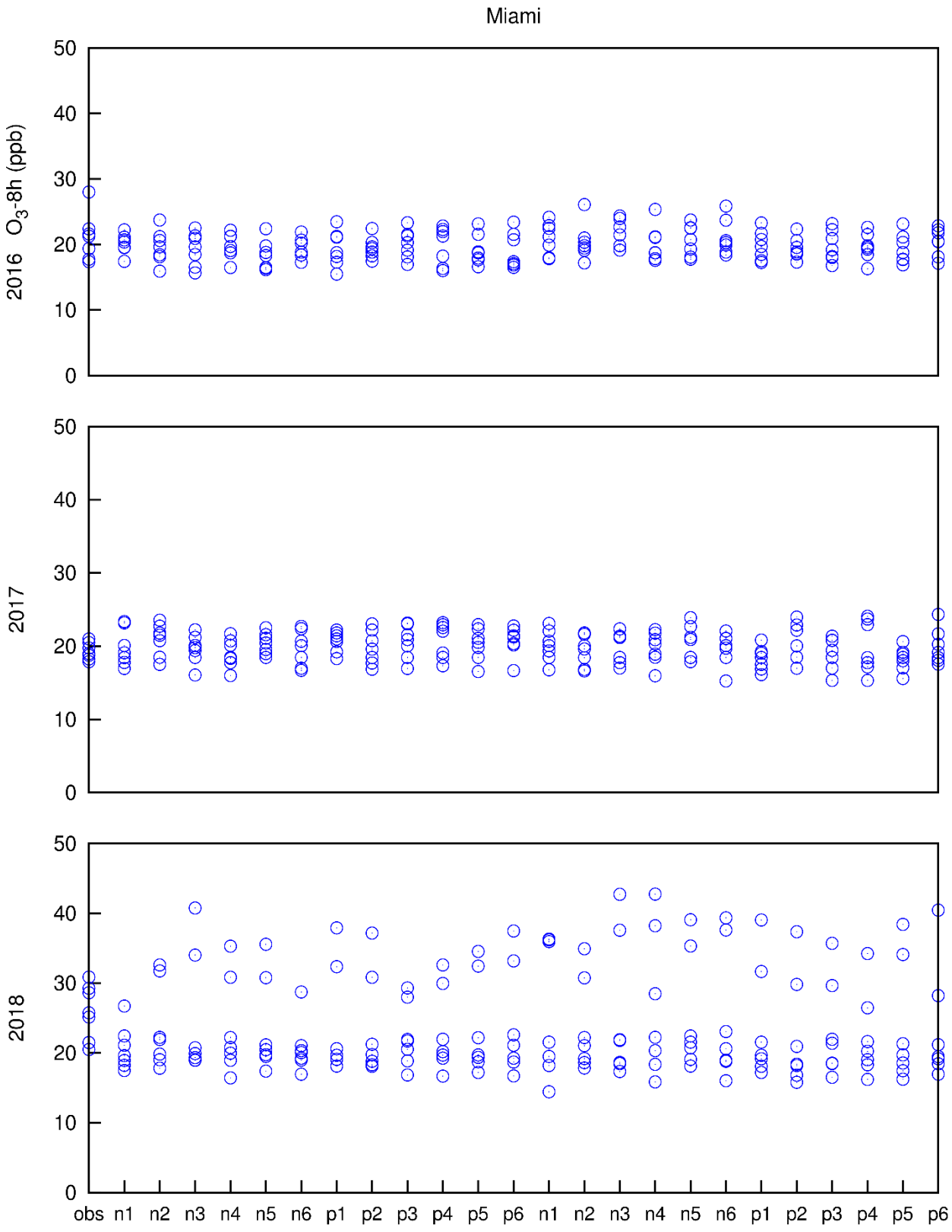

Figure 27. MDA8 O_3 concentrations of observation and ensemble prediction along with RMSE in Miami in three years.

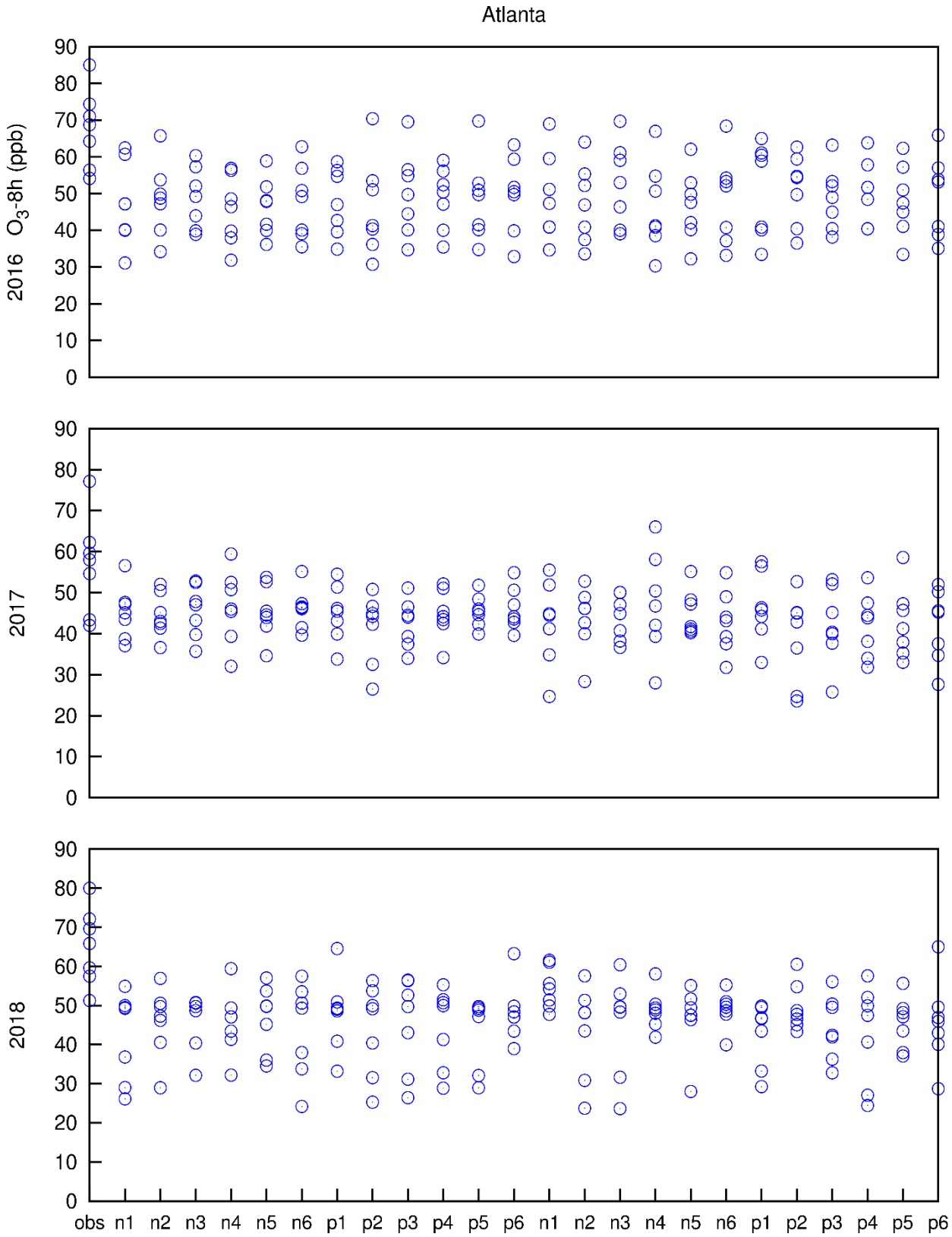

Figure 28. MDA8 O_3 concentrations of observation and ensemble prediction along with RMSE in Atlanta in three years.

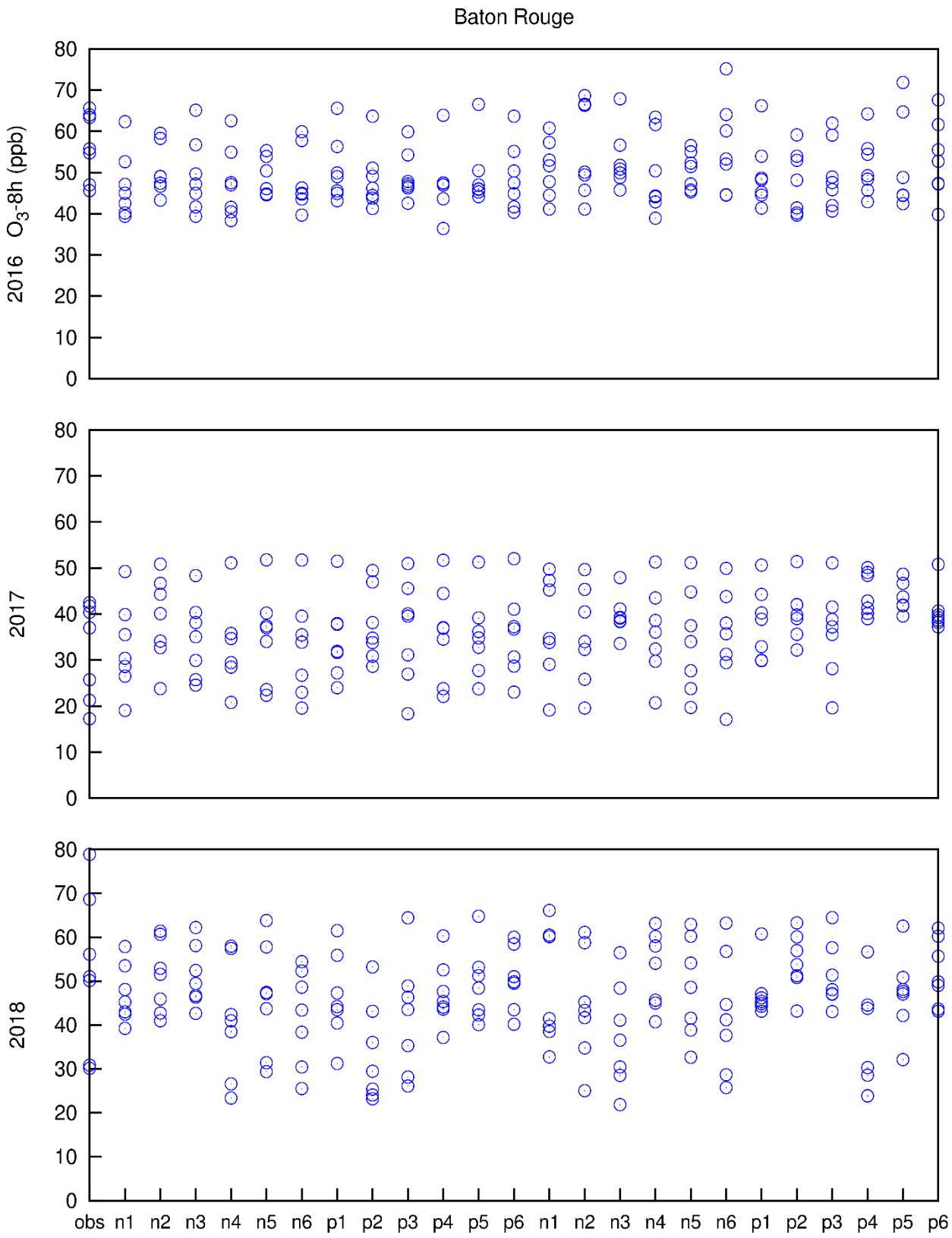

Figure 29. MDA8 O_3 concentrations of observation and ensemble prediction along with RMSE in Baton Rouge in three years.

Miami showed great performance in 2016 since there were no extreme high or low bars. The model showed 40% overprediction in 2017 while the model was underpredicted for almost 50% in Miami. Atlanta showed clearly underprediction in all three years. More than 70% of underprediction was found in 2016 and 2018 and almost 40% of underprediction was observed in 2017. Baton Rouge was in a large variance while 2016 had a 30% underprediction and 2017 had a 30% overprediction while a relatively good performance was found in 2018.

4.4 Conclusion

In this study, simulation of O_3 over the Southeast U.S. was conducted for one week in the summer of each year from 2016 to 2018 using the WRF/Chem model with ensemble meteorology. The contribution of meteorology uncertainties to the air quality forecasting was conducted. Ensemble averaged concentration showed good performance in predicting O_3, especially along the coastal areas. The largest fluctuations of O_3 were 4–6 ppb during the three years especially in the coastal areas along Louisiana, Florida, and Virginia. The O_3 changes due to meteorology uncertainties accounted for at least 10% of averaged O_3 concentration in the domain. Although the ensemble model underpredicted O_3 in Atlanta in all three years in this study, the ensemble method was still more reliable than any individual run. This is not only because the ensemble offered more simulation options than a single run but also because it has optimization potential by calculating and using the weighting factors of all the ensemble members. Ensemble offers a way to improve the chemical transport model performance.

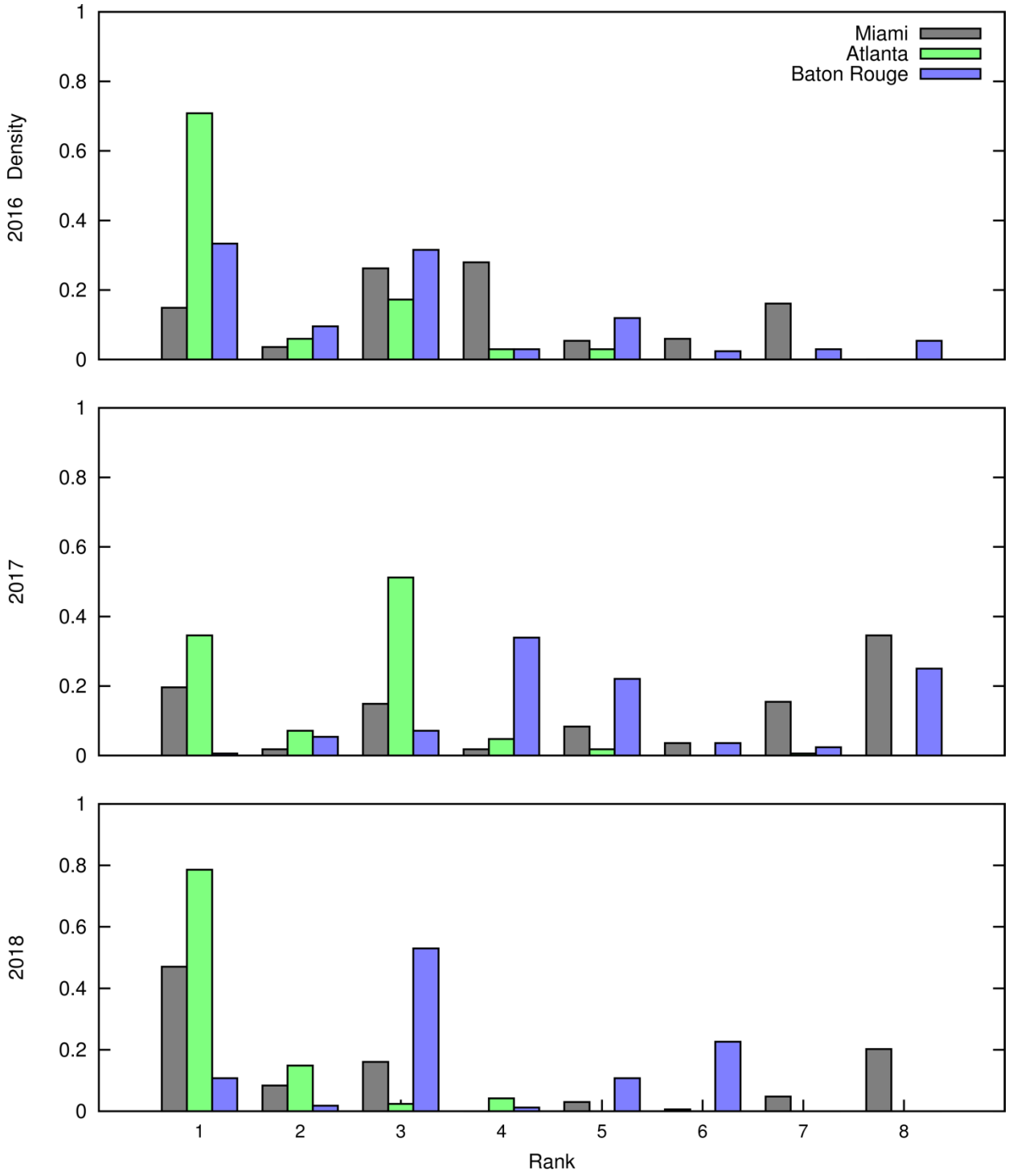

Figure 30. Ranked histogram of MDA8 O_3 for ensemble in three cities in three years.

CHAPTER 5. AIR POLLUTION AND ITS METEOROLOGICAL FEEDBACKS IN AFRICA

5.1 Introduction

Africa is the second-largest continent in the world with the second highest population. The past air quality studies in Africa were highly dust-related since the Middle East and North Africa are the most insistent source of mineral dust [206, 207]. It is estimated that more than 50% of the global dust mass was emitted from this region [208].

Air pollution problems happen globally, especially the areas with a large population and rapid economic development, which result in large anthropogenic emissions [67, 209-212]. Africa is now suffering air pollution problems like $PM_{2.5}$ and ground-level O_3 due to the rapid population growth and urbanization [213-215]. It was estimated that 54% of population growth would be in urban areas by 2030 in Africa [216]. Traffic and industry are the major $PM_{2.5}$ sources along with the urbanization in developing countries [217, 218]. Assamoi and Liousse [218] indicated the fuel consumption ratios of vehicles between their study and the United Nation database could be as large as 169%, 264%, and 628% in three countries in West Africa. Africa is a continent with high distributions of coal and oil sources, phosphate, and metal ores in all five regions [219]. Large numbers of tractors, machinery, and delivery vehicles are used underground and on the surface of mines. Those gasoline and diesel engines are huge emission sources [220]. Besides traffic and industry emission, other kinds of typical $PM_{2.5}$ sources were found in Africa as well, such as cooking emission from the combustion of biomass fuels like charcoal, wood, crop wastes, and animal dung[221]. Indoor emission of residual insecticides for malaria control and smoke emission from the agriculture waste burning are large sources as well [222, 223].

In addition to particulate pollution, O_3 pollution is becoming severe in recent years in Africa as well [224-226]. High level of ground-level O_3 was found in southern Africa because of the huge

emission from vegetation, biomass burning with the help of intensive solar radiation [227]. Compared with dust, $PM_{2.5}$ showed more severe health effects on human beings since it has a smaller size and could be easily breathed into our lungs and even dissolved in blood [13, 228, 229]. Being a powerful oxidant, high concentration O_3 on the ground level could damage the plant cell as well as the skin of human beings and lead to crop loss and skin and respiratory disease of human beings [230, 231].

Besides emission, the meteorological condition is another key factor in air pollution. Meteorology plays a significant role in the processes of transport, transformation, and deposition of air pollutants and their precursors [86, 232]. With a big range of latitude, there are several climates in Africa such as the tropical monsoon climate, the equatorial climate, the tropical dry and wet climate, the desert and semi-desert climate, and the subtropical highland climate [233]. The emitted pollutants would show different feedback effects under these various kinds of climates. For example, there are two main Monsoons in Africa. The West African Monsoon prevails in the summer and the East African Monsoon, which usually brought precipitation in spring and autumn [234, 235]. From a WRF/Chem simulation over the West Africa Monsoon region, Zhao et al. [236] found dust showed warming up effect (6.94 W/m^2) and cooling down effect (-6.11 W/m^2) at the surface in the atmosphere during January 2016. Through a 6-year simulation conducted by the RegCM3 model over southern Africa, Tummon et al. [237] found an up to 60 W/m^2 decrease in surface radiation was found in the biomass burning region. The study of aerosol radiation in Africa is limited while mostly focused on dust [238, 239].

In this study, model simulation of air pollutants like PM and O_3 with aerosol radiation feedbacks effects over the whole continent of Africa at 36-km grid resolution was conducted for eight days in January (09-16) and August (05-12) 2015 using the WRF/Chem model. This study would

provide information for evaluating WRF/Chem model performance and meteorological feedbacks for the areas where have large meteorology variations and emission potentials like Africa.

5.2 Methods

5.2.1 Model description and application

WRF/Chem is the WRF model online coupled with a chemistry module to predict chemical components and meteorological at the same time [141, 142]. The gas-phase chemical mechanism of RACM-KPP (Regional Atmospheric Chemistry Mechanism of using the Kinetic Pre-Processor) and the aerosol scheme of GOCART (Goddard Global Ozone Chemistry Aerosol Radiation and Transport) are used [240, 241]. YSU boundary layer physics was used as meteorological physics option [149], land surface model of NOAH was used [148], and RRTM schemes were chosen for longwave and Goddard shortwave radiation prediction [150, 151]. WRF outputs were processed by Meteorology-Chemistry Interface Processor (MCIP). The common case is using FNL Operational Global Analysis data from the NCAR [242].The configuration of WRF/Chem is defined in Table 13.

Table 13. The configuration of WRF/Chem.

Process	**WRF/Chem**
Aerosol model	GOCART
Dust option	GOCART-AFWA
Gas-phase mechanism	RACM-KPP
Boundary layer scheme	YSU
Photolysis scheme	Fast-J
Land-surface model	NOAH
Short-wave radiation	Goddard
Long-wave radiation	RRTM

To explore the aerosol radiation feedback effects on air pollutants on meteorology, two simulation situations were steed up. The base case is a simulation without feedbacks (WOF). The comparative case (WF) is simulating with aerosol direct radiation effects. Except for the radiation feedback effects difference, the two cases were the same in everything including model setup and emission

inputs. The difference between the two cases indicates the consequence of aerosol radiation direct effects.

5.2.2 Emission Inventory

Anthropogenic emissions of $PM_{2.5}$, PM_{10}, SO_2, NOx, CO, VOCs, OC, and EC were offered by EDGAR v4.3 with a spatial resolution of 0.1° × 0.1°. The anthropogenic emissions are grouped into six categories: energy agriculture, on-road transportation, industries, off-road transportation, residential activities. The hourly anthropogenic emission files are processed base on weekly and diurnal profiles. Since no local information on Africa was available, the profiles used here are originally designed for U.S. and described in detail by Zhang et al. [153]. The details can be found in Section 3.2.2 and Table 7 and 8. The Model for MEGAN v2.1 was used to generate the biogenic emissions [243].

5.2.3. Model validation

Meteorology and model performances were certified by evaluating meteorological observations and air pollutant concentrations with simulation outcomes. By comparing the prediction results generated by WRF/Chem model with the observation results from the NASA earth science data of aerosol optical depth (AOD) results obtained from Moderate Resolution Imaging Spectroradiometer (MODIS), the performance of WRF/Chem model was validated. Meteorology performance was justified by comparing WRF simulation results with meteorological observations. Meteorological observations were acquired from NCDC, including WD and WS at 10 meters AGL, RH and air temperature at 2 meters AGL. The meteorological stations in Africa of 36 km resolution are marked as red crosses in Figure 31.

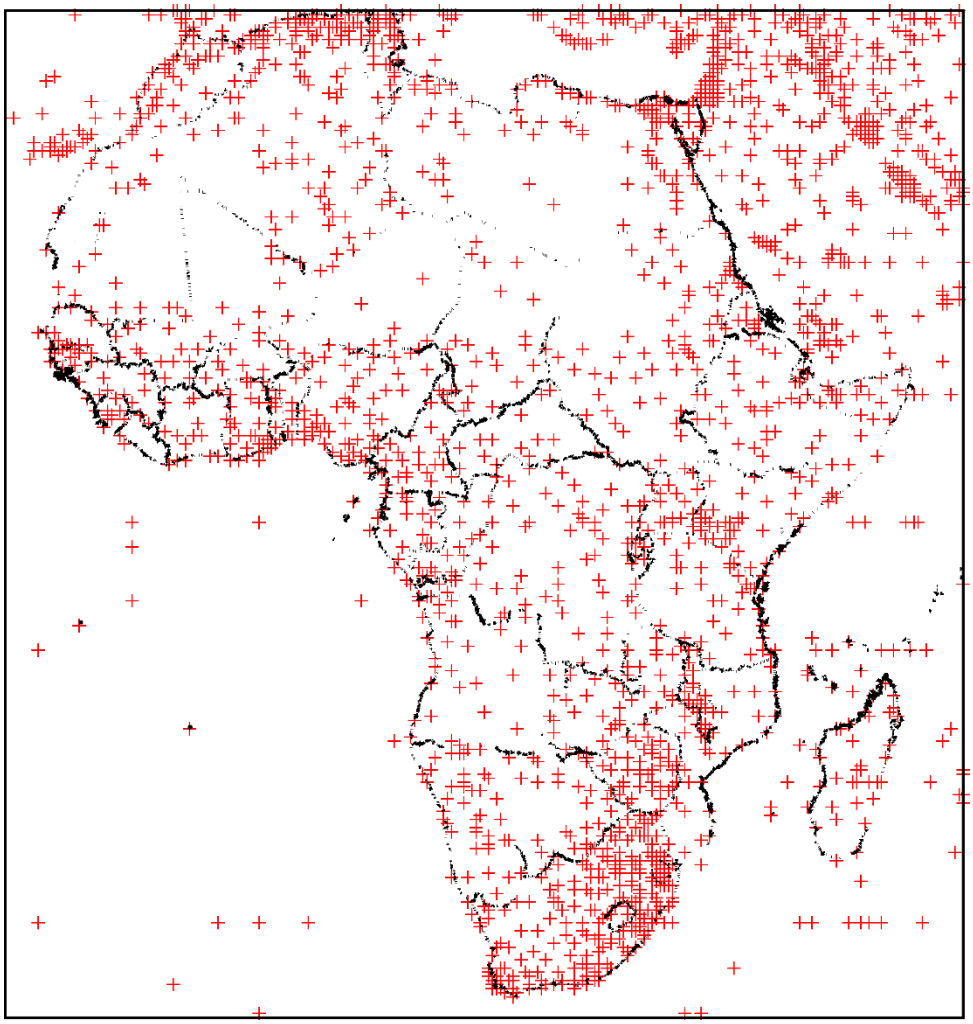

Figure 31. Locations of domains with meteorological stations (red cross X) in Africa.

5.3 Results and discussions

5.3.1 Model validation

5.3.1.1 Meteorology

The WRF model performance was certified during the eight days in January and August of 2015. Simulations results were evaluated by calculating the statistics of MB, RMSE, and GE. Details were shown in Table 14 together with the benchmarks suggested by Emery et al.[107]. T2 was slightly under-estimated in both January and August since MBs values are negative (-0.46 K and -0.59 K, respectively). Whereas WS was over-estimated, as MBs are 0.86 m/s in January and 0.64 m/s in

August. MBs of WD in both months was within the benchmark. The statistics results were also compared with related benchmarks. In terms of T2, GE was surpassing benchmarks by 10% in two months and MB was exceeding benchmark by 20% in August while within benchmark in January. MB of WS was larger than benchmarks by 30% to 70% while GE achieved the benchmarks. RMSE of WS is higher than the benchmark in by 5%-10% in two months. MB of WD was inside the benchmark range while GE was higher than benchmarks by 100% in both months. Since the benchmarks were based on MM5 simulations with finer resolutions of 12km and 4 km for the eastern United States, it cannot be concluded a simulation failure for exceeding the benchmark values.

Table 14. Meteorology performance of January and August in 2015. OBS means observation, PRE means prediction, MB means bias, GE is gross error, and RMSE is root mean square error. The benchmarks are suggested by Emery et al. [107]. Values exceeded the benchmark are represented in bold.

		Jan	Aug	Benchmark
T2(K)	OBS	289.57	300.14	
	PRE	289.10	299.54	
	MB	-0.46	**-0.59**	≤±0.5
	GE	**2.26**	**2.26**	≤2.0
	RMSE	2.98	2.99	
WS(m/s)	OBS	3.80	3.87	
	PRE	4.66	4.50	
	MB	**0.86**	**0.64**	≤±0.5
	GE	1.68	1.63	≤2.0
	RMSE	**2.18**	**2.11**	≤2.0
WD(°)	OBS	167.40	192.42	
	PRE	166.67	188.33	
	MB	2.00	-0.38	≤±10
	GE	**39.92**	**41.74**	≤±30
	RMSE	56.36	58.86	
RH(%)	OBS	63.76	55.33	
	PRE	63.30	56.78	
	MB	-0.45	1.46	
	GE	12.97	12.01	
	RMSE	16.78	16.01	

5.3.1.2 $PM_{2.5}$ and AOD

It is difficult to obtain surface observed air pollutant data because air quality monitoring sites are seldom set in Africa, especially in the whole continent. AOD is widely used as an indicator of $PM_{2.5}$ concentration. Averaged AOD from MODIS and WRF/Chem simulation during the eight days in January and August is showed in Figure 32 and Figure 33. In January, large AOD was found in North Africa and the middle area. Peak AOD values were observed along with the coastal areas in West Africa (Figure 32a). All those patterns of AOD spatial distribution were well captured by the WRF/Chem simulation (Figure 32b). In August, except for some missing in the middle, the model predicted the AOD in the north including the high values in the Red sea area (Figure 33b).

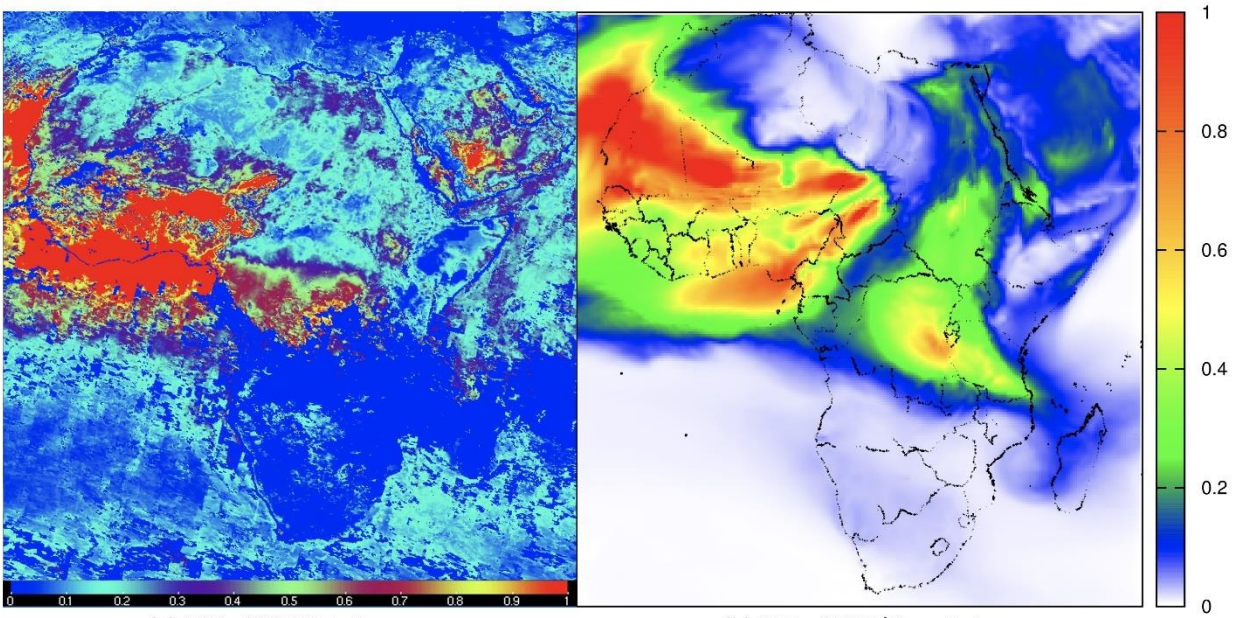

Figure 32. Averaged AOD from MODIS and WRF/Chem simulation during the eight days in January.

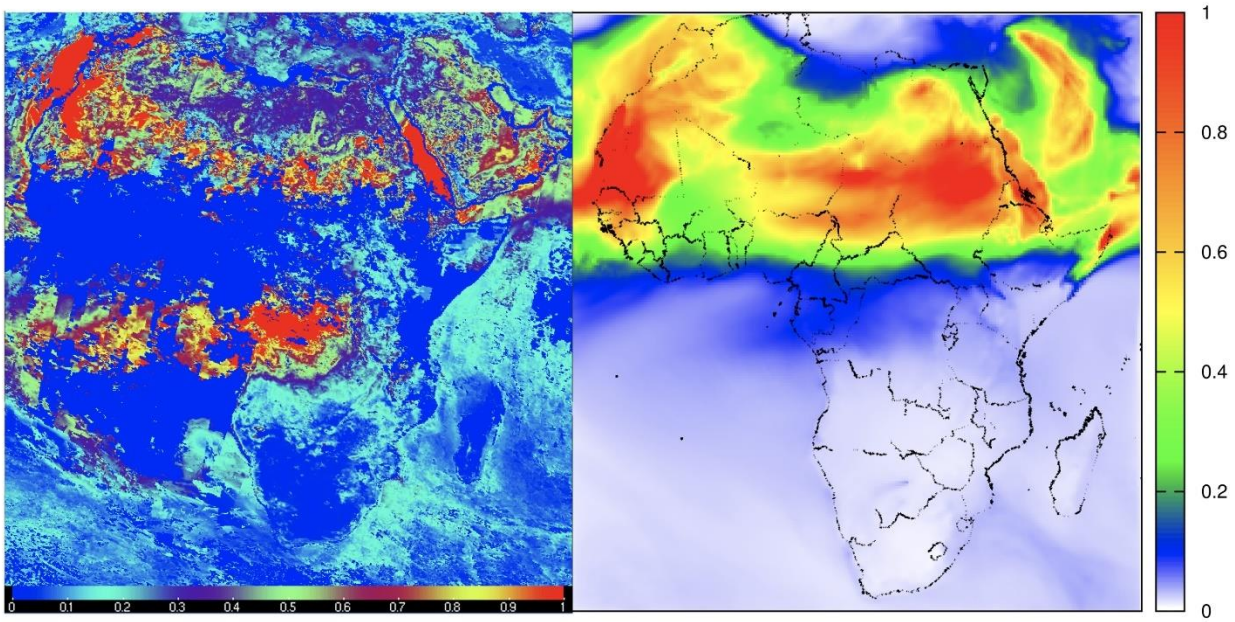

(a) AOD of MODIS in August (b) AOD of WRF/Chem in August

Figure 33. Averaged AOD from MODIS and WRF/Chem simulation during the eight days in August.

5.3.2 Effects of aerosol radiation feedbacks

5.3.2.1 Seasonal and spatial variations

$PM_{2.5}$ concentrations in Africa have obvious variations season and spatial distribution (Figure. 35, Figure. 36). Large areas in west Africa were suffering the $PM_{2.5}$ pollution with more than 500 $\mu g/m^3$ in averaged concentration in January. The peak value of 1600 $\mu g/m^3$ was observed in the middle of the Sahara Desert area (Figure 34a). While in August, high $PM_{2.5}$ concentration was observed in North Africa with an average of ~200 $\mu g/m^3$. Extreme values of more than 400 $\mu g/m^3$ were found near the coastal area of the North Atlantic Ocean and Red sea (Figure 35a).

O_3 showed similar patterns in distribution and range in the two months (Figure. 34c, Figure. 35c). High O_3 concentrations around 35 ppb were found in North and South Africa while low values were found in the middle part. While the difference between peak and valley values in August (~30 ppb) is larger than January (~15 ppb).

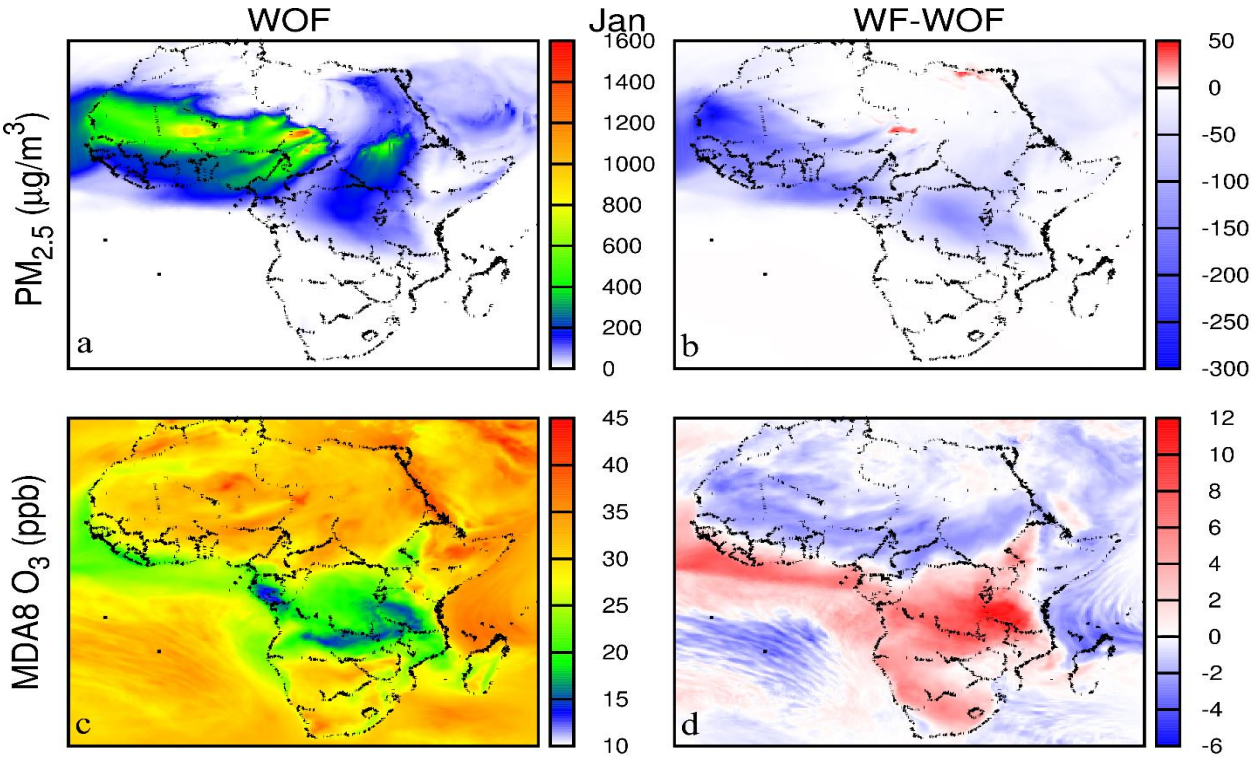

Figure 34. Spatial distribution of predicted $PM_{2.5}$ ($\mu g/m^3$) and MDA8 O_3 concentrations (ppb) in January 2015 without feedback and differences between WF and WOF of Africa.

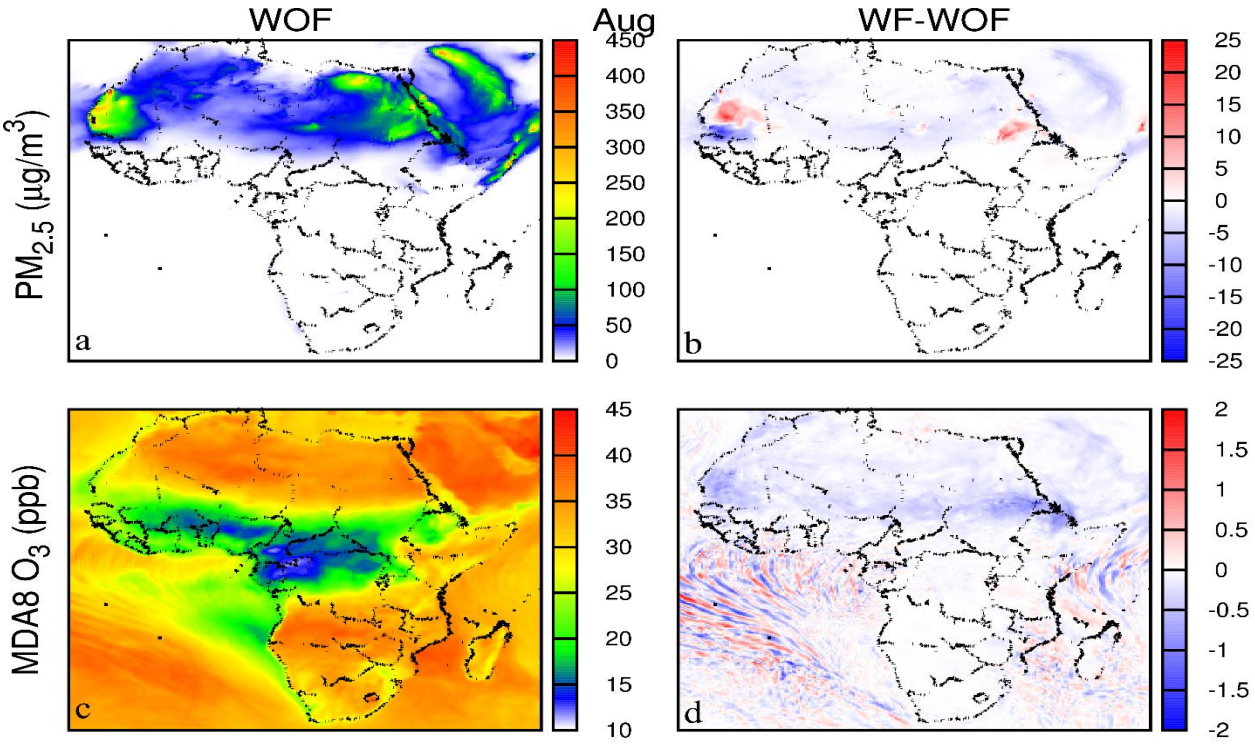

Figure 35. Spatial distribution of predicted $PM_{2.5}$ ($\mu g/m^3$) and MDA8 O_3 concentrations (ppb) in August 2015 without feedback and differences between WF and WOF of Africa.

5.3.2.2 Aerosol radiation feedbacks

Differences between WF and WOF in $PM_{2.5}$ and MDA8 O_3 in January and August are shown in Figure. 34b, Figure. 35b. In January, feedback brought west Africa an up to 300 $\mu g/m^3$ decrease and north and middle Sahara an up to 50 $\mu g/m^3$ increase of $PM_{2.5}$ in concentration. The changes of $PM_{2.5}$ in August were less than 25 $\mu g/m^3$ on average and all were distributed in the north and west Africa. The increase of $PM_{2.5}$ resulted from the decreases in temperature (up to 1 °C in both months) and PBL (up to 120 m in both months) (Figure. 36). Decreased PBL height revealed a more stable atmosphere, which further diminished the spreading of air pollutants. Aerosol radiation feedback effects reduced MDA8 O_3 concentration in North Africa by as much as 6 ppb and increased MDA8 O_3 concentration in South Africa by up to 12 ppb during January (Figure 34d). While only slightly decrease (less than 1 ppb) was found in North Africa in August (Figure 35d). The O_3 reductions in concentration were due to the reduced temperature (around 1 °C in both months) and solar radiation (20-40 w/m^2), which directly lowered photolysis rates and slashed the formation of O_3 (Figure. 36).

5.4 Conclusion

WRF/Chem V3.7.1 was used to simulate $PM_{2.5}$ and O_3 and their aerosol direct radiation feedbacks on meteorology over Africa. Model showed reasonable performance both in predicting meteorology parameters and air pollutants. The meteorology conditions showed big differences in the south and north Africa in January and August of 2015. $PM_{2.5}$ concentration was greater in January with the peak value of 1600 $\mu g/m^3$ in the middle of the Sahara Desert area while extreme values of more than 400 $\mu g/m^3$ were found near the coastal area of North Atlantic Ocean and the Red Sea in August. O_3 concentrations were less than 45 ppb in January and August. The distribution patterns were similar with higher values in north and south and lower values in the

middle in both seasons. Aerosol radiative effects reduced the ground solar radiation by up to 20 w/m^2 in January and 40 w/m^2 in August, lowered the temperature by 1 °C in January and 0.5 °C in August in average, reduced WS by ~0.1 m/s, reduced PBL height by up to 120 m in both months, while slightly increased RH (2-4%). All changes led to decreases of O_3 and $PM_{2.5}$ concentrations. This study indicates the importance of feedbacks from air pollutants and offers a basis for future source apportionment and health-related studies in Africa.

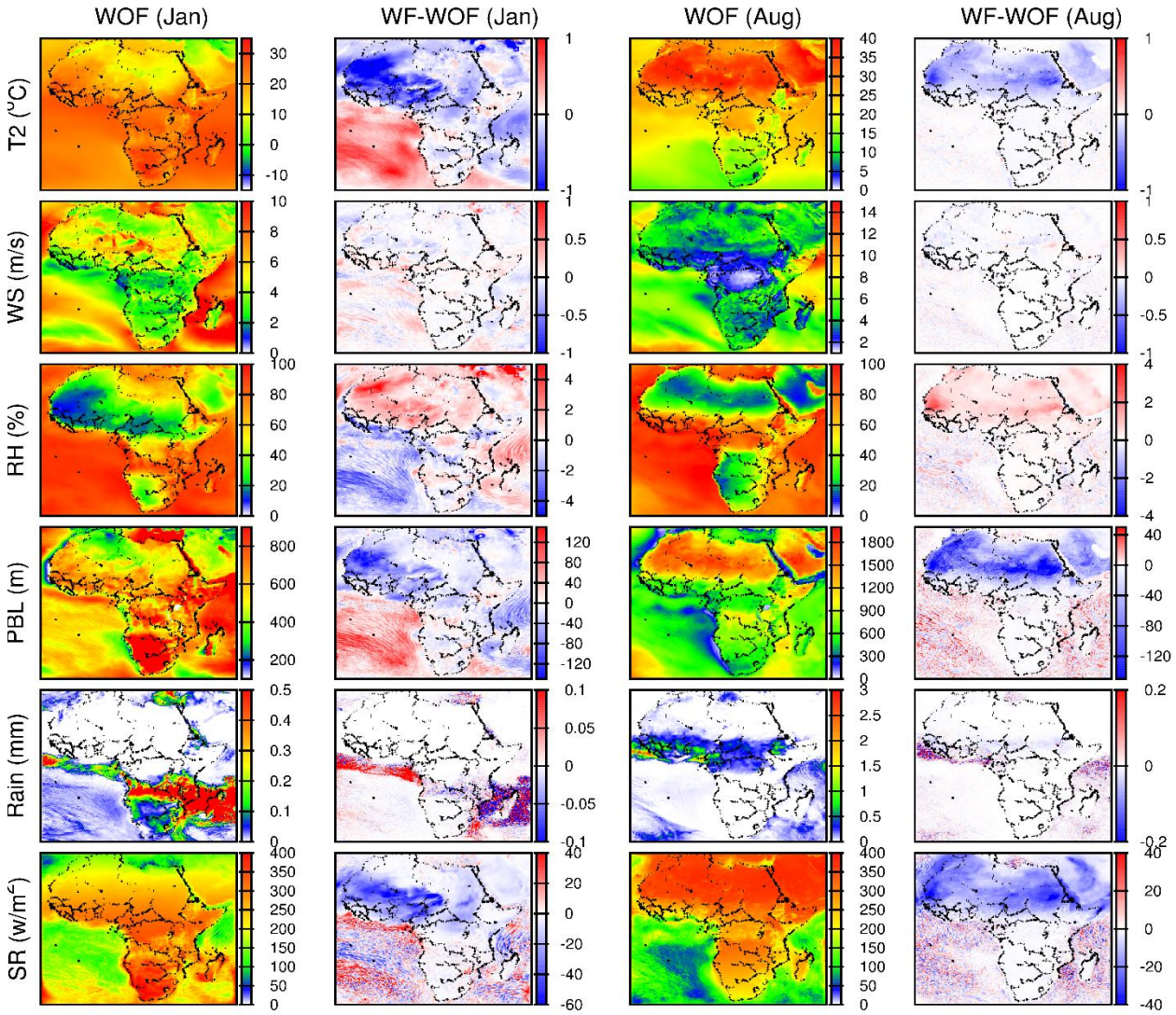

Figure 36. Averaged meteorology in January and August 2015 and the differences from with feedback and without feedback. T2 is temperature at 2 meters above ground, WS is wind speed, RH is relative humidity, PBL is planetary boundary layer height, and SR is the shortwave radiation at surface.

CHAPTER 6. CONCLUSION

Meteorology also plays a vital role in air quality simulation besides emission. In this work, a comprehensive understanding of the communications between air pollution and meteorology was built using chemical transport models. From Chapters 2 to 5, the major analysis and findings based on WRF/Chem and WRF/CMAQ model systems are presented.

In Chapter 2, the responses of $PM_{2.5}$ and O_3 concentrations to changes in emission and meteorology from 2013 to 2015 were investigated based on ambient measurements and CMAQ model simulations with anthropogenic emissions. It is found that emission reductions in 2014 and 2015 effectively reduced $PM_{2.5}$ concentrations by 23.9 and 43.5 $\mu g/m^3$, respectively, but was partially counteracted by unfavorable meteorology. The negative effects of unfavorable meteorology were significant in extreme pollution events. For example, in December 2015, unfavorable meteorology caused a great increase (90 $\mu g/m^3$) of $PM_{2.5}$ in Beijing. Reduction of primary PM and gaseous precursors led to 13.4 and 16.5 ppb increase of MDA8 O_3 daily concentrations in the summertime in 2014 and 2015 in comparison of 2013, which was likely caused by the increase of solar actinic flux due to PM reduction. Besides, the reduction of NOx emissions in areas with negative NOx-O_3 sensitivity could lead to an increase in O_3 formation when the reduction of VOCs was not enough. This unintended enhanced O_3 formation could also lead to higher O_3 in downwind areas. This chapter emphasizes the role of meteorology in pollution control, validates the effectiveness of $PM_{2.5}$ control measures in China, and highlights the importance of appropriate joint reduction of NOx and VOCs to simultaneously decrease O_3 and $PM_{2.5}$ for higher air quality.

In Chapter 3, simulation of $PM_{2.5}$ and O_3 over the SCB with a horizontal resolution of 36 km over China and 12 km was conducted for summer (July) and winter (January) in 2015 using the WRF/Chem model. The model well captured the variations of $PM_{2.5}$ and daily maximum MDA8

O_3 in the 18 cities, especially O_3 in July and $PM_{2.5}$ in January. From rim to the center, averaged $PM_{2.5}$ increased from 40 μg/m^3 to 100 μg/m^3 in January while averaged O_3 ranged from 60 to 90 ppb in July. Aerosol radiation decreased surface temperature by 1–2 °C, WS by ~0.3 m/s, PBL height by 10–20%, SR by ~30%, and precipitation by 0.02–0.2 mm, while increased RH by up to 2-4% in January, which resulted in up to 10 μg/m^3 increase of $PM_{2.5}$ in January and 2 ppb decrease of O_3 in July. The effect increased as the increase of $PM_{2.5}$ concentration and can be up to 18% in January and 25% in July. This chapter highlights the importance of considering meteorology feedbacks in understanding and controlling air pollution in the SCB.

In Chapter 4, simulation of O_3 prediction over the Southeast U.S. at 12km × 12 km grid resolution was conducted for three week-long episodes during summer 2016 to 2018 using WRF/Chem with ensemble meteorological inputs. Ensemble WRF/Chem predictions led by the SREF outputs are accomplished to observe the influence of meteorological uncertainties on the estimating of O_3. Ensemble average showed good performance in predicting O_3 in the Southeast U.S., especially in the Gulf of Mexico coastal and U.S. East Coast areas. O_3 variations were highly related to meteorological conditions such as precipitation, solar radiation, temperature, and wind. The largest fluctuations of O_3 were 4–6 ppb and the O_3 changes due to meteorology uncertainties accounted for at least 10% of averaged O_3 concentration in the Southeast U.S.. The ensemble method was more reliable than any individual run and offered a way to improve CTM performance.

In Chapter 5, simulation of air pollutants like $PM_{2.5}$ and O_3 with effects of aerosol radiation feedbacks over the whole continent of Africa at 36-km grid resolution was conducted for eight days in January (09-16) and August (05-12) 2015 by using Weather Research and Forecasting model coupled with Chemistry (WRF/Chem). $PM_{2.5}$ concentration was higher in January with the peak value of 1600 μg/m^3 in the middle of the Sahara Desert area while extreme values of more

than 400 $\mu g/m^3$ were found near the coastal area of North Atlantic Ocean and Red sea in August. O_3 concentrations were less than 45 ppb in January and August. The distribution patterns were similar in both seasons with higher values in north and south and lower values in the middle. Aerosol radiative effects decreased the ground solar radiation by as much as 20 w/m^2 in January and 40 w/m^2 in August, lowering the temperature by 1 °C in January and 0.5 °C in August in average, reduced WS by ~0.1 m/s, reduced PBL height by up to 120 m in both months, while slightly increased RH (2-4%). All changes led to decreases of O_3 and $PM_{2.5}$ in concentrations. This chapter indicates the importance of study aerosol radiative feedbacks in the areas where have large meteorology variation and emission potential.

Besides the extensive work in this study, there still are many potentials to be investigated and achieved. First indirect, second indirect and semidirect aerosol radiative effects could be included in the simulation of the current WRF/Chem model to completely explore all the physical and chemical reactions that happened between air pollutants and meteorological conditions. Study of health risk, years of life lost, premature mortality, and economic loss due to $PM_{2.5}$ and O_3 could be conducted as well. To couple current WRF/Chem model with Vegetation Photosynthesis and Respiration Model (VPRM) to get more precise biogenic emission or to develop a source-oriented version WRF/Chem for source apportionment will also be another two interesting and achievable topics.

REFERENCES

1. Xu, P.; Chen, Y.; Ye, X., Haze, air pollution, and health in China. *The Lancet* **2013,** *382* (9910).

2. Ma, Z.; Hu, X.; Sayer, A. M.; Levy, R.; Zhang, Q.; Xue, Y.; Tong, S.; Bi, J.; Huang, L.; Liu, Y., Satellite-Based Spatiotemporal Trends in PM2.5 Concentrations: China, 2004-2013. *Environ Health Perspect* **2016,** *124* (2), 184-92.

3. Jacobson, M. Z., Control of fossil-fuel particulate black carbon and organic matter, possibly the most effective method of slowing global warming. *Journal of Geophysical Research* **2002,** *107* (D19).

4. Pui, D. Y. H.; Chen, S.-C.; Zuo, Z., PM 2.5 in China: Measurements, sources, visibility and health effects, and mitigation. *Particuology* **2014,** *13*, 1-26.

5. Lonati, G.; Ozgen, S.; Giugliano, M., Primary and secondary carbonaceous species in PM2.5 samples in Milan (Italy). *Atmospheric Environment* **2007,** *41* (22), 4599-4610.

6. Gelencsér, A.; May, B.; Simpson, D.; Sánchez-Ochoa, A.; Kasper-Giebl, A.; Puxbaum, H.; Caseiro, A.; Pio, C.; Legrand, M., Source apportionment of PM2.5 organic aerosol over Europe: Primary/secondary, natural/anthropogenic, and fossil/biogenic origin. *Journal of Geophysical Research* **2007,** *112* (D23).

7. Wang, D.; Hu, J.; Xu, Y.; Lv, D.; Xie, X.; Kleeman, M.; Xing, J.; Zhang, H.; Ying, Q., Source contributions to primary and secondary inorganic particulate matter during a severe wintertime PM2.5 pollution episode in Xi'an, China. *Atmospheric Environment* **2014,** *97*, 182-194.

8. Hu, J.; Wu, L.; Zheng, B.; Zhang, Q.; He, K.; Chang, Q.; Li, X.; Yang, F.; Ying, Q.; Zhang, H., Source contributions and regional transport of primary particulate matter in China. *Environ Pollut* **2015,** *207*, 31-42.

9. Lu, F.; Xu, D.; Cheng, Y.; Dong, S.; Guo, C.; Jiang, X.; Zheng, X., Systematic review and meta-analysis of the adverse health effects of ambient PM2.5 and PM10 pollution in the Chinese population. *Environ Res* **2015,** *136*, 196-204.

10. Lin, H.; Liu, T.; Xiao, J.; Zeng, W.; Li, X.; Guo, L.; Zhang, Y.; Xu, Y.; Tao, J.; Xian, H.; Syberg, K. M.; Qian, Z. M.; Ma, W., Mortality burden of ambient fine particulate air pollution in six Chinese cities: Results from the Pearl River Delta study. *Environ Int* **2016,** *96*, 91-97.

11. Pope III, C. A.; Burnett, R. T.; Thurston, G. D.; Thun, M. J.; Calle, E. E.; Krewski, D.; Godleski, J. J., Cardiovascular mortality and long-term exposure to particulate air pollution: epidemiological evidence of general pathophysiological pathways of disease. *Circulation* **2004,** *109* (1), 71-77.

12. Boldo, E.; Linares, C.; Lumbreras, J.; Borge, R.; Narros, A.; García-Pérez, J.; Fernández-Navarro, P.; Pérez-Gómez, B.; Aragonés, N.; Ramis, R., Health impact assessment of a reduction in ambient PM2. 5 levels in Spain. *Environment International* **2011,** *37* (2), 342-348.

13. Xing, Y.-F.; Xu, Y.-H.; Shi, M.-H.; Lian, Y.-X., The impact of PM2. 5 on the human respiratory system. *Journal of thoracic disease* **2016,** *8* (1), E69.

14. Wu, R.; Dai, H.; Geng, Y.; Xie, Y.; Masui, T.; Liu, Z.; Qian, Y., Economic impacts from PM2. 5 pollution-related health effects: a case study in Shanghai. *Environmental science & technology* **2017,** *51* (9), 5035-5042.

15. Etchie, T. O.; Sivanesan, S.; Adewuyi, G. O.; Krishnamurthi, K.; Rao, P. S.; Etchie, A. T.; Pillarisetti, A.; Arora, N. K.; Smith, K. R., The health burden and economic costs averted by ambient PM2. 5 pollution reductions in Nagpur, India. *Environment international* **2017,** *102*, 145-156.

16. Squizzato, S.; Masiol, M.; Rich, D. Q.; Hopke, P. K., PM2. 5 and gaseous pollutants in New York State during 2005–2016: Spatial variability, temporal trends, and economic influences. *Atmospheric Environment* **2018,** *183*, 209-224.

17. Kita, K.; Fujiwara, M.; Kawakami, S., Total ozone increase associated with forest fires over the Indonesian region and its relation to the El Nino-Southern oscillation. *Atmospheric Environment* **2000,** *34* (17), 2681-2690.

18. Logan, J. A.; Staehelin, J.; Megretskaia, I. A.; Cammas, J. P.; Thouret, V.; Claude, H.; De Backer, H.; Steinbacher, M.; Scheel, H. E.; Stübi, R.; Fröhlich, M.; Derwent, R., Changes in ozone over Europe: Analysis of ozone measurements from sondes, regular aircraft (MOZAIC) and alpine surface sites. *Journal of Geophysical Research: Atmospheres* **2012,** *117* (D9), n/a-n/a.

19. Verstraeten, W. W.; Neu, J. L.; Williams, J. E.; Bowman, K. W.; Worden, J. R.; Boersma, K. F., Rapid increases in tropospheric ozone production and export from China. *Nature Geoscience* **2015,** *8* (9), 690-695.

20. Ahmadov, R.; McKeen, S.; Trainer, M.; Banta, R.; Brewer, A.; Brown, S.; Edwards, P. M.; de Gouw, J. A.; Frost, G. J.; Gilman, J.; Helmig, D.; Johnson, B.; Karion, A.; Koss, A.; Langford, A.; Lerner, B.; Olson, J.; Oltmans, S.; Peischl, J.; Pétron, G.; Pichugina, Y.; Roberts, J. M.; Ryerson, T.; Schnell, R.; Senff, C.; Sweeney, C.; Thompson, C.; Veres, P. R.; Warneke, C.; Wild, R.; Williams, E. J.; Yuan, B.; Zamora, R., Understanding high wintertime ozone pollution events in an oil- and natural gas-producing region of the western US. *Atmospheric Chemistry and Physics* **2015,** *15* (1), 411-429.

21. Monks, P. S.; Archibald, A.; Colette, A.; Cooper, O.; Coyle, M.; Derwent, R.; Fowler, D.; Granier, C.; Law, K. S.; Mills, G., Tropospheric ozone and its precursors from the urban to the global scale from air quality to short-lived climate forcer. **2015**.

22. Wang, H.; Kiang, C. S.; Tang, X.; Zhou, X.; Chameides, W. L., Surface ozone: A likely threat to crops in Yangtze delta of China. *Atmospheric Environment* **2005,** *39* (21), 3843-3850.

23. Marr, L. C.; Harley, R. A., Spectral analysis of weekday–weekend differences in ambient ozone, nitrogen oxide, and non-methane hydrocarbon time series in California. *Atmospheric Environment* **2002,** *36* (14), 2327-2335.

24. Seinfeld, J. H.; Pandis, S. N., *Atmospheric chemistry and physics: from air pollution to climate change*. John Wiley & Sons: 2012.

25. Wang, X.; Mauzerall, D. L., Characterizing distributions of surface ozone and its impact on grain production in China, Japan and South Korea: 1990 and 2020. *Atmospheric Environment* **2004,** *38* (26), 4383-4402.

26. WHO, Health aspects of air pollution with particulate matter, ozone and nitrogen dioxide: report on a WHO working group. *Copenhagen: WHO Regional Office for Europe* **2003**.

27. Avnery, S.; Mauzerall, D. L.; Liu, J.; Horowitz, L. W., Global crop yield reductions due to surface ozone exposure: 1. Year 2000 crop production losses and economic damage. *Atmospheric Environment* **2011,** *45* (13), 2284-2296.

28. Morgan, P. B.; Mies, T. A.; Bollero, G. A.; Nelson, R. L.; Long, S. P., Season-long elevation of ozone concentration to projected 2050 levels under fully open-air conditions substantially decreases the growth and production of soybean. *New Phytol* **2006,** *170* (2), 333-43.

29. Wang, T.; Xue, L.; Brimblecombe, P.; Lam, Y. F.; Li, L.; Zhang, L., Ozone pollution in China: A review of concentrations, meteorological influences, chemical precursors, and effects. *Sci Total Environ* **2017,** *575*, 1582-1596.

30. Zheng, B.; Tong, D.; Li, M.; Liu, F.; Hong, C.; Geng, G.; Li, H.; Li, X.; Peng, L.; Qi, J.; Yan, L.; Zhang, Y.; Zhao, H.; Zheng, Y.; He, K.; Zhang, Q., Trends in China's anthropogenic emissions since 2010 as the consequence of clean air actions. *Atmospheric Chemistry and Physics* **2018,** *18* (19), 14095-14111.

31. Wang, G.; Zhang, R.; Gomez, M. E.; Yang, L.; Levy Zamora, M.; Hu, M.; Lin, Y.; Peng, J.; Guo, S.; Meng, J.; Li, J.; Cheng, C.; Hu, T.; Ren, Y.; Wang, Y.; Gao, J.; Cao, J.; An, Z.; Zhou, W.; Li, G.; Wang, J.; Tian, P.; Marrero-Ortiz, W.; Secrest, J.; Du, Z.; Zheng, J.; Shang, D.; Zeng, L.; Shao, M.; Wang, W.; Huang, Y.; Wang, Y.; Zhu, Y.; Li, Y.; Hu, J.; Pan, B.; Cai, L.; Cheng, Y.; Ji, Y.; Zhang, F.; Rosenfeld, D.; Liss, P. S.; Duce, R. A.; Kolb, C. E.; Molina, M. J., Persistent sulfate formation from London Fog to Chinese haze. *Proc Natl Acad Sci U S A* **2016,** *113* (48), 13630-13635.

32. Cheng, Y.; Zheng, G.; Wei, C.; Mu, Q.; Zheng, B.; Wang, Z.; Gao, M.; Zhang, Q.; He, K.; Carmichael, G.; Pöschl, U.; Su, H., Reactive nitrogen chemistry in aerosol water as a source of sulfate during haze events in China. *Science Advances* **2016,** *2(12), e1601530.*

33. Han, L.; Cheng, S.; Zhuang, G.; Ning, H.; Wang, H.; Wei, W.; Zhao, X., The changes and long-range transport of PM2. 5 in Beijing in the past decade. *Atmospheric Environment* **2015,** *110*, 186-195.

34. Seinfeld, J. H.; Pandis, S. N., *Atmospheric chemistry and physics: from air pollution to climate change*. John Wiley & Sons: 2016.

35. Grambsch, A., Climate change and air quality. *The Potential Impacts of Climate Change on Transportation, US Department of Transportation* **2002**, 225-235.

36. Zhao, X.; Zhang, X.; Xu, X.; Xu, J.; Meng, W.; Pu, W., Seasonal and diurnal variations of ambient PM2. 5 concentration in urban and rural environments in Beijing. *Atmospheric Environment* **2009,** *43* (18), 2893-2900.

37. Chaloulakou, A.; Kassomenos, P.; Spyrellis, N.; Demokritou, P.; Koutrakis, P., Measurements of PM10 and PM2. 5 particle concentrations in Athens, Greece. *Atmospheric Environment* **2003,** *37* (5), 649-660.

38. Witkowska, A.; Lewandowska, A. U., Water soluble organic carbon in aerosols (PM1, PM2. 5, PM10) and various precipitation forms (rain, snow, mixed) over the southern Baltic Sea station. *Science of the Total Environment* **2016,** *573*, 337-346.

39. Pu, W.-w.; Zhao, X.-j.; Zhang, X.-l.; Ma, Z.-q., Effect of meteorological factors on PM2. 5 during July to September of Beijing. *Procedia Earth and Planetary Science* **2011,** *2*, 272-277.

40. Tai, A. P.; Mickley, L. J.; Jacob, D. J., Correlations between fine particulate matter (PM2. 5) and meteorological variables in the United States: Implications for the sensitivity of PM2. 5 to climate change. *Atmospheric Environment* **2010,** *44* (32), 3976-3984.

41. Jacob, D. J.; Winner, D. A., Effect of climate change on air quality. *Atmospheric Environment* **2009,** *43* (1), 51-63.

42. Rasmussen, D.; Fiore, A.; Naik, V.; Horowitz, L.; McGinnis, S.; Schultz, M., Surface ozone-temperature relationships in the eastern US: A monthly climatology for evaluating chemistry-climate models. *Atmospheric Environment* **2012,** *47*, 142-153.

43. Bloomer, B. J.; Stehr, J. W.; Piety, C. A.; Salawitch, R. J.; Dickerson, R. R., Observed relationships of ozone air pollution with temperature and emissions. *Geophysical Research Letters* **2009,** *36* (9).

44. Shan, W.; Yin, Y.; Zhang, J.; Ding, Y., Observational study of surface ozone at an urban site in East China. *Atmospheric Research* **2008,** *89* (3), 252-261.

45. Nakicenovic, N.; Swart, R., Emissions scenarios. Special report of the Intergovernmental panel on climate change. Cambridge University Press, Cambridge: 2000.

46. Charlson, R. J.; Schwartz, S.; Hales, J.; Cess, R. D.; Coakley, J. J.; Hansen, J.; Hofmann, D., Climate forcing by anthropogenic aerosols. *Science* **1992,** *255* (5043), 423-430.

47. Houghton, J. T.; Jenkins, G. J.; Ephraums, J. J., *Climate change*. 1991.

48. Forster, P.; Ramaswamy, V.; Artaxo, P.; Berntsen, T.; Betts, R.; Fahey, D. W.; Haywood, J.; Lean, J.; Lowe, D. C.; Myhre, G., Changes in atmospheric constituents and in radiative forcing. Chapter 2. In *Climate Change 2007. The Physical Science Basis*, 2007.

49. Ackerman, A. S.; Toon, O.; Stevens, D.; Heymsfield, A.; Ramanathan, V.; Welton, E., Reduction of tropical cloudiness by soot. *Science* **2000,** *288* (5468), 1042-1047.

50. Law, K., Atmospheric chemistry: more ozone over North America. *Nature* **2010,** *463* (7279), 307.

51. Ainsworth, E. A.; Yendrek, C. R.; Sitch, S.; Collins, W. J.; Emberson, L. D., The effects of tropospheric ozone on net primary productivity and implications for climate change. *Annual review of plant biology* **2012,** *63*, 637-661.

52. Cho, K.; Tiwari, S.; Agrawal, S.; Torres, N.; Agrawal, M.; Sarkar, A.; Shibato, J.; Agrawal, G. K.; Kubo, A.; Rakwal, R., Tropospheric ozone and plants: absorption, responses, and consequences. In *Reviews of Environmental Contamination and Toxicology Volume 212*, Springer: 2011; pp 61-111.

53. Karnosky, D. F.; Skelly, J. M.; Percy, K. E.; Chappelka, A. H., Perspectives regarding 50 years of research on effects of tropospheric ozone air pollution on US forests. *Environmental pollution* **2007,** *147* (3), 489-506.

54. Wang, J.; Wang, Y.; Liu, H.; Yang, Y.; Zhang, X.; Li, Y.; Zhang, Y.; Deng, G., Diagnostic identification of the impact of meteorological conditions on PM2. 5 concentrations in Beijing. *Atmospheric environment* **2013,** *81*, 158-165.

55. Huang, X.; Wang, Z.; Ding, A., Impact of Aerosol-PBL Interaction on Haze Pollution: Multiyear Observational Evidences in North China. *Geophysical Research Letters* **2018,** *45* (16), 8596-8603.

56. Filleul, L.; Cassadou, S.; Médina, S.; Fabres, P.; Lefranc, A.; Eilstein, D.; Le Tertre, A.; Pascal, L.; Chardon, B.; Blanchard, M., The relation between temperature, ozone, and mortality in nine French cities during the heat wave of 2003. *Environmental health perspectives* **2006,** *114* (9), 1344-1347.

57. Wang, J.; Wang, S.; Jiang, J.; Ding, A.; Zheng, M.; Zhao, B.; Wong, D. C.; Zhou, W.; Zheng, G.; Wang, L.; Pleim, J. E.; Hao, J., Impact of aerosol–meteorology interactions on fine particle pollution during China's severe haze episode in January 2013. *Environmental Research Letters* **2014,** *9(9), 094002.*

58. Forkel, R.; Werhahn, J.; Hansen, A. B.; McKeen, S.; Peckham, S.; Grell, G.; Suppan, P., Effect of aerosol-radiation feedback on regional air quality–A case study with WRF/Chem. *Atmospheric Environment* **2012,** *53*, 202-211.

59. Wang, H.; Shi, G.; Zhang, X.; Gong, S.; Tan, S.; Chen, B.; Che, H.; Li, T., Mesoscale modelling study of the interactions between aerosols and PBL meteorology during a haze episode in China Jing–Jin–Ji and its near surrounding region–Part 2: Aerosols' radiative feedback effects. *Atmospheric Chemistry and Physics* **2015,** *15* (6), 3277-3287.

60. Werner, M.; Kryza, M.; Skjøth, C. A.; WAŁASZEK, K.; Dore, A. J.; Ojrzyńska, H.; Kapło, J., Aerosol-radiation feedback and PM 10 air concentrations over Poland. In *Geoinformatics and Atmospheric Science*, Springer: 2018; pp 93-110.

61. Pearce, J. L.; Beringer, J.; Nicholls, N.; Hyndman, R. J.; Tapper, N. J., Quantifying the influence of local meteorology on air quality using generalized additive models. *Atmospheric Environment* **2011,** *45* (6), 1328-1336.

62. Langner, J.; Engardt, M.; Baklanov, A.; Christensen, J. H.; Gauss, M.; Geels, C.; Hedegaard, G. B.; Nuterman, R.; Simpson, D.; Soares, J., A multi-model study of impacts of climate change on surface ozone in Europe. *Atmospheric Chemistry and Physics* **2012,** *12* (21), 10423-10440.

63. Kampa, M.; Castanas, E., Human health effects of air pollution. *Environ Pollut* **2008,** *151* (2), 362-7.

64. Zhai, Y.; Liu, X.; Chen, H.; Xu, B.; Zhu, L.; Li, C.; Zeng, G., Source identification and potential ecological risk assessment of heavy metals in PM2.5 from Changsha. *Sci Total Environ* **2014,** *493*, 109-15.

65. WHO, World Health Organization Air Quality Guidelines-global update. *Report on a Working Group meeting* **2005**, Bonn, Germany.

66. Hu, J.; Wang, Y.; Ying, Q.; Zhang, H., Spatial and temporal variability of PM2.5 and PM10 over the North China Plain and the Yangtze River Delta, China. *Atmospheric Environment* **2014,** *95*, 598-609.

67. Chan, C. K.; Yao, X., Air pollution in mega cities in China. *Atmospheric environment* **2008,** *42* (1), 1-42.

68. Hu, J.; Huang, L.; Chen, M.; Liao, H.; Zhang, H.; Wang, S.; Zhang, Q.; Ying, Q., Premature Mortality Attributable to Particulate Matter in China: Source Contributions and Responses to Reductions. *Environ Sci Technol* **2017,** *51* (17), 9950-9959.

69. Patz, J. A.; Campbell-Lendrum, D.; Holloway, T.; Foley, J. A., Impact of regional climate change on human health. *Nature* **2005,** *438* (7066), 310-7.

70. China, T. S. C. o. t. P. s. R. o., Air Pollution Prevention andControl Action Plan. *http://www.gov.cn/zwgk/2013-09/12/content_2486773.htm* **2013**, (in Chinese).

71. Zheng, Y.; Xue, T.; Zhang, Q.; Geng, G.; Tong, D.; Li, X.; He, K., Air quality improvements and health benefits from China's clean air action since 2013. *Environmental Research Letters* **2017,** *12* (11).

72. Chang, L.; Xu, J.; Tie, X.; Wu, J., Impact of the 2015 El Nino event on winter air quality in China. *Scientific Reports* **2016,** *6*, 34275.

73. Hu, D.; Wu, J.; Tian, K.; Liao, L.; Xu, M.; Du, Y., Urban air quality, meteorology and traffic linkages: Evidence from a sixteen-day particulate matter pollution event in December 2015, Beijing. *Journal of Environmental Sciences* **2017,** *59* (Supplement C), 30-38.

74. Wang, W. N.; Cheng, T. H.; Gu, X. F.; Chen, H.; Guo, H.; Wang, Y.; Bao, F. W.; Shi, S. Y.; Xu, B. R.; Zuo, X.; Meng, C.; Zhang, X. C., Assessing Spatial and Temporal Patterns of Observed Ground-level Ozone in China. *Sci Rep* **2017,** *7* (1), 3651.

75. Iny, J.; Brent, A. C.; Joel, S.; Bryan, H.; Petros, K., The impact of weather changes on air quality and health in the United States in 1994–2012. *Environmental Research Letters* **2015,** *10* (8), 084009.

76. Fujita, E. M.; Campbell, D. E.; Stockwell, W. R.; Saunders, E.; Fitzgerald, R.; Perea, R., Projected ozone trends and changes in the ozone-precursor relationship in the South Coast Air Basin in response to varying reductions of precursor emissions. *Journal of the Air & Waste Management Association* **2016,** *66* (2), 201-214.

77. Wu, S.; Mickley, L. J.; Jacob, D. J.; Rind, D.; Streets, D. G., Effects of 2000–2050 changes in climate and emissions on global tropospheric ozone and the policy-relevant background surface ozone in the United States. *Journal of Geophysical Research: Atmospheres* **2008,** *113* (D18).

78. Huang, R. J.; Zhang, Y.; Bozzetti, C.; Ho, K. F.; Cao, J. J.; Han, Y.; Daellenbach, K. R.; Slowik, J. G.; Platt, S. M.; Canonaco, F.; Zotter, P.; Wolf, R.; Pieber, S. M.; Bruns, E. A.; Crippa, M.; Ciarelli, G.; Piazzalunga, A.; Schwikowski, M.; Abbaszade, G.; Schnelle-Kreis, J.; Zimmermann, R.; An, Z.; Szidat, S.; Baltensperger, U.; El Haddad, I.; Prevot, A. S., High secondary aerosol contribution to particulate pollution during haze events in China. *Nature* **2014,** *514* (7521), 218-22.

79. Jiménez, P., Ozone response to precursor controls in very complex terrains: Use of photochemical indicators to assess O3-NOx-VOC sensitivity in the northeastern Iberian Peninsula. *Journal of Geophysical Research* **2004,** *109* (D20).

80. Li, K.; Jacob, D. J.; Liao, H.; Shen, L.; Zhang, Q.; Bates, K. H., Anthropogenic drivers of 2013-2017 trends in summer surface ozone in China. *Proc Natl Acad Sci U S A* **2019,** *116* (2), 422-427.

81. Afroz, R.; Hassan, M. N.; Ibrahim, N. A., Review of air pollution and health impacts in Malaysia. *Environmental Research* **2003,** *92* (2), 71-77.

82. Wang, K.; Zhang, Y.; Jang, C.; Phillips, S.; Wang, B., Modeling intercontinental air pollution transport over the trans-Pacific region in 2001 using the Community Multiscale Air Quality modeling system. *Journal of Geophysical Research* **2009,** *114* (D4).

83. Leibensperger, E. M.; Mickley, L. J.; Jacob, D. J.; Barrett, S. R. H., Intercontinental influence of NOx and CO emissions on particulate matter air quality. *Atmospheric Environment* **2011,** *45* (19), 3318-3324.

84. Shen, L.; Jacob, D. J.; Mickley, L. J.; Wang, Y.; Zhang, Q., Insignificant effect of climate change on winter haze pollution in Beijing. *Atmos. Chem. Phys.* **2018,** *18* (23), 17489-17496.

85. Mahmud, A.; Hixson, M.; Kleeman, M. J., Quantifying population exposure to airborne particulate matter during extreme events in California due to climate change. *Atmos. Chem. Phys.* **2012,** *12* (16), 7453-7463.

86. Zhang, H.; Wang, Y.; Hu, J.; Ying, Q.; Hu, X.-M., Relationships between meteorological parameters and criteria air pollutants in three megacities in China. *Environmental research* **2015,** *140*, 242-254.

87. USEPA, Air quality criteria for ozone and related photochemical oxidants. *US Environmental Protection Agency* **2006**, Washington, DC.

88. Michael Jerrett; Richard T. Burnett; C. Arden Pope III; Kazuhiko Ito; George Thurston; Daniel Krewski; Yuanli Shi; Eugenia Calle; Thun, M., Long-Term Ozone Exposure and Mortality. *New England Journal of Medicine* **2009**, 360(11), 1085-1095.

89. Ghude, S. D.; Chate, D. M.; Jena, C.; Beig, G.; Kumar, R.; Barth, M. C.; Pfister, G. G.; Fadnavis, S.; Pithani, P., Premature mortality in India due to PM2.5

and ozone exposure. *Geophysical Research Letters* **2016,** *43* (9), 4650-4658.

90. Zhang, Q.; Ma, Q.; Zhao, B.; Liu, X.; Wang, Y.; Jia, B.; Zhang, X., Winter haze over North China Plain from 2009 to 2016: Influence of emission and meteorology. *Environ Pollut* **2018,** *242* (Pt B), 1308-1318.

91. Atkinson, R., Atmospheric chemistry of VOCs and NOx. *Atmospheric Environment* **2000,** *34* (12-14), 2063-2101.

92. Megaritis, A. G.; Fountoukis, C.; Charalampidis, P. E.; Denier van der Gon, H. A. C.; Pilinis, C.; Pandis, S. N., Linking climate and air quality over Europe: effects of meteorology on PM2.5 concentrations. *Atmos. Chem. Phys.* **2014,** *14* (18), 10283-10298.

93. Zhang, H.; Hu, J.; Kleeman, M.; Ying, Q., Source apportionment of sulfate and nitrate particulate matter in the Eastern United States and effectiveness of emission control programs. *Science of the Total Environment* **2014,** *490*, 171-181.

94. Kota, S. H.; Guo, H.; Myllyvirta, L.; Hu, J.; Sahu, S. K.; Garaga, R.; Ying, Q.; Gao, A.; Dahiya, S.; Wang, Y.; Zhang, H., Year-long simulation of gaseous and particulate air pollutants in India. *Atmospheric Environment* **2018,** *180*, 244-255.

95. Wang, Y.; Ying, Q.; Hu, J.; Zhang, H., Spatial and temporal variations of six criteria air pollutants in 31 provincial capital cities in China during 2013–2014. *Environment International* **2014,** *73* (0), 413-422.

96. Hu, J.; Wang, Y.; Ying, Q.; Zhang, H., Spatial and temporal variability of PM2.5 and PM10 over the North China Plain and the Yangtze River Delta, China. *Atmospheric Environment* **2014,** *95* (0), 598-609.

97. Hu, J.; Ying, Q.; Wang, Y.; Zhang, H., Characterizing multi-pollutant air pollution in China: Comparison of three air quality indices. *Environment International* **2015,** *84*, 17-25.

98. Ying, Q.; Li, J.; Kota, S. H., Significant Contributions of Isoprene to Summertime Secondary Organic Aerosol in Eastern United States. *Environmental Science & Technology* **2015,** *49* (13), 7834-7842.

99. Hu, J.; Wang, P.; Ying, Q.; Zhang, H.; Chen, J.; Ge, X.; Li, X.; Jiang, J.; Wang, S.; Zhang, J.; Zhao, Y.; Zhang, Y., Modeling biogenic and anthropogenic secondary organic aerosol in China. *Atmos. Chem. Phys.* **2017,** *17* (1), 77-92.

100. Kurokawa, J.; Ohara, T.; Morikawa, T.; Hanayama, S.; Janssens-Maenhout, G.; Fukui, T.; Kawashima, K.; Akimoto, H., Emissions of air pollutants and greenhouse gases over Asian regions during 2000–2008: Regional Emission inventory in ASia (REAS) version 2. *Atmos. Chem. Phys.* **2013,** *13* (21), 11019-11058.

101. Zhang, H.; Li, J.; Ying, Q.; Yu, J. Z.; Wu, D.; Cheng, Y.; He, K.; Jiang, J., Source apportionment of PM2.5 nitrate and sulfate in China using a source-oriented chemical transport model. *Atmospheric Environment* **2012,** *62* (0), 228-242.

102. Hu, J.; Li, X.; Huang, L.; Ying, Q.; Zhang, Q.; Zhao, B.; Wang, S.; Zhang, H., Ensemble Predictions of Air Pollutants in China in 2013 for Health Effects Studies Using WRF/CMAQ Modeling System with Four Emission Inventories. *Atmos. Chem. Phys. Discuss.* **2017,** *2017*, 1-32.

103. Hu, J.; Chen, J.; Ying, Q.; Zhang, H., One-year simulation of ozone and particulate matter in China using WRF/CMAQ modeling system. *Atmos. Chem. Phys.* **2016,** *16* (16), 10333-10350.

104. Shi, Z.; Li, J.; Huang, L.; Wang, P.; Wu, L.; Ying, Q.; Zhang, H.; Lu, L.; Liu, X.; Liao, H.; Hu, J., Source apportionment of fine particulate matter in China in 2013 using a source-oriented chemical transport model. *Science of The Total Environment* **2017,** *601-602*, 1476-1487.

105. Hu, J.; Chen, J.; Ying, Q.; Zhang, H., One-year simulation of ozone and particulate matter in China using WRF/CMAQ modeling system. *Atmospheric Chemistry and Physics* **2016,** *16* (16), 10333-10350.

106. Emery, C.; Tai, E.; Yarwood, G. *Enhanced meteorological modeling and performance evaluation for two texas episodes*; Novato, CA, 2001.

107. Emery, C.; Tai, E.; Yarwood, G., Enhanced meteorological modeling and performance evaluation for two Texas ozone episodes. *Prepared for the Texas natural resource conservation commission, by ENVIRON International Corporation* **2001**.

108. EPA, U., Guidance on the use of models and other analyses for demonstrating attainment of air quality goals for ozone, PM2. 5, and regional haze. *US Environmental Protection Agency, Office of Air Quality Planning and Standards* **2007**.

109. EPA, U. *Guidance on the Use of Models and Other Analyses in Attainment Demonstrations for the 8-hour Ozone NAAQS*; EPA-454/R-05-002: 2005.

110. Boylan, J. W.; Russell., A. G., PM and light extinction model performance metrics, goals, and criteria for three-dimensional air quality models. *Atmospheric environment* **2006,** *40.26*, 4946-4959.

111. Fu, X.; Wang, S.; Chang, X.; Cai, S.; Xing, J.; Hao, J., Modeling analysis of secondary inorganic aerosols over China: pollution characteristics, and meteorological and dust impacts. *Scientific Reports* **2016,** *6*, 35992.

112. Sun, J.; Liu, L.; Xu, L.; Wang, Y.; Wu, Z.; Hu, M.; Shi, Z.; Li, Y.; Zhang, X.; Chen, J.; Li, W., Key Role of Nitrate in Phase Transitions of Urban Particles: Implications of Important Reactive Surfaces for Secondary Aerosol Formation. *Journal of Geophysical Research: Atmospheres* **2018,** *123* (2), 1234-1243.

113. Cheng, Y.; He, K.-b.; Du, Z.-y.; Zheng, M.; Duan, F.-k.; Ma, Y.-l., Humidity plays an important role in the PM2.5 pollution in Beijing. *Environmental Pollution* **2015,** *197*, 68-75.

114. Fine, P. M.; Sioutas, C.; Solomon, P. A., Secondary Particulate Matter in the United States: Insights from the Particulate Matter Supersites Program and Related Studies. *J Air Waste Manag Assoc* **2008,** *58* (2), 234-253.

115. Aw, J.; Kleeman, M. J., Evaluating the first-order effect of intraannual temperature variability on urban air pollution. *Journal of Geophysical Research* **2003,** *108* (D12).

116. Hu, J.; Zhu, Y.; Huang, L.; Zhang, H.; Ying, Q., Unintentional Ozone Increase Due to Particulate Matter Controls in China. *Nature Geoscience* **2018,** *In preparation*.

117. Guo, H.; Chen, K.; Wang, P.; Hu, J.; Ying, Q.; Gao, A.; Zhang, H., Simulation of summer ozone and its sensitivity to emission changes in China. *Atmospheric Pollution Research* **2019,** *10* (5), 1543-1552.

118. Lim, S. S.; Vos, T.; Flaxman, A. D.; Danaei, G.; Shibuya, K.; Adair-Rohani, H.; AlMazroa, M. A.; Amann, M.; Anderson, H. R.; Andrews, K. G., A comparative risk assessment of burden of disease and injury attributable to 67 risk factors and risk factor clusters in 21 regions, 1990–2010: a systematic analysis for the Global Burden of Disease Study 2010. *The lancet* **2012,** *380* (9859), 2224-2260.

119. GRID-Arendal, Time to act - To reduce short-lived climate pollutants, https://www.grida.no/resources/7544. 2014.

120. WHO *Health aspects of air pollution with particulate matter, ozone and nitrogen dioxide: report on a WHO working group, Bonn, Germany 13-15 January 2003*; Copenhagen: WHO Regional Office for Europe: 2003.

121. Luo, C., Sensitivity study of meteorological parameters on mineral aerosol mobilization, transport, and distribution. *Journal of Geophysical Research* **2003,** *108* (D15).

122. Stanier, C. O.; Khlystov, A. Y.; Pandis, S. N., Nucleation Events During the Pittsburgh Air Quality Study: Description and Relation to Key Meteorological, Gas Phase, and Aerosol Parameters Special Issue ofAerosol Science and Technologyon Findings from the Fine Particulate Matter Supersites Program. *Aerosol Science and Technology* **2004,** *38* (sup1), 253-264.

123. Johnson, B.; Shine, K.; Forster, P., The semi-direct aerosol effect: Impact of absorbing aerosols on marine stratocumulus. *Quarterly Journal of the Royal Meteorological Society* **2004,** *130* (599), 1407-1422.

124. Hatzianastassiou, N.; Matsoukas, C.; Drakakis, E.; Stackhouse Jr, P.; Koepke, P.; Fotiadi, A.; Pavlakis, K.; Vardavas, I., The direct effect of aerosols on solar radiation based on satellite observations, reanalysis datasets, and spectral aerosol optical properties from Global Aerosol Data Set (GADS). **2007**.

125. Tao, J.; Ho, K.-F.; Chen, L.; Zhu, L.; Han, J.; Xu, Z., Effect of chemical composition of PM2.5 on visibility in Guangzhou, China, 2007 spring. *Particuology* **2009,** *7* (1), 68-75.

126. Shen, L.; Jacob, D. J.; Mickley, L. J.; Wang, Y.; Zhang, Q., Insignificant effect of climate change on winter haze pollution in Beijing. *Atmospheric Chemistry and Physics* **2018,** *18* (23), 17489-17496.

127. Qiao, X.; Guo, H.; Wang, P.; Tang, Y.; Ying, Q.; Zhao, X.; Deng, W.; Zhang, H., Fine Particulate Matter and Ozone Pollution in the 18 Cities of the Sichuan Basin in Southwestern China: Model Performance and Characteristics. *Aerosol and Air Quality Research* **2019,** *19* (10), 2308-2319.

128. Qiao, X.; Guo, H.; Tang, Y.; Wang, P.; Deng, W.; Zhao, X.; Hu, J.; Ying, Q.; Zhang, H., Local and regional contributions to fine particulate matter in the 18 cities of Sichuan Basin, southwestern China. *Atmospheric Chemistry and Physics* **2019,** *19* (9), 5791-5803.

129. Ning, G.; Wang, S.; Ma, M.; Ni, C.; Shang, Z.; Wang, J.; Li, J., Characteristics of air pollution in different zones of Sichuan Basin, China. *Sci Total Environ* **2018,** *612*, 975-984.

130. Li, Y.; Chen, Q.; Zhao, H.; Wang, L.; Tao, R., Variations in PM10, PM2.5 and PM1.0 in an Urban Area of the Sichuan Basin and Their Relation to Meteorological Factors. *Atmosphere* **2015,** *6* (1), 150-163.

131. Liu, X.; Chen, Q.; Che, H.; Zhang, R.; Gui, K.; Zhang, H.; Zhao, T., Spatial distribution and temporal variation of aerosol optical depth in the Sichuan basin, China, the recent ten years. *Atmospheric Environment* **2016,** *147*, 434-445.

132. Liao, T.; Wang, S.; Ai, J.; Gui, K.; Duan, B.; Zhao, Q.; Zhang, X.; Jiang, W.; Sun, Y., Heavy pollution episodes, transport pathways and potential sources of PM2. 5 during the winter of 2013 in Chengdu (China). *Science of the Total Environment* **2017,** *584*, 1056-1065.

133. Zhang, L.; Guo, X.; Zhao, T.; Gong, S.; Xu, X.; Li, Y.; Luo, L.; Gui, K.; Wang, H.; Zheng, Y., A modelling study of the terrain effects on haze pollution in the Sichuan Basin. *Atmospheric environment* **2019,** *196*, 77-85.

134. Zhang, H.; Li, J.; Ying, Q.; Yu, J.; Wu, D.; Cheng, Y.; He, K.; Jiang, J., Source apportionment of PM2.5 nitrate and sulfate in China using a source-oriented chemical transport model. *Atmospheric Environment* **2012,** *62*, 228-242.

135. Gao, Y.; Zhang, M.; Liu, Z.; Wang, L.; Wang, P.; Xia, X.; Tao, M.; Zhu, L., Modeling the feedback between aerosol and meteorological variables in the atmospheric boundary layer during a severe fog–haze event over the North China Plain. *Atmospheric Chemistry and Physics* **2015,** *15* (8), 4279-4295.

136. Zhuang, B.; Jiang, F.; Wang, T.; Li, S.; Zhu, B., Investigation on the direct radiative effect of fossil fuel black-carbon aerosol over China. *Theoretical and Applied Climatology* **2010,** *104* (3-4), 301-312.

137. Gao, Y.; Zhao, C.; Liu, X.; Zhang, M.; Leung, L. R., WRF-Chem simulations of aerosols and anthropogenic aerosol radiative forcing in East Asia. *Atmospheric Environment* **2014,** *92*, 250-266.

138. Wang, K.; Zhang, Y.; Yahya, K.; Wu, S.-Y.; Grell, G., Implementation and initial application of new chemistry-aerosol options in WRF/Chem for simulating secondary organic aerosols and aerosol indirect effects for regional air quality. *Atmospheric Environment* **2015,** *115*, 716-732.

139. Forkel, R.; Werhahn, J.; Hansen, A. B.; McKeen, S.; Peckham, S.; Grell, G.; Suppan, P., Effect of aerosol-radiation feedback on regional air quality – A case study with WRF/Chem. *Atmospheric Environment* **2012,** *53*, 202-211.

140. Wu, J.; Bei, N.; Hu, B.; Liu, S.; Zhou, M.; Wang, Q.; Li, X.; Liu, L.; Feng, T.; Liu, Z.; Wang, Y.; Cao, J.; Tie, X.; Wang, J.; Molina, L. T.; Li, G., Aerosol–radiation feedback deteriorates the wintertime haze in the North China Plain. *Atmospheric Chemistry and Physics* **2019,** *19* (13), 8703-8719.

141. Fast, J. D.; Gustafson, W. I.; Easter, R. C.; Zaveri, R. A.; Barnard, J. C.; Chapman, E. G.; Grell, G. A.; Peckham, S. E., Evolution of ozone, particulates, and aerosol direct radiative forcing in the vicinity of Houston using a fully coupled meteorology-chemistry-aerosol model. *Journal of Geophysical Research* **2006,** *111* (D21).

142. Grell, G. A.; Peckham, S. E.; Schmitz, R.; McKeen, S. A.; Frost, G.; Skamarock, W. C.; Eder, B., Fully coupled "online" chemistry within the WRF model. *Atmospheric Environment* **2005,** *39* (37), 6957-6975.

143. Buchholz, R. R.; Emmons, L. K.; Tilmes, S.; Team, T. C. D., CESM2.1/CAM-chem Instantaneous Output for Boundary Conditions. *UCAR/NCAR - Atmospheric Chemistry Observations and Modeling Laboratory* **2019,** *Subset used† Lat: -90 to 90, Lon: 0 to 360, January 2015 - December 2015*, https://doi.org/10.5065/NMP7-EP60.

144. Wang, H.; Tian, M.; Chen, Y.; Shi, G.; Liu, Y.; Yang, F.; Zhang, L.; Deng, L.; Yu, J.; Chao, P., Seasonal characteristics, formation mechanisms and source origins of PM 2.5 in two megacities in Sichuan Basin, China. *Atmospheric Chemistry and Physics* **2018,** *18* (2), 865.

145. Liu, H.; Liu, S.; Xue, B.; Lv, Z.; Meng, Z.; Yang, X.; Xue, T.; Yu, Q.; He, K., Ground-level ozone pollution and its health impacts in China. *Atmospheric Environment* **2018,** *173*, 223-230.

146. Liu, L.; Zhang, X.; Xu, W.; Liu, X.; Lu, X.; Chen, D.; Zhang, X.; Wang, S.; Zhang, W., Estimation of monthly bulk nitrate deposition in China based on satellite NO2 measurement by the Ozone Monitoring Instrument. *Remote Sensing of Environment* **2017,** *199*, 93-106.

147. Ying, Q.; Wu, L.; Zhang, H., Local and inter-regional contributions to PM2. 5 nitrate and sulfate in China. *Atmospheric environment* **2014,** *94*, 582-592.

148. Chen, F.; Dudhia, J., Coupling an advanced land surface–hydrology model with the Penn State–NCAR MM5 modeling system. Part I: Model implementation and sensitivity. *Monthly Weather Review* **2001,** *129.4*, 569-585.

149. Hong, S.-Y.; Noh., Y.; Dudhia, J., A new vertical diffusion package with an explicit treatment of entrainment processes. *Monthly weather review* **2006,** *134.9*, 2318-2341.

150. Chou, M.-D.; Suarez, M. J., An efficient thermal infrared radiation parameterization for use in general circulation models. **1994**, 1-85.

151. Mlawer, E. J.; Taubman, S. J.; Brown, P. D.; Iacono, M. J.; Clough, S. A., Radiative transfer for inhomogeneous atmospheres: RRTM, a validated correlated-k model for the longwave. *Journal of Geophysical Research: Atmospheres* **1997,** *102* (D14), 16663-16682.

152. Grell, G. A.; Dévényi, D., A generalized approach to parameterizing convection combining ensemble and data assimilation techniques. *Geophysical Research Letters* **2002,** *29* (14), 38-1-38-4.

153. Zhang, H.; Li, J.; Ying, Q.; Yu, J. Z.; Wu, D.; Cheng, Y.; He, K.; Jiang, J., Source apportionment of PM2. 5 nitrate and sulfate in China using a source-oriented chemical transport model. *Atmospheric environment* **2012,** *62*, 228-242.

154. Wang, X.; Liang, X.-Z.; Jiang, W.; Tao, Z.; Wang, J. X.; Liu, H.; Han, Z.; Liu, S.; Zhang, Y.; Grell, G. A., WRF-Chem simulation of East Asian air quality: Sensitivity to temporal and vertical emissions distributions. *Atmospheric Environment* **2010,** *44* (5), 660-669.

155. Pollack, A. K.; Chan, L.; Chandraker, P.; Grant, J.; Lindhjem, C.; Rao, S.; Russell, J.; Tran, C., WRAP Mobile Source Emission Inventories Update. *ENVIRON International Corporation, Novato, CA. May. http://www. wrapair. org/forums/ef/UMSI/0606_WRAP_Mobile_Source_EI_Final_Report. pdf* **2006**.

156. Lindhjem, C., Development Work for Improved Heavy-Duty Vehicle Modeling Capability Data Mining FHWA Datasets Phase II: Final Report. *EPA Contract* **2004,** (68-C), 02-022.

157. Chinkin, L. R.; Ryan, P. A.; Coe, D. L.; Koerber, M., Recommended improvements to the CMU ammonia emission inventory model for use by LADCO. *Revised final report* **2003**, 902350-2249.

158. Olivier, J.; Peters, J.; Granier, C.; Petron, G.; Müller, J.; Wallens, S. *Present and future surface emissions of atmospheric compounds, POET report {#} 2, EU project EVK2-1999-00011*; Tech. rep., European Union: 2003.

159. Emmons, L. K.; Walters, S.; Hess, P. G.; Lamarque, J. F.; Pfister, G. G.; Fillmore, D.; Granier, C.; Guenther, A.; Kinnison, D.; Laepple, T.; Orlando, J.; Tie, X.; Tyndall, G.; Wiedinmyer, C.; Baughcum, S. L.; Kloster, S., Description and evaluation of the Model for Ozone and Related chemical Tracers, version 4 (MOZART-4). *Geoscientific Model Development* **2010,** *3* (1), 43-67.

160. Hu, J.; Li, X.; Huang, L.; Ying, Q.; Zhang, Q.; Zhao, B.; Wang, S.; Zhang, H., Ensemble Predictions of Air Pollutants in China in 2013 for Health Effects Studies Using WRF/CMAQ Modeling System with Four Emission Inventories. *Atmospheric Chemistry and Physics Discussions* **2017**, 1-32.

161. Zhao, S.; Yu, Y.; Yin, D.; Qin, D.; He, J.; Dong, L., Spatial patterns and temporal variations of six criteria air pollutants during 2015 to 2017 in the city clusters of Sichuan Basin, China. *Sci Total Environ* **2018,** *624*, 540-557.

162. Wang, P.; Guo, H.; Hu, J.; Kota, S. H.; Ying, Q.; Zhang, H., Responses of PM2. 5 and O3 concentrations to changes of meteorology and emissions in China. *Science of the Total Environment* **2019,** *662*, 297-306.

163. Jacobson, M. Z., Studying the effects of aerosols on vertical photolysis rate coefficient and temperature profiles over an urban airshed. *Journal of Geophysical Research: Atmospheres* **1998,** *103* (D9), 10593-10604.

164. Wilkinson, S.; Mills, G.; Illidge, R.; Davies, W. J., How is ozone pollution reducing our food supply? *Journal of Experimental Botany* **2012,** *63* (2), 527-536.

165. WHO, Review of evidence on health aspects of air pollution–REVIHAAP project: final technical report. *Bonn: WHO European Centre for Environment and Health* **2013**.

166. Madrigano, J.; Jack, D.; Anderson, G. B.; Bell, M. L.; Kinney, P. L., Temperature, ozone, and mortality in urban and non-urban counties in the northeastern United States. *Environmental Health* **2015,** *14* (1), 3.

167. CR, O. L.; Chang, H. H.; Kramer, M. R.; Winquist, A.; Mulholland, J. A.; Friberg, M. D.; Sarnat, S. E., Ozone and childhood respiratory disease in three US cities: evaluation of effect measure modification by neighborhood socioeconomic status using a Bayesian hierarchical approach. *Environ Health* **2017,** *16* (1), 36.

168. Sheffield, P. E.; Knowlton, K.; Carr, J. L.; Kinney, P. L., Modeling of regional climate change effects on ground-level ozone and childhood asthma. *Am J Prev Med* **2011,** *41* (3), 251-7; quiz A3.

169. Sousa, S. I.; Alvim-Ferraz, M. C.; Martins, F. G., Health effects of ozone focusing on childhood asthma: what is now known--a review from an epidemiological point of view. *Chemosphere* **2013,** *90* (7), 2051-8.

170. Bell, M. L.; McDermott, A.; Zeger, S. L.; Samet, J. M.; Dominici, F., Ozone and short-term mortality in 95 US urban communities, 1987-2000. *Jama* **2004,** *292* (19), 2372-2378.

171. Nuvolone, D.; Petri, D.; Voller, F., The effects of ozone on human health. *Environ Sci Pollut Res Int* **2018,** *25* (9), 8074-8088.

172. Maji, K. J.; Ye, W. F.; Arora, M.; Nagendra, S. M. S., Ozone pollution in Chinese cities: Assessment of seasonal variation, health effects and economic burden. *Environ Pollut* **2019,** *247*, 792-801.

173. Ghude, S. D.; Chate, D. M.; Jena, C.; Beig, G.; Kumar, R.; Barth, M. C.; Pfister, G. G.; Fadnavis, S.; Pithani, P., Premature mortality in India due to PM2.5 and ozone exposure. *Geophysical Research Letters* **2016,** *43* (9), 4650-4658.

174. McGrath, J. M.; Betzelberger, A. M.; Wang, S.; Shook, E.; Zhu, X. G.; Long, S. P.; Ainsworth, E. A., An analysis of ozone damage to historical maize and soybean yields in the United States. *Proc Natl Acad Sci U S A* **2015,** *112* (46), 14390-5.

175. Feng, Z.; De Marco, A.; Anav, A.; Gualtieri, M.; Sicard, P.; Tian, H.; Fornasier, F.; Tao, F.; Guo, A.; Paoletti, E., Economic losses due to ozone impacts on human health, forest productivity and crop yield across China. *Environ Int* **2019,** *131*, 104966.

176. Ritter, M.; Müller, M. D.; Jorba, O.; Parlow, E.; Liu, L.-J. S., Impact of chemical and meteorological boundary and initial conditions on air quality modeling: WRF-Chem sensitivity evaluation for a European domain. *Meteorology and Atmospheric Physics* **2013,** *119* (1-2), 59-70.

177. Zhong, M.; Saikawa, E.; Liu, Y.; Naik, V.; Horowitz, L. W.; Takigawa, M.; Zhao, Y.; Lin, N.-H.; Stone, E. A., Air quality modeling with WRF-Chem v3. 5 in East Asia: sensitivity to emissions and evaluation of simulated air quality. *Geosci Model Dev* **2016,** *9* (3), 1201-1218.

178. Zhang, Y.; Wang, Y., Climate-driven ground-level ozone extreme in the fall over the Southeast United States. *Proc Natl Acad Sci U S A* **2016,** *113* (36), 10025-30.

179. Jing, P.; Lu, Z.; Xing, J.; Streets, D. G.; Tan, Q.; O'Brien, T.; Kamberos, J., Response of the summertime ground-level ozone trend in the Chicago area to emission controls and temperature changes, 2005–2013. *Atmospheric Environment* **2014,** *99*, 630-640.

180. Seaman, N. L., Meteorological modeling for air-quality assessments. *Atmospheric environment* **2000,** *34* (12-14), 2231-2259.

181. Kim, S. W.; Heckel, A.; McKeen, S.; Frost, G.; Hsie, E. Y.; Trainer, M.; Richter, A.; Burrows, J.; Peckham, S.; Grell, G., Satellite-observed US power plant NOx emission reductions and their impact on air quality. *Geophysical Research Letters* **2006,** *33* (22).

182. Zhou, Y.; Brunner, D.; Hueglin, C.; Henne, S.; Staehelin, J., Changes in OMI tropospheric NO2 columns over Europe from 2004 to 2009 and the influence of meteorological variability. *Atmospheric Environment* **2012,** *46*, 482-495.

183. Pugliese, S. C.; Murphy, J. G.; Geddes, J. A.; Wang, J. M., The impacts of precursor reduction and meteorology on ground-level ozone in the Greater Toronto Area. *Atmospheric Chemistry and Physics Discussions* **2014,** *14* (7), 10209-10239.

184. Jaffe, D.; Zhang, L., Meteorological anomalies lead to elevated O3 in the western US in June 2015. *Geophysical Research Letters* **2017,** *44* (4), 1990-1997.

185. Stensrud, D. J.; Brooks, H. E.; Du, J.; Tracton, M. S.; Rogers, E., Using ensembles for short-range forecasting. *Monthly Weather Review* **1999,** *127* (4), 433-446.

186. Delle Monache, L.; Stull, R., An ensemble air-quality forecast over western Europe during an ozone episode. *Atmospheric Environment* **2003,** *37* (25), 3469-3474.

187. Gilliam, R. C.; Hogrefe, C.; Godowitch, J. M.; Napelenok, S.; Mathur, R.; Rao, S. T., Impact of inherent meteorology uncertainty on air quality model predictions. *Journal of Geophysical Research: Atmospheres* **2015,** *120* (23), 12,259-12,280.

188. Stevenson, D. S.; Dentener, F. J.; Schultz, M. G.; Ellingsen, K.; van Noije, T. P. C.; Wild, O.; Zeng, G.; Amann, M.; Atherton, C. S.; Bell, N.; Bergmann, D. J.; Bey, I.; Butler, T.; Cofala, J.; Collins, W. J.; Derwent, R. G.; Doherty, R. M.; Drevet, J.; Eskes, H. J.; Fiore, A. M.; Gauss, M.; Hauglustaine, D. A.; Horowitz, L. W.; Isaksen, I. S. A.; Krol, M. C.; Lamarque, J. F.; Lawrence, M. G.; Montanaro, V.; Müller, J. F.; Pitari, G.; Prather, M. J.; Pyle, J. A.; Rast, S.; Rodriguez, J. M.; Sanderson, M. G.; Savage, N. H.; Shindell, D. T.; Strahan, S. E.; Sudo, K.; Szopa, S., Multimodel ensemble simulations of present-day and near-future tropospheric ozone. *Journal of Geophysical Research* **2006,** *111* (D8).

189. Vautard, R.; Van Loon, M.; Schaap, M.; Bergström, R.; Bessagnet, B.; Brandt, J.; Builtjes, P. J. H.; Christensen, J. H.; Cuvelier, C.; Graff, A.; Jonson, J. E.; Krol, M.; Langner, J.; Roberts, P.; Rouil, L.; Stern, R.; Tarrasón, L.; Thunis, P.; Vignati, E.; White, L.; Wind, P., Is regional air quality model diversity representative of uncertainty for ozone simulation? *Geophysical Research Letters* **2006,** *33* (24).

190. van Loon, M.; Vautard, R.; Schaap, M.; Bergström, R.; Bessagnet, B.; Brandt, J.; Builtjes, P. J. H.; Christensen, J. H.; Cuvelier, C.; Graff, A.; Jonson, J. E.; Krol, M.; Langner, J.; Roberts, P.; Rouil, L.; Stern, R.; Tarrasón, L.; Thunis, P.; Vignati, E.; White, L.; Wind, P., Evaluation of long-term ozone simulations from seven regional air quality models and their ensemble. *Atmospheric Environment* **2007,** *41* (10), 2083-2097.

191. Solazzo, E.; Bianconi, R.; Vautard, R.; Appel, K. W.; Moran, M. D.; Hogrefe, C.; Bessagnet, B.; Brandt, J.; Christensen, J. H.; Chemel, C., Model evaluation and ensemble modelling of surface-level ozone in Europe and North America in the context of AQMEII. *Atmospheric environment* **2012,** *53*, 60-74.

192. Delle Monache, L.; Deng, X.; Zhou, Y.; Stull, R., Ozone ensemble forecasts: 1. A new ensemble design. *Journal of Geophysical Research* **2006,** *111* (D5).

193. Mallet, V.; Sportisse, B., Ensemble-based air quality forecasts: A multimodel approach applied to ozone. *Journal of Geophysical Research* **2006,** *111* (D18).

194. Mallet, V.; Sportisse, B., Uncertainty in a chemistry-transport model due to physical parameterizations and numerical approximations: An ensemble approach applied to ozone modeling. *Journal of Geophysical Research* **2006,** *111* (D1).

195. Bei, N.; Lei, W.; Zavala, M.; Molina, L. T., Ozone predictabilities due to meteorological uncertainties in the Mexico City basin using ensemble forecasts. *Atmospheric Chemistry and Physics* **2010,** *10* (13), 6295-6309.

196. Boynard, A.; Beekmann, M.; Foret, G.; Ung, A.; Szopa, S.; Schmechtig, C.; Coman, A., An ensemble assessment of regional ozone model uncertainty with an explicit error representation. *Atmospheric Environment* **2011,** *45* (3), 784-793.

197. Žabkar, R.; Koračin, D.; Rakovec, J., A WRF/Chem sensitivity study using ensemble modelling for a high ozone episode in Slovenia and the Northern Adriatic area. *Atmospheric Environment* **2013,** *77*, 990-1004.

198. Dawson, J. P.; Adams, P. J.; Pandis, S. N., Sensitivity of ozone to summertime climate in the eastern USA: A modeling case study. *Atmospheric Environment* **2007,** *41* (7), 1494-1511.

199. Du, J.; DiMego, G.; Tracton, M.; Zhou, B., NCEP short-range ensemble forecasting (SREF) system: multi-IC, multi-model and multi-physics approach. *Research activities in atmospheric and oceanic modelling* **2003,** *33*, 5.09-5.10.

200. Du, J. In *Recent upgrade of NCEP short-range ensemble forecast (SREF) system*, 23rd Conference on Weather Analysis and Forecasting/19th Conference on Numerical Weather Prediction, 2009.

201. USEPA, Air Quality System Data Mart [internet database] available via https://www.epa.gov/airdata. Accessed 03 02, 2020. **2020**.

202. Tracton, M. S.; Du, J.; Toth, Z.; Juang, H., Short range ensemble forecasting (SREF) at NCEP/EMC. *WORLD METEOROLOGICAL ORGANIZATION-PUBLICATIONS-WMO TD* **1998**, 5.58-5.59.

203. USEPA, Air Pollutant Emissions Trends Data, https://www.epa.gov/air-emissions-inventories/air-pollutant-emissions-trends-data. **2018**.

204. Wiedinmyer.; Christine.; Akagi., S. K.; Yokelson., R. J.; Emmons., L. K.; Al-Saadi., J. A.; Orlando., J. J.; Soja, A. J., The Fire INventory from NCAR (FINN): A high resolution global model to estimate the emissions from open burning. *Geoscientific Model Development* **2011,** *4.3*, 625.

205. Chan, E.; Vet, R., Baseline levels and trends of ground level ozone in Canada and the United States. *Atmospheric Chemistry and Physics* **2010,** *10* (18), 8629.

206. Prospero, J. M.; Ginoux, P.; Torres, O.; Nicholson, S. E.; Gill, T. E., Environmental characterization of global sources of atmospheric soil dust identified with the Nimbus 7 Total Ozone Mapping Spectrometer (TOMS) absorbing aerosol product. *Reviews of geophysics* **2002,** *40* (1), 2-1-2-31.

207. Washington, R.; Todd, M.; Middleton, N. J.; Goudie, A. S., Dust-storm source areas determined by the total ozone monitoring spectrometer and surface observations. *Annals of the Association of American Geographers* **2003,** *93* (2), 297-313.

208. Goudie, A.; Middleton, N., Saharan dust storms: nature and consequences. *Earth-science reviews* **2001,** *56* (1-4), 179-204.

209. Khajuria, A.; Yamamoto, Y.; Morioka, T., Estimation of municipal solid waste generation and landfill area in Asian developing countries. *Journal of Environmental Biology* **2010,** *31* (5), 649-654.

210. Kan, H.; Chen, R.; Tong, S., Ambient air pollution, climate change, and population health in China. *Environment international* **2012,** *42*, 10-19.

211. McGranahan, G., *Air pollution and health in rapidly developing countries*. Earthscan: 2012.

212. Guttikunda, S. K.; Calori, G., A GIS based emissions inventory at 1 km× 1 km spatial resolution for air pollution analysis in Delhi, India. *Atmospheric Environment* **2013,** *67*, 101-111.

213. Ezeh, A. C.; Bongaarts, J.; Mberu, B., Global population trends and policy options. *The Lancet* **2012,** *380* (9837), 142-148.

214. Petkova, E. P.; Jack, D. W.; Volavka-Close, N. H.; Kinney, P. L., Particulate matter pollution in African cities. *Air Quality, Atmosphere & Health* **2013,** *6* (3), 603-614.

215. Shen, L.; Shuai, C.; Jiao, L.; Tan, Y.; Song, X., Dynamic sustainability performance during urbanization process between BRICS countries. *Habitat International* **2017,** *60*, 19-33.

216. Antonel, J.; Chowdhury, Z., Measuring ambient particulate matter in three cities in Cameroon, Africa. *Atmospheric Environment* **2014,** *95*, 344-354.

217. Eliasson, I.; Jonsson, P.; Holmer, B., Diurnal and intra-urban particle concentrations in relation to windspeed and stability during the dry season in three African cities. *Environmental monitoring and assessment* **2009,** *154* (1-4), 309.

218. Assamoi, E.-M.; Liousse, C., A new inventory for two-wheel vehicle emissions in West Africa for 2002. *Atmospheric Environment* **2010,** *44* (32), 3985-3996.

219. Nriagu, J. O., Toxic metal pollution in Africa. *Science of the Total Environment* **1992,** *121*, 1-37.

220. Van Niekerk, W.; Simpson, D.; Fourie, M.; Mouton, G., Diesel particulate emission in the South African mining industry. **2002**.

221. Armah, F. A.; Odoi, J. O.; Luginaah, I., Indoor air pollution and health in Ghana: Self-reported exposure to unprocessed solid fuel smoke. *EcoHealth* **2015,** *12* (2), 227-243.

222. Sam, R.; Ofosu, F.; Atiemo, S.; Aboh, I.; Gyampo, O.; Ahiamadjie, H.; Adeti, J.; Arthur, J., Heavy metal contamination levels in topsoil at selected auto workshops in Accra. *International Journal of Science and Technology* **2015,** *4* (5), 222-9.

223. Gaspar, F. W.; Chevrier, J.; Bornman, R.; Crause, M.; Obida, M.; Barr, D. B.; Bradman, A.; Bouwman, H.; Eskenazi, B., Undisturbed dust as a metric of long-term indoor insecticide exposure: Residential DDT contamination from indoor residual spraying and its association with serum levels in the VHEMBE cohort. *Environment international* **2015,** *85*, 163-167.

224. Van Tienhoven, A. M.; Otter, L.; Lenkopane, M.; Zunckel, M.; Venjonoka, K., Assessment of ozone impacts on vegetation in southern Africa and directions for future research: commentary. *South African journal of science* **2005,** *101* (3), 143-148.

225. Van Tienhoven, A.; Scholes, M., Air pollution impacts on vegetation in South Africa. *Air pollution impacts on crops and forests: A global assessment* **2003**, 237-262.

226. Kirkmana, G.; Piketha, S.; Andreae, M.; Annegarn, H.; Helas, G., Distribution of aerosols, ozone and carbon monoxide over southern Africa. **2017**.

227. Laakso, L.; Beukes, J. P.; Van Zyl, P. G.; Pienaar, J. J.; Josipovic, M.; Venter, A.; Jaars, K.; Vakkari, V.; Labuschagne, C.; Chiloane, K., Ozone concentrations and their potential impacts on vegetation in southern Africa. In *Developments in Environmental Science*, Elsevier: 2013; Vol. 13, pp 429-450.

228. Feng, S.; Gao, D.; Liao, F.; Zhou, F.; Wang, X., The health effects of ambient PM2. 5 and potential mechanisms. *Ecotoxicology and environmental safety* **2016,** *128*, 67-74.

229. Zhang, X.; Kang, J.; Chen, H.; Yao, M.; Wang, J., PM2. 5 meets blood: In vivo damages and immune defense. *Aerosol and Air Quality Research* **2018,** *18* (2), 456-470.

230. McGrath, J. M.; Betzelberger, A. M.; Wang, S.; Shook, E.; Zhu, X.-G.; Long, S. P.; Ainsworth, E. A., An analysis of ozone damage to historical maize and soybean yields in the United States. *Proceedings of the National Academy of Sciences* **2015,** *112* (46), 14390-14395.

231. Karlsson, P. E.; Klingberg, J.; Engardt, M.; Andersson, C.; Langner, J.; Karlsson, G. P.; Pleijel, H., Past, present and future concentrations of ground-level ozone and potential impacts on ecosystems and human health in northern Europe. *Science of the Total Environment* **2017,** *576*, 22-35.

232. Arya, S. P., *Air pollution meteorology and dispersion*. Oxford University Press New York: 1999; Vol. 6.

233. Leroux, M., *The meteorology and climate of tropical Africa*. Springer Science & Business Media: 2001.

234. Rossignol-Strick, M., African monsoons, an immediate climate response to orbital insolation. *Nature* **1983,** *304* (5921), 46-49.

235. Funk, C.; Hoell, A.; Shukla, S.; Husak, G.; Michaelsen, J., The east african monsoon system: Seasonal climatologies and recent variations. In *The Monsoons and Climate Change*, Springer: 2016; pp 163-185.

236. Zhao, C.; Liu, X.; Leung, L.; Hagos, S., Radiative impact of mineral dust on monsoon precipitation variability over West Africa. *Atmospheric Chemistry and Physics Discussions* **2010,** *10* (11), 27185-27226.

237. Tummon, F.; Solmon, F.; Liousse, C.; Tadross, M., Simulation of the direct and semidirect aerosol effects on the southern Africa regional climate during the biomass burning season. *Journal of Geophysical Research: Atmospheres* **2010,** *115* (D19).

238. Zhao, C.; Liu, X.; Leung, L.; Johnson, B.; McFarlane, S. A.; Gustafson Jr, W.; Fast, J. D.; Easter, R., The spatial distribution of mineral dust and its shortwave radiative forcing over North Africa: modeling sensitivities to dust emissions and aerosol size treatments. *Atmospheric Chemistry and Physics* **2010,** *10* (18), 8821.

239. Zhao, C.; Chen, S.; Leung, L. R.; Qian, Y.; Kok, J.; Zaveri, R.; Huang, J., Uncertainty in modeling dust mass balance and radiative forcing from size parameterization. *Atmospheric Chemistry & Physics Discussions* **2013,** *13* (7).

240. Stockwell, W. R.; Kirchner, F.; Kuhn, M.; Seefeld, S., A new mechanism for regional atmospheric chemistry modeling. *Journal of Geophysical Research: Atmospheres* **1997,** *102* (D22), 25847-25879.

241. Chin, M.; Ginoux, P.; Kinne, S.; Torres, O.; Holben, B. N.; Duncan, B. N.; Martin, R. V.; Logan, J. A.; Higurashi, A.; Nakajima, T., Tropospheric aerosol optical thickness from the GOCART model and comparisons with satellite and Sun photometer measurements. *Journal of the atmospheric sciences* **2002,** *59* (3), 461-483.

242. Wiedinmyer, C.; Yokelson, R. J.; Gullett, B. K., Global emissions of trace gases, particulate matter, and hazardous air pollutants from open burning of domestic waste. *Environmental science & technology* **2014,** *48* (16), 9523-9530.

243. Guenther, A.; Jiang, X.; Heald, C.; Sakulyanontvittaya, T.; Duhl, T.; Emmons, L.; Wang, X., The Model of Emissions of Gases and Aerosols from Nature version 2.1 (MEGAN2. 1): an extended and updated framework for modeling biogenic emissions. **2012**.

APPENDIX A. PUBLICATION AGREEMENTS

For Chapter 2

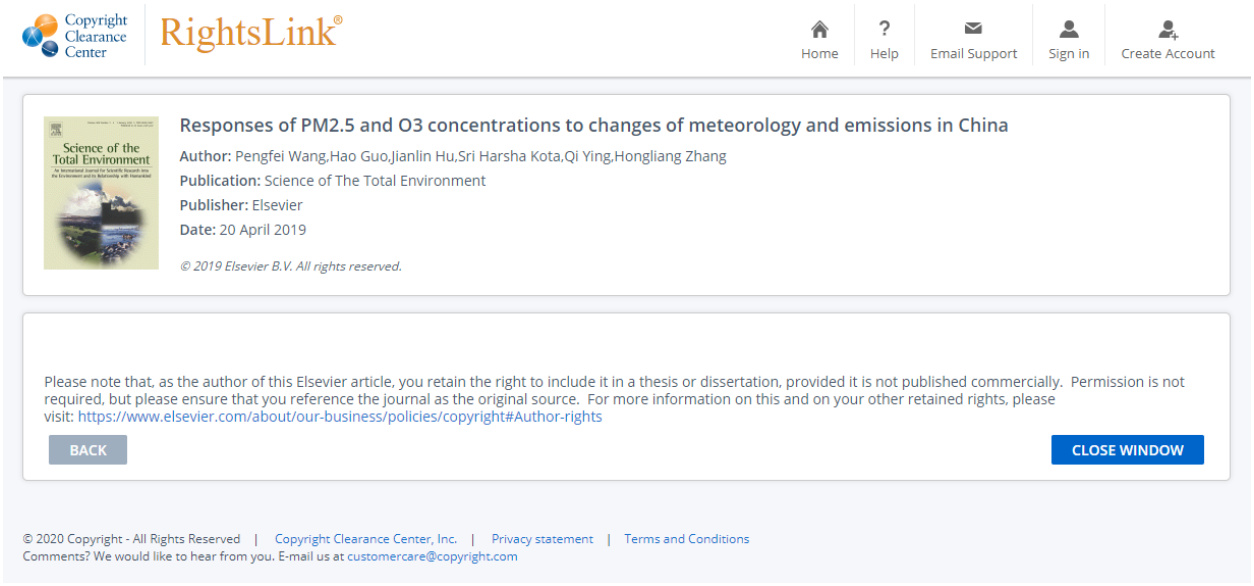

For Chapter 3

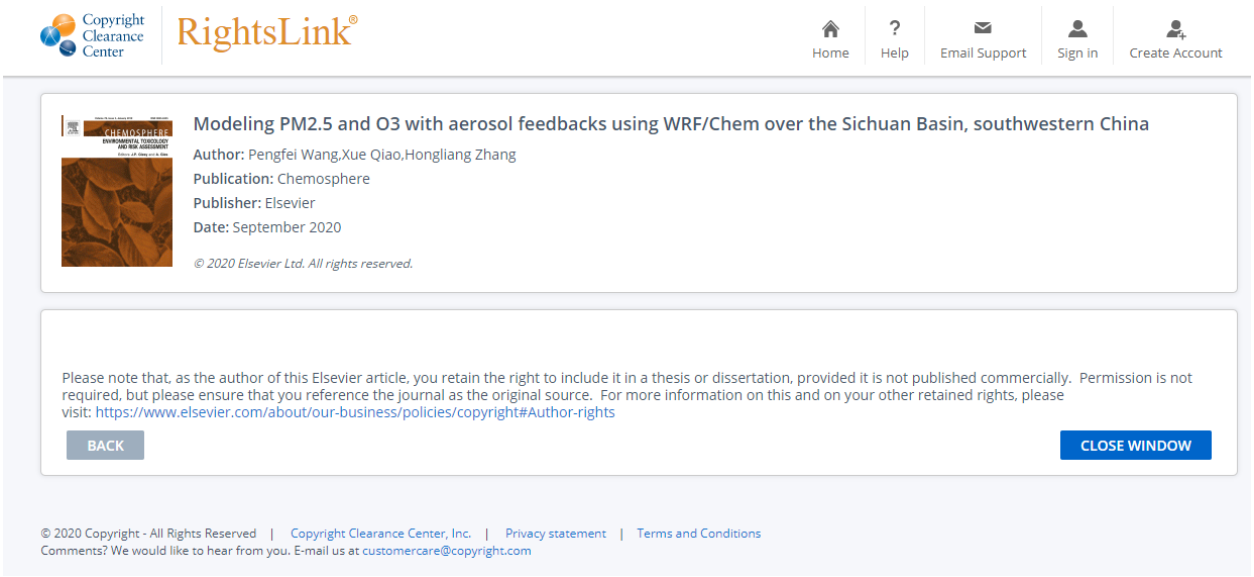

VITA

Pengfei Wang was born in 1989 in Yantai, Shandong Province, People's Republic of China. He graduated with a Bachelor of Science in Environmental Engineering in 2012 from Shandong University of Science and Technology, Qingdao, China. He received his Master of Science in Advanced Engineering in 2015 from Nagasaki University, Nagasaki, Japan.